Aus dem Zentrum für Translationale Lungenforschung
Abteilung Translationale Pneumologie
Ärztlicher Direktor: Prof. Dr. med. Hans-Ulrich Kauczor

Role of the epithelial Cl^- channel SLC26A9 in the murine airway epithelium

Inauguraldisssertation
zur Erlangung des Doctor scientiarum humanarum (Dr. sc. hum.)
an der
Medizinischen Fakultät Heidelberg
an der
Ruprecht-Karls-Universität

Vorgelegt von
Pamela Millar Büchner
aus
Valdivia, Chile
2019

Prodekan: Prof. Dr. Hans-Georg Kräusslich

Doktorvater: Prof. Dr. Marcus A. Mall

Table of contents

TABLE OF CONTENTS III

ABBREVIATIONS VI

1 INTRODUCTION 1

1.1 Cystic fibrosis lung disease 1

1.1.1 Pathogenesis of CF lung disease 1

1.1.2 Novel therapeutic treatments in CF 4

1.2 The alternative Cl^- channel SLC26A9 5

1.2.1 Structure, expression and regulation of SLC26A9 5

1.2.2 Role of the epithelial Cl^- channel SLC26A9 in CF lung disease 5

1.3 βENaC-Tg mice as model to study genetic modifiers of CF lung disease 7

1.4 Aim of the study 7

2 MATERIAL AND METHODS 9

2.1 Experimental animals 9

2.2 Survival rates 9

2.3 Phenotypic appearance, physical condition and oxygen saturation measurements 9

2.4 Lung liquid content 9

2.5 Lung volume measurements 10

2.6 Histology and morphometry 10

2.6.1 Fixation, embedding and tissue sectioning 10

2.6.2 Airway mucus content 11

2.6.3 Airway morphology and mean linear intercepts 12

2.6.4 Immunohistochemistry 13

2.7 Mouse perfusion and *ex-vivo* µCT scanning 13

2.8 Electrophysiological experiments 14

2.8.1 Cultured-tracheal explants 14

2.8.2 Ussing chamber 15

2.9 Flow cytometry 18

2.9.1 Isolation of single cells from lung homogenates for flow cytometry 18

2.9.2 Flow cytometry measurements 18

2.10 Bronchoalveolar lavage 19

2.11 Cytokine quantification 20

2.11.1 Enzyme-linked immunosorbent assay (ELISA) 20

2.11.2 Cytometric bead assay (CBA) 21

2.12 Microbiology experiments 21

2.13 RNA extraction and reverse transcription (RT) qPCR 21

2.13.1 RNA extraction 21

2.13.2 RT-qPCR 22

2.14 Statistics 22

3 RESULTS 23

3.1 Genetic deletion of *Slc26a9* causes high mortality rate in newborn mice 23

3.2 Genetic deletion of *Slc26a9* causes spontaneous lung disease in newborn mice 23

3.2.1 Genetic deletion of *Slc26a9* produces early neonatal mortality due to deficient ventilation 24

3.2.2 Genetic deletion of *Slc26a9* is associated with airway mucus obstruction in newborn mice 25

3.2.3 Lack of *Slc26a9* changes ion transport in the airway epithelium of newborn mice 32

3.2.4 Airway mucus obstruction of the newborn *Slc26a9*$^{-/-}$ mice is associated with hypoxic epithelial cell degeneration and inflammation in absence of detectable lung infection 34

3.3 Developmental role of the SLC26A9 Cl^- channel in the lung 38

3.3.1 SLC26A9-mediated Cl^- secretion is not essential for transepithelial ion transport at postnatal day 5 39
3.3.2 Effects of genetic deletion of *Slc26a9* on mucus airway obstruction in juvenile and adult mice 41
3.3.3 Effects of genetic deletion of *Slc26a9* on airway morphology and lung structure in juvenile and adult mice 43
3.3.4 Resolution of inflammation in surviving juvenile and adult *Slc26a9*$^{-/-}$ mice 44

3.4 Genetic deletion of *Slc26a9* decreases survival of βENaC-Tg mice with CF-like lung disease 46

4 DISCUSSION 49

4.1 Role of the epithelial Cl^- channel SLC26A9 in the early neonatal lung 49
4.1.1 SLC26A9-mediated Cl^- secretion is constitutively active in the airways after birth..... 49
4.1.2 Lack of SLC26A9-mediated Cl^- secretion is associated with airway mucus obstruction and inflammation in newborn mice 51

4.2 Resolution of airway mucus obstruction and inflammation in surviving *Slc26a9*$^{-/-}$ mice 54

4.3 Role of the epithelial Cl^- channel SLC26A9 as a modifier of muco-obstructive lung diseases 55

4.4 Genetic deletion of *Slc26a9* does not generate a model of CF-like lung disease..... 56

4.5 Conclusions 58

5 SUMMARY 59

5.1 Summary 59

5.2 Zusammenfassung 60

6 REFERENCES 63

OWN PUBLICATIONS 79

CURRICULUM VITAE **81**

ACKNOWLEDGEMENTS **82**

EIDESSTATTLICHE VERSICHERUNG **83**

Abbreviations

ABC	ATP-binding cassette transporter protein family
AB-PAS	Alcian-blue periodic acid Schiff
Actb	β-actin gene
αENaC$^{-/-}$	Alpha-ENaC deficient mice
ASL	Airway surface layer
BAL	Bronchoalveolar lavage
βENaC-Tg	Transgenic overexpression of β subunit of ENaC in mice
βENaC-Tg/*Slc26a9*$^{-/-}$	Transgenic overexpression of β subunit of ENaC with additional deletion of *Slc26a9*
Ca^{2+}	Calcium ion
cAMP	Cyclic adenosine monophosphate
CBA	Cytometric bead array
CCSP	Club cell secretory protein
CD	Cluster differentiation
CF	Cystic Fibrosis
CFTR	Cystic fibrosis transmembrane regulation
Cftr$^{-/-}$	*Cftr*- deficient mice
CFU	Colony forming units
Cl^-	Chloride ion
COPD	Chronic obstructive pulmonary disease
dd	Doubled distilled
F508del	Deletion of the codon for phenylalanine at position 508 of *CFTR* gene
ELISA	Enzyme-Linked ImmunoSorbent Assay
ENaC	Epithelial sodium channel

FSK	Forskoline
G551D	Substitution of the aminoacid glycine by aspartate at position 551 of *CFTR* gene
HBE	Human bronchial epithelial cells
$HCO3^-$	Bicarbonate
H&E	Hematoxylin-eosin
IBMX	3-Isobutyl-1-methylxanthin
IL	Interleukin
I_{sc}	Short circuit current
KC	Keratinocyte-derived chemokine
Ly6G	Lymphocyte antigen 6 complex locus G6D
MHCII	Major Histocompatibility complex
MCC	Mucociliary clearance
MIP-2	Macrophage inflammatory protein 2
Na^+-K^+-ATPase	Sodium, potassium, ATPase pump
Na^+	Sodium ion
NACl	Sodium chloride
NBD	Nucleotide binding domain
NKCC1	Co-transporter Na^+-K^+-$2Cl^-$
PBS	Phosphate buffered saline
PCL	Periciliary layer
PCR	Polymerase chain reaction
RT	Reverse transcription
R_{te}	Transepithelial resistance
Scnn1a	Gene of the alpha subunit of the epithelial sodium channel, ENaC
Scnna1b	Gene of the beta subunit of the epithelial sodium channel, ENaC

Scnn1g	Gene of the gamma subunit of the epithelial sodium channel, ENaC
SiglecF	Sialic acid binding immunoglobulin-like lection
Slc26a9	Solute carrier family 26, member 9 gene
SLC26A9	Solute carrier family 26, member 9 protein
Slc26a9$^{-/-}$	*Slc26a9*- deficient mice
Slc26a9$^{-/-}$/*Cftr*$^{-/-}$	*Slc26a9*- and *Cftr*-deficient mice
SNP	Single nucleotide polymorphism
STAS	Sulphate Transporter and AntiSigma factor antagonist
TMD	Transmembrane domain
TMEM16A	Calcium- activated Cl^- channel transmembrane membrane 16A
TNF-α	Tumor necrosis factor alpha
µCT	Micro-computed tomography
UTP	Uridine-5'-triphosphate
V_{te}	Transepithelial potential difference

1 Introduction

1.1 Cystic fibrosis lung disease

Cystic fibrosis (CF) is a lethal autosomal recessive disease affecting primarily Caucasian populations (1). It is a multiorgan disease, but the main cause of morbidity and mortality in patients with CF is determined by chronic lung disease (2). CF is caused by mutations in the cystic fibrosis transmembrane regulator *(CFTR)* gene, which encodes a cyclic adenosine monophosphate (cAMP)-dependent chloride (Cl^-) channel (1, 3, 4). CFTR is an integral membrane protein (1) that belongs to the ATP-binding cassette (ABC) family (sub-family C, member 7; ABCC7) and conserves the general architecture of the ABC family proteins, which consist of four canonical domains: two transmembrane domains (TMD), two cytosolic nucleotide binding domains (NBD) and a cytosolic regulatory (R) domain (5). The anion pore of CFTR Cl^- channel permeates mainly Cl^- ions, but also bicarbonate (HCO_3^-) (6, 7) and its regulated by cAMP-dependent proteinase kinase phosphorylation (8, 9).

1.1.1 Pathogenesis of CF lung disease

In the lung, CFTR is expressed in epithelial cells of the airway surfaces and of submucosal glands (10, 11). CFTR is crucially involved in regulating the activity of other ion channels such as the epithelial sodium (Na^+) channel, ENaC (12) and thereby maintaining airway surface liquid (ASL) homeostasis, which in turn is critical for efficient mucociliary clearance (MCC) (13). In the healthy airway epithelium, ASL is formed by two layers: an upper phase, also known as mucus layer and an inner phase, the periciliary liquid layer (PCL) (Figure 1A). The mucus layer is formed by 98% water and 3% solids (14). This 3% of solids is composed mainly of salt, lipids, cellular debris and the secreted mucins MUC5B and MUC5AC, which represent the two major macromolecular components of the airway (14, 15). The PCL is a 7 µm layer of lower viscosity compared to the mucus layer (14, 16, 17).

Proper hydration of the ASL is essential to enable the coordinated beating of cilia that propel the mucus layer in cranial direction to remove inhaled irritants and pathogens from the lower airways (13). ASL hydration is tightly regulated by coordinated movement of ions coupled with water flow. Na^+ absorption from ASL is mediated by apical ENaC channels, while Cl^- secretion into the airway lumen involves transport via apical and basolateral channels, transporters and pumps (12). Cl^- ions enter the cell through basolateral Na^+-K^+-Cl^- co-transporter (NKCC1), driven by the electrochemical Na^+ gradient generated by the basolateral Na^+-K^+-ATPase pump. On the apical

side, Cl^- exits the cell predominantly via CFTR accompanied by paracellular water flow (12). The alternative Cl^- channels, calcium (Ca^{2+})-activated Cl^- channel transmembrane membrane 16A (TMEM16A; also known as anoctamin 1 [ANO1]) and solute carrier SLC26A9 Cl^- channel may contribute to Cl^- secretion in airway epithelia (18) (Figure 1A).

In the CF airways, defective CFTR-mediated Cl^- secretion in the airway epithelium generates both increased Na^+ absorption and defective Cl^- secretion (19, 20). The impaired regulation of epithelial ion transport in CF airways results in an increased percentage of solids (>8%) in the mucus layer, which represent elevated concentrations of MUC5B and MUC5AC and intracellular components such as DNA (14). The resultant dehydrated and hyperconcentrated mucus compressed the PCL impairing ciliary beating and MCC (13, 21). As a consequence of ineffective MCC, airway mucus obstruction leads to hypoxic necrotic cells in the airway epithelium, which passively release pro-inflammatory cytokines such as IL-1α triggering sterile neutrophilic inflammation (22–25). In the long term, the defective removal of irritants and pathogens from the CF lung causes persistent inflammatory response and favor chronic infection with bacteria (e.g *Pseudomonas aeruginosa*) and further induces mucus hypersecretion (Figure 1B). Thus, the vicious circle of increased mucin secretion, inflammation, and bacterial infection can further aggravate mucus stasis and plugging that characterize the CF airways (13), which may lead to atelectasis (26). Furthermore, the muco-inflammatory phenotype observed in patients with CF leads to irreversible structural lung damage that affect lung function (27), causing progressive organ destruction and ultimately leading to respiratory failure and death.

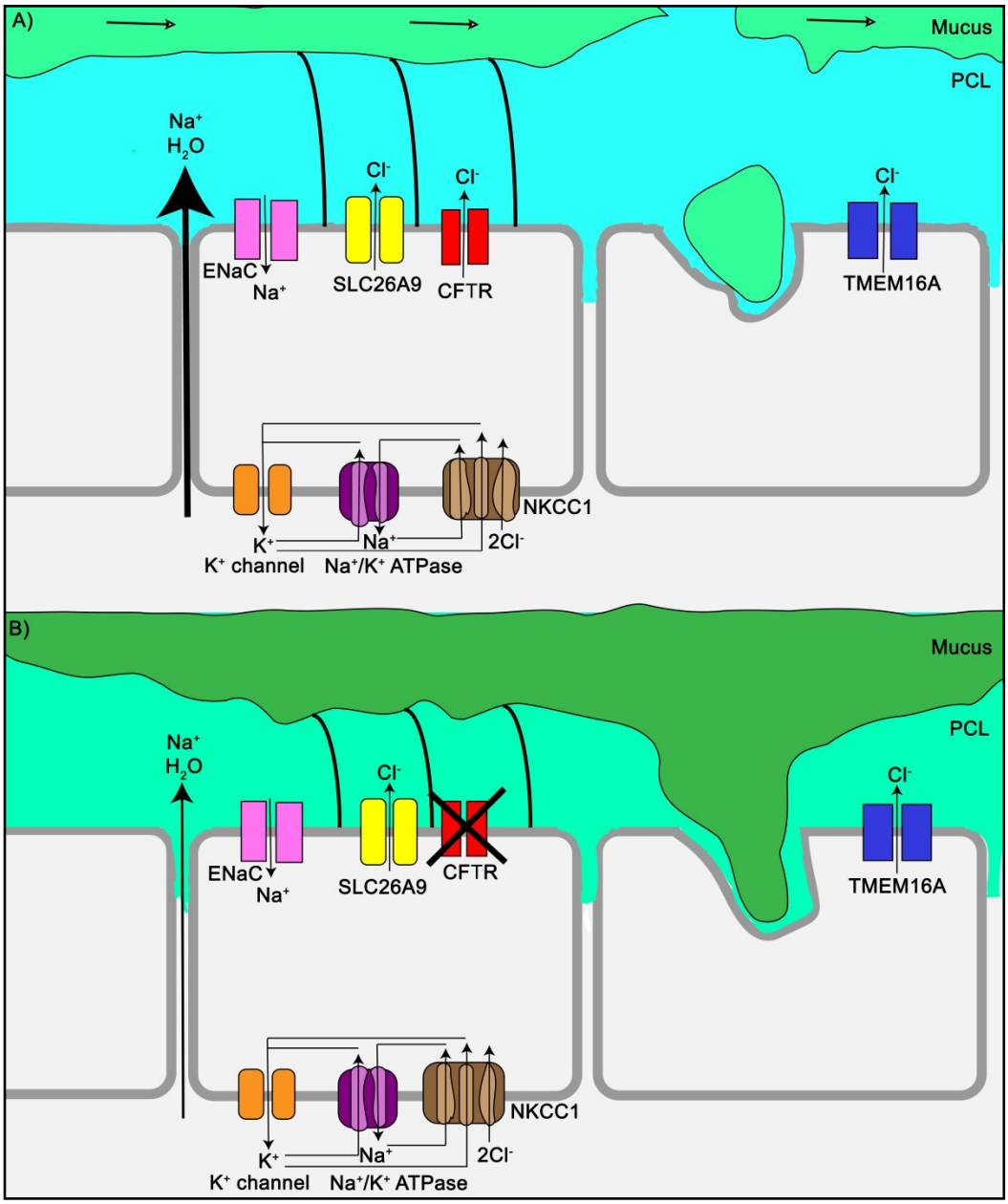

Figure 1. Cell models illustrating epithelial ion transport and fluid secretion in healthy and CF airway epithelium. (A) In the healthy airways, the epithelium is covered by the ASL, which is further divided into the mucus layer and the PCL. Hydration of ASL occurs by coordinate movement of Cl^- secretion through CFTR, which is passively followed by paracellular fluid secretion, and ENaC-mediated Na^+ absorption. To a lesser extend the epithelial Cl^- channels TMEM16A and SLC26A9, which are expressed in mucus-producing cells and epithelial cells respectively, might contribute to epithelial secretion. Cl^- secretion is maintained by the basolateral cotransporter NKCC1, Na^+/K^+-ATPase and K^+ channels. Proper ASL hydration enables ciliary beating and thus, the mucus layer moves towards the oral cavity (as indicated by the arrows). **(B)** In the CF airways, the defective CFTR-mediated Cl^-/fluid secretion causes the accumulation of dehydrated and hyperconcentrated mucus layer. In consequence, ASL is depleted and MCC is impaired. This muco-obstructive phenotype is further aggravated by increased ENaC-mediated Na^+ absorption.

1.1.2 Novel therapeutic treatments in CF

More than 2000 mutations of the *CFTR* gene have been identified (http://www.genet.sickkids.on.ca/), although the functional consequences of many of them are largely unknown. The high diversity of mutations has led to classify them into six classes (Class I to Class VI) according to their molecular and cellular consequences. Class I mutations result in the loss of *CFTR* protein (e.g. premature stop codon). Impaired protein processing and misfolding mutations are summarized as Class II, including the most common mutation, the deletion of a phenylalanine at position 508 (F508del) (2). Mutations resulting in defective protein regulation are grouped in Cass III (also known as gating mutations). Class IV contains mutations leading to decreased CFTR conductance. Other mutations affect mRNA splicing of the CFTR protein (Class V) or CFTR protein stability in the plasma membrane (Class VI) (28). These enormous amounts of mutations hamper the development of an effective CFTR-directed pharmacotherapy. However, intense ongoing research in the CF field has led to the development and optimization of small-molecule compounds (CFTR modulators), which are able to partially restore CFTR function in patients with CF carrying specific mutations (e.g. Class III and F508del mutation) (18, 29–32). CFTR modulators are further divided into two types: CFTR potentiators and CFTR correctors. The first ones are designed to increase CFTR expression at the cell surface, while CFTR correctors improve defective protein processing and trafficking to the cell surface (30). Nevertheless, the CFTR-directed therapies are mutation specific and rely on the biosynthesis of CFTR protein that then, can be transported and stabilized in the plasma membrane. This is particularly important for individuals carrying CFTR mutations that do not synthesize CFTR protein (Class I mutations) and therefore, they are not amenable to treatment with small molecule CFTR modulators.

Patients carrying the same CFTR mutation exhibit different clinical phenotype and responsiveness to treatment (33–37). In addition to genetic defects, differences on clinical outcomes in patients with CF have been associated to environmental factors and non-CFTR genetic variations (38–40). In this context, mutation independent therapies that circumvent CFTR dysfunction such as the potential activation of alternative Cl^- channels (TMEM16A and SLC26A9) are a promising therapeutic option (41).

1.2 The alternative Cl^- channel SLC26A9

1.2.1 Structure, expression and regulation of SLC26A9

In contrast to other members of the SLC26 family, the epithelial Cl^- channel SLC26A9 functions as an uncoupled fast transporter of Cl^- (42). The tertiary structure of SLC26A9 consist of: N-terminal SLC26/sulphate permease transmembrane domain followed by 14 TDM and a cytoplasmic sulphate transporter and sulphate transporter and antisigma factor antagonist (STAS) domain and PDZ-binding domain at the C-terminus (42–44). The STAS and the PDZ-binding domains are known to play a role in membrane targeting, interaction with scaffolding proteins and other ion channels, such as CFTR (21, 51, 54, 55).

SLC26A9 is expressed in several organs, but most prominently in the lung and gastrointestinal tract (stomach and duodenum) (46, 48, 49). In the lung, on a cellular level, SLC26A9 has been localized in bronchial epithelial cells (50, 51), AT1 and AT2 cells (52), and very recently, in neuroendocrine cells (53). In the gastrointestinal tract SLC26A9 was found in gastric epithelial cells (51). Lysine deficient protein kinase (WNKs) and osmotic stress conditions have been describe to participate in the regulation of SLC26A9 (54, 55).

1.2.2 Role of the epithelial Cl^- channel SLC26A9 in CF lung disease

Several lines of evidence suggest a critical role of SLC26A9 in muco-obstructive lung diseases. Single nucleotide polymorphisms (SNPs) on the *SLC26A9* gene have been correlated with a higher risk of developing muco-obstructive lung diseases including diffuse bronchiectasis (56) and childhood asthma (57). In this last study, it was also shown that the SNP in 3` untranslated region of the *SLC26A9* gene (rs228230) reduce protein expression of SLC26A9 (57). Interestingly, one of the allelic forms of the SNP rs7512462 in the *SLC26A9* gene also improved the response to CFTR-directed treatment in patients with CF carrying the class III mutation G551D (58). Furthermore, several genetic studies have associated SNPs in the *SLC26A9* gene with a higher susceptibility to develop CF-associated phenotypes such as prenatal exocrine pancreatic damage (50, 59), CF-related diabetes (60, 61) and meconium ileus (62).

Interestingly, experiments in heterologous systems have demonstrated that SLC26A9 is constitutively active in the airway epithelium (47, 48, 51, 63–65). Furthermore, co-expression of SLC26A9 and CFTR in human embryonic kidney (HEK) 293 cells detected synergetic regulation of cAMP-mediated Cl^- secretion, suggesting a functional interaction between both channels (63). I*n vitro* studies revealed that interaction between both channels begin before reaching the

plasma membrane by showing that the intracellularly retained F508del-CFTR protein binds SLC26A9 via its PDZ domain and thereby inhibits the trafficking of SLC26A9 to the plasma membrane (63). This interaction is reflected in the effect of the SNP rs7512462 of the *SLC26A9* gene, on the responsiveness to CFTR potentiator ivacaftor in patients with G551D and F508del CFTR mutation (58). Patients carrying the G551D mutation (gating mutation) and specific allelic forms of the *SLC26A9* gene showed better lung function when treated with CFTR potentiator ivacaftor. However, homozygous F508del patients (processing mutation) did not show positive modulation of lung function independently of the *SLC26A9* genotype. Interestingly, rescue of F508del CFTR mutation with CFTR corrector VX-809 in primary bronchial epithelial cells showed improvement of lung function, suggesting that both channels are required in the plasma membrane to trigger the beneficial effect of *SLC26A9* genotype (58).

Despite the previous publications indicating that the epithelial Cl^- SLC26A9 plays a role in CF and other muco-obstructive lung diseases, little is known about the *in vivo* function of SLC26A9 at different developmental stages. The *Slc26a9*-deficient mouse (*Slc26a9*$^{-/-}$) was generated by eliminating the exons 2 – 5, including the initiation codon (66). Initially, *Slc26a9*$^{-/-}$ mice were characterized based on their gastrointestinal phenotype (49, 66–70). Adult *Slc26a9*$^{-/-}$ mice showed alterations of gastric acid secretion regulation and reduce number of parietal cells in the stomach (66, 69, 71). Furthermore, SLC26A9 expression was elevated in the gastric mucosa when infected with *Helicobacter pilori* or challenged with IL-11, suggesting that SLC26A9 is important for gastric mucosal defense under pathophysiological conditions (29, 69, 70). To study the role of SLC26A9 as a modifier of intestinal CF phenotype, *Slc26a9*$^{-/-}$ mice were bred with *Cftr*-deficient mice (*Cftr*$^{-/-}$) to generate the double mutant *Slc26a9*$^{-/-}$/*Cftr*$^{-/-}$ mice. The experiments revealed that the genetic deletion of *Slc26a9* increases the mortality of *Cftr*$^{-/-}$ mice, most likely due to intestinal obstruction (29, 49).

The importance of SLC26A9 in the airway epithelium *in vivo* has been demonstrated in experiments performed in *Slc26a9*$^{-/-}$ mice treated with IL-13, as a model of allergic disease. This study revealed that lack of SLC26A9-mediated Cl^- secretion leads to severe airway mucus obstruction (57), suggesting that SLC26A9-mediated Cl^- secretion is critical for ASL hydration and thus, for efficient MCC under pathophysiological conditions (57). Nevertheless, further research is essential to determine the contribution of SLC26A9 in the airway epithelium in both health physiology and muco-obstructive lung disease at different developmental stages.

1.3 βENaC-Tg mice as model to study genetic modifiers of CF lung disease

Cftr$^{-/-}$ mice do not develop CF-like lung disease, limiting their usefulness to study the pathophysiology of CF lung disease (72–76). Therefore, mice with lung specific overexpression of the beta subunit of ENaC (βENaC-Tg mice) were generated to phenocopy CF-like ASL hydration (77). The club cell secretory protein (CCSP) promoter was used to ensure the overexpression of βENaC only in the airways (77). βENaC-Tg mice share features of the human CF pulmonary disease (78, 79) and thus, provide a model to study the effect of ion transport dysregulation in the airway epithelium.

Bioelectric studies demonstrated that basal and amiloride-sensitive currents were elevated in the airway epithelium of βENaC-Tg mice at the neonatal and adult stage, while the cAMP and the Ca^{2+} activated Cl^- secretion remained unchanged (77). Increased airway Na^+ transport causes ASL depletion and consequently, severe and spontaneous airway mucus plugging, impaired MCC, chronic airway inflammation and slowed clearance of bacterial pathogens (25). Longitudinal analysis of the βENaC-Tg mice revealed severe tracheal mucus plugging that is initiated at the neonatal stage (3 days old). In juvenile and adult βENaC-Tg mice, airway mucus obstruction is propagated towards the proximal and distal intrapulmonary main axial bronchi (25). Chronic airway inflammation in the βENaC-Tg mice is characterized by influx of macrophages and increase recruitment of neutrophils. Consistently, keratinocyte-derived chemokine (KC) and macrophage-inflammatory protein 2 (MIP-2), both neutrophils chemoattractant, were elevated in bronchoalveolar lavage (BAL) fluid. Transient eosinophilic inflammation and increase expression of Th2 markers was also detected in the βENaC-Tg mice (80).

βENaC-Tg mice have been particularly useful to study the contribution of other genes (e.g. IL-1Ra, neutrophil elastase and matrix metalloproteinase 12, among others) to the pathogenesis of CF-like lung disease (22, 81–83). Crossing the βENaC-Tg mice with genetically modified mice that lack potential disease modifiers of CF lung disease provides information on the contribution of these genes to the pathogenesis of CF lung disease, how the airway epithelium is impacted and potential therapeutic strategies.

1.4 Aim of the study

Understanding the role of SLC26A9 Cl^- channel in an *in vivo* system is pivotal to determine how SLC26A9 contribute to lung health and the pathophysiology of muco-obstructive lung diseases such as CF. Therefore, the overall aim of this study was to characterize the pulmonary

phenotype of the *Slc26a9*$^{-/-}$ mice in a longitudinal manner (newborn, juvenile and adult mice) by comparing WT and *Slc26a9*$^{-/-}$ littermates.

The first goal of this project was to determine if and how the genetic deletion of *Slc26a9* affects the survival of the mice by monitoring the mortality rate and phenotypic appearance of WT and *Slc26a9*$^{-/-}$ mice from birth up to the age of 6 weeks. To elucidate the role of SLC26A9 Cl^- channel on lung health, morphology and airway structure histological preparations were analyzed in newborn, juvenile and adult WT and *Slc26a9*$^{-/-}$ mice. Lung structure of newborn WT and *Slc26a9*$^{-/-}$ mice was further investigated by µCT-imaging analysis. The bioelectrical properties of tracheas from newborn and 5-day-old WT and *Slc26a9*$^{-/-}$ mice were studied to evaluate the contribution of SLC26A9-mediated Cl^- secretion to the transpithelial ion transport of the airway epithelium. Furthermore, the potential impact of the genetic deletion of *Slc26a9* on other epithelial ion channels was also determined at a transcriptional level. To explore if and how the genetic deletion of *Slc26a9* impacts the inflammatory phenotype of the airway epithelium, the relative distribution of inflammatory cells was quantified from lung homogenates of newborn mice and BAL of juvenile and adult WT and *Slc26a9*$^{-/-}$ mice. Additionally, levels of pro- and anti-inflammatory cytokines were determined from lung homogenates of newborn WT and *Slc26a9*$^{-/-}$ mice. To evaluate if the genetic deletion of *Slc26a9* leads to airway bacterial infection, colony forming units (CFU) were determine from lung homogenates of newborn mice. Finally to determine if the genetic deletion of *Slc26a9* modifies survival in the context of CF-like lung disease, *Slc26a9*-heterozygous (*Slc26a9*$^{+/-}$) mice were intercrossed with βENaC-Tg mice to generate double mutant mice (βENaC-Tg/*Slc26a9*$^{-/-}$). The mortality rate of βENaC-Tg/*Slc26a9*$^{-/-}$ mice and βENaC-Tg mice were compared from birth up to the age of 6 weeks.

2 Material and Methods

2.1 Experimental animals

All animal studies were approved by the animal welfare authority responsible for the University of Heidelberg (Regierungspräsidium Karlsruhe). Experimental animals were generated from *Slc26a9*$^{+/-}$ breeding pairs on C57BL/6J genetic background. Wild-type (WT) and *Slc26a9*$^{-/-}$ (71) mice were studied. βENaC-Tg mice were generated as previously described (77) and intercrossed with *Slc26a9*$^{+/-}$ mice to obtain βENaC-Tg/*Slc26a9*$^{-/-}$ mice. This breeding strategy also generated WT, *Slc26a9*$^{+/-}$, *Slc26a9*$^{-/-}$, βENaC-Tg and βENaC-Tg/*Slc26a9*$^{+/-}$ mice.

All animals were genotyped from tail or ear biopsies by polymerase chain reaction (PCR) as previously described (71, 77). Mice were studied as newborn (within the first hours of life), at postnatal day 5 (5-day-old), juvenile stage (2-week-old) or adult stage (6-week-old). Mice were housed in a specific pathogen-free animal facility with standard 12 hours day/night light cycles at 22°C and free access to food and water.

2.2 Survival rates

To determine the effects of the genetic deletion of *Slc26a9* on survival, pups were monitored from birth up to the age of 6 weeks. Cages were checked 3 times a day during the first two weeks, and then, once a day until week 6. The cadavers were collected and genotyped.

2.3 Phenotypic appearance, physical condition and oxygen saturation measurements

The phenotype and physical conditions of the newborn mice were determined by monitoring and annotating the phenotypic appearance of pups as normal breathing or respiratory distress and non-cyanotic appearance or cyanotic appearance. Weight was also determined for each mouse.

Oxygen saturation was determined on newborn WT and *Slc26a9*$^{-/-}$ mice at room air using a non-invasive pulse oximeter for laboratory animals (MouseOx Plus, STARR Life Science Corporation, Oakmont, Pennsylvania, USA). Arterial blood oxygen saturation, respiratory rate and heart rate were recorded with a thigh clip sensor. Percent oxygen saturation was measured after stabilization of respiratory rate and heart rate.

2.4 Lung liquid content

Experiments were performed in newborn WT and *Slc26a9*$^{-/-}$ mice. Lungs were dissected from

the heart and connective tissue and blotted with filter paper to remove excessive liquid. Lungs were weight to determine the wet weight. Following incubation for 48 hours at 72°C, and weighed again to obtain the dry weight. Results are shown as the ratio between lung wet to dry weight.

2.5 Lung volume measurements

For assessment of lung volume the juvenile and adult right lung lobes from juvenile and adult WT and *Slc26a9*$^{-/-}$ mice were inflated with 4% buffered formalin (Otto Fischar, Saarbrücken, Germany) at a constant pressure of 25 cm column. Once the right lung lobes were inflated, the tissue was submerged in formalin for 24 hours. Then, the lung volume was determined using the volume displacement method (84, 85) as followed: a container was filled with 2/3 of PBS, placed on a balance and the weight recorded (W_1). Next, the fixed right lung lobes were submerged in the container with PBS, kept in place with a thin wire without touching the wall container or the bottom, and the second weight (W_2) was read off. The weight of the fluid displaced by the right lung lobes was determined by W_{organ}= W2 – W1 and it is a direct indicator of the right lung lobes volume.

2.6 Histology and morphometry

2.6.1 Fixation, embedding and tissue sectioning

For fixation left and right lung lobes were treated differently. Newborn, juvenile and adult left lung lobes were directly immersed in 4% buffered formalin immediately after dissection (Otto Fischar, Saarbrücken, Germany) and used to quantify airway mucus obstruction and epithelial cell degeneration. The right lung lobes of juvenile and adult mice (2- and 6-week-old) were inflated as previously described (See section 2.5), stored in 4% buffered formalin at 4°C overnight and used for measurements of mean linear intercepts (MLI), as an indicator of alveolar diameters.

After 24 hours, left and right lung lobes were washed with PBS (Thermo Fisher Scientific, Darmstadt, Germany) and transferred to ethanol 70% (Carl Roth, Karlsruhe, Germany). The apical part of the lung lobes was cropped transversally, transferred to biopsy cassettes (Steinbrenner Laborsysteme, Wiesenbach, Germany) and dehydrated at room temperature according to the following protocol: 2 x 30 minutes in 96% ethanol (Carl Roth, Karlsruhe, Germany), 2 x 45 minutes in 100% ethanol (Carl Roth, Karlsruhe, Germany) and overnight in xylene (Carl Roth, Karlsruhe, Germany).

For embedding, the specimens were immersed in paraffin (Carl Roth, Karlsruhe, Germany) and

vacuum was applied for two hours to assist penetration of the embedding agent, followed by one hour at atmospheric pressure. For correct orientation during tissue sectioning the lung lobes were placed in molds with the cropped surface facing downwards. Paraffin blocks were kept for 12 to 16 hours at 4°C to harden completely.

Sectioning of the lungs was performed in a microtome (Leica Microsystems, Nussloch, Germany). Left lung lobes were sectioned transversally at the level of the proximal and distal intra-pulmonary main axial airway near the hilus in sections of 5 µm or 1.5 µm thickness. Right lung lobes were cut to sections of 5 µm. Lung sections were deparaffinized in xylene (Carl Roth, Karlsruhe, Germany) and rehydrated 2 x 10 minutes in 100% ethanol (Carl Roth, Karlsruhe, Germany), 2 x 2 minutes in 96% ethanol (Carl Roth, Karlsruhe, Germany), 2 minutes in 70% ethanol (Carl Roth, Karlsruhe, Germany), and finally rinsed with double distilled water (ddH_2O).

2.6.2 Airway mucus content

To study airway mucus content and determine goblet cell counts in the proximal and distal main axial airways, 5 µm and 1.5 µm sections were stained with Alcian blue-Periodic acid Schiffs (AB-PAS) staining. In brief, samples were immersed 30 minutes in Alcian blue solution containing 3% acetic acid (Carl Roth, Karlsruhe, Germany), 1% Alcian Blue 8GX (Sigma-Aldrich, Steimheim, Germany), and 1 crystal of Thymol (Sigma-Aldrich, Steinheim, Germany) for 30 minutes and afterwards rinsed with tap water for 2 minutes. Then, sections were stained with 0.5% periodic acid solution (Sigma-Aldrich, Steinheim, Germany) for 5 minutes and rinsed 3 x in ddH_2O, followed by Schiff's reagent (Sigma-Aldrich, Steinheim, Germany) for 15 minutes and 1 minute in sulfur solution containing 1% 5 M HCl (Merck, Darmstadt, Germany), 0.6% sodium metabisulfite (Sigma-Aldrich, Steinheim, Germany), and subsequently rinsed in tap water. Finally, AB-PAS-stained sections were immersed in 96% ethanol for 1 minute, 2 x 1 minute in 100% ethanol, cleared in xylene for 3 minutes, and mounted with permanent mounting medium (Sigma-Aldrich, Steinheim, Germany). Images of stained-lungs were captured with Olympus IX-71 microscope interfaced with a SIS Colorview I Camera Set (Olympus, Hamburg, Germany) interfaced with a DP73 camera (Olympus, Hamburg, Germany). For quantitative stereological assessment of airway mucus obstruction in the main proximal and distal airways, Cell^F analysis software (Olympus Soft Imaging Solutions, Münster, Germany) was used as previously described (3). Briefly, the length of the airway boundary, defined as the epithelial basement membrane, was measured using the interactive image measurement tool, and the AB-PAS positive surface area within the boundary was measured by phase analysis according to the automatic threshold settings of the software. The volume density of airway mucus, representing the volume of airway

mucus content per surface of the basement membrane (nl/mm^2), was calculated from the surface area of AB-PAS positive mucus and the total basement membrane length.

To quantify the AB-PAS positive staining in the terminal bronchioles open source image processing program ImageJ 1.52a was used. Briefly, AB-PAS-stained images were converted into grayscale and then, the picture was split into three colors channels. The green channel was selected because showed the highest contrast between background and the AB-PAS positive staining. The threshold was adjusted to obtain the percentage of AB-PAS positive area staining and normalized to the total area of the picture.

2.6.3 Airway morphology and mean linear intercepts

In order to analyze airway epithelial cell degeneration, 5 µm sections of left lung lobes from newborn, juvenile and adult WT and *Slc26a9*$^{-/-}$ mice were stained with hematoxylin-eosin (H&E). Juvenile and adult right lung lobes from WT and *Slc26a9*$^{-/-}$ mice were also stained with H&E and used to analyze MLI. Lung tissues were placed 3 minutes in hematoxylin (Sigma-Aldrich, Steimheim, Germany), rinsed with ddH_2O and placed 1 minute in hydrochloric acid (HCl)/ethanol solution containing 50% ethanol (Carl Roth, Karlsruhe, Germany) and 1.3% 5M HCl (Merck, Darmstadt, Germany), and subsequently washed with tap water. Slides were transferred to the eosin solution containing 0.1% eosin (Carl Roth, Karlsruhe, Germany), 63% ethanol (Carl Roth, Karlsruhe, Germany), and 1% acetic acid (Carl Roth, Karlsruhe, Germany), for 45 seconds before rinsing again with ddH_2O. Tissue sections were then dehydrated, and mounted with permanent mounting medium (Sigma-Aldrich, Steinheim, Germany), as described above.

To study airway epithelial cell degeneration, Cell^F analysis software was used for quantitative stereological assessment. Degenerative cells were identified by morphologic criteria (i.e., cell swelling with cytoplasmic vacuolization), and numeric cell densities were quantified by counting epithelial cells per mm of the basement membrane, as previously described (25).

The 4 inflated-right lung lobes of the lung from juvenile and adult mice were used to measure distal air space enlargement by quantifying MLI. MLI was determined by dividing the sum of the lengths of all lines in all frames by the number of intercepts between alveolar septum and counting lines, as previously described (25). For each animal, 8 – 10 fields were measured in different lung lobes.

2.6.4 Immunohistochemistry

To localize the mucin MUC5B, immunohistochemistry was performed in formalin-fixed, paraffin-embedded 1.5 µm left lobe sections from newborn mice. The antibody rabbit-anti mouse MUC5B at a dilution of 1:2000 in PBS (H-300; Santa Cruz, Heidelberg, Germany) was used.

Unstained and hydrated paraffin section were pre-treated with 3% hydrogen peroxide for 10 minutes at room temperature and rinsed 3 x 3 minutes in PBS, followed by antigen retrieval with Citra plus buffer (BioGenex, San Ramon, California, USA) for 30 minutes at 97°C. Lung sections were incubated with a non-specific protein-blocking solution containing animal serum (Vector Laboratories, Burlingame, California, USA). Lung sections were incubated overnight at 4°C with primary antibody as indicated. Lung sections were rinsed 3 x 2 minutes in PBS and incubated with goat anti-rabbit IgG antibody (dilution of 1: 200 in PBS) as secondary antibody for 30 minutes at room temperature. Immunoreactivity was visualized using Vectastain ABC HRP Kit (Vector Laboratories, Burlingame, California, USA), followed by 3, 3'-diaminobenzidine (DAB) substrate kit (Vector Laboratories, Burlingame, California, USA). After visualization of the reaction, the sections were counterstained with H&E (Sigma-Aldrich, Steinheim, Germany) for 5 seconds, dehydrated, cleared and mounted as previously described. As negative control, each experiment included lung sections stained with secondary antibody only.

2.7 Mouse perfusion and *ex-vivo* µCT scanning

Lungs from newborn WT and *Slc26a9*$^{-/-}$ mice were perfused and fixed *in situ* for subsequent µCT imaging. Lungs were fixed by vasculature perfusion as previously described (86). To preserve airway mucus in its original position, the trachea was tied to preserve a residual volume of air in the lungs and no positive airway pressure was applied to inflate the lungs. The thoracic cavity was longitudinally opened and the thymus and ribs were removed to have a better access to the heart. The right ventricle was cannulated using a 22G cannula (Venisystems, Abbocath, UK) and the left atrium was cut for drainage. Lungs were perfused with pre-flush solution (1L Ringer solution (B Braun, Germany), 5% Dextran 70 (Roth, Germany), 5 IU/ml heparin (Ratiopharm, Ulm, Germany) and 0.02% lidocaine (Jenapharm, Jena, Germany) to remove coagulated blood from pulmonary vessels. For fixation, lungs were perfused with fixative solution (25% Polyethynelglycol (PEG; Roth, Karlsruhe, Germany), 10% ethanol (Roth, Karlsruhe, Germany), 3.7% formaldehyde (AppliChem, Darmstadt, Germany) for 30 minutes at 20 cm column pressure. Then, lungs were removed and stained with osmium as previously described (87).

Osmium-stained lungs were scanned using the SkyScan1176 (Bruker microCT, Kontich,

Belgium). Images were obtained without contrast agent with the following settings: 50 kV, 500 µA source current, 0.5 mm aluminum filter, 9 µm resolution and a rotation range of 180°. Reconstruction and analyses of the scans were performed with NRecon programme (version: 1.7.0.4, Burker microCT, Kontich, Belgium). Airways in the tracheobronchial tree were classified as previously described (88) and each airway segment was evaluated for airway occlusion, using a semi-quantitatively system from 0 to 2 (0= non, 1= mild and 2= severe airway occlusion). Researchers were blinded to the genotype and results are shown as the mean of all airway segments analyzed.

2.8 Electrophysiological experiments

The conventional method to study transepithelial ion transport from freshly excised tissue is the Ussing chamber. However, in our case the use of this technique limits the study of all newborn mice at a similar time point, and therefore, cultured-tracheal explants were generated to evaluate transepithelial ion transport. The bioelectrical properties of mice at later time points were investigated by performing Ussing chamber.

2.8.1 Cultured-tracheal explants

This protocol was modified from Hummler, E., *et al* (89). Tracheas were dissected from newborn WT and *Slc26a9*$^{-/-}$ mice, placed in petri dishes (Thermo scientific, Roskilde, Denmark) containing 1 ml of medium (F12 Nutrient Mixture (Ham) + L-Glutamine (Gibco, Schwerte, Germany), supplemented with 10% FBS (Gibco, Schwerte, Germany), 5 mg/ml Penicillin/Streptomycin (Gibco, Schwerte, Germany), 5 mM HEPES buffer (Millipore, Darmstadt, Germany), and incubated at 37°C in an atmosphere of 5% CO_2 and 95% O_2. A mixture of 400 µl Matrigel Matrix high concentration (Corning, Wiesbaden, Germany) and 200 µl of cold medium was prepared and filled into a bottom glass petri dish (Cellvis, Mountain view, California, USA). Tissues were transferred into the matrigel filled petri dishes and gelation was performed according to manufacturer's instructions. After solidification of the Matrigel Matrix, the tissues were covered with medium and incubated for 6 – 8 days. Medium was changed every second day.

After 6 – 8 days of culture, the tracheal tissues form a cyst-like structure filled with liquid secreted by the airway epithelial cells (89). 15 – 30 minutes before the electrophysiological experiment the culture medium was replaced with Ringer solution (145 mM NaCl (Sigma-Aldrich, Steinheim, Germany), 0.4 mM KH_2PO_4 (Millipore, Darmstadt, Germany), 1.6 mM K_2HPO_4*$3H_2O$ (Millipore, Darmstadt, Germany), 5 mM glucose (Millipore, Darmstadt, Germany), 1 mM $MgCl_2$*$6H_2O$ (Millipore, Darmstadt, Germany) and 1.3 mM Ca- gluconate*$1H_2O$ (Aplichem,

Darmstadt, Germany)). The cyst was impaled with a glass microelectrode (tip resistance 14.9 MΩ) filled with Ringer solution and the transepithelial potential difference (V_{te}) was continuously recorded using a standardized voltmeter set-up (Figure 2). The recording electrode was referenced to the bath solution. Impalements were accepted if they met the following criteria: (i) the electrode tip was seen to penetrate the explant wall, (ii) base-line readings before and after impalement differed by less than 1 mV, (iii) the recording was stable for at least 2 minutes, and (iv) there was not a visible hole in the cyst when the microelectrode was withdrawn (90). Data was analyzed using Lab chart (Lab Chart7, ADInstruments Pty Ltd, 13/22 Lexington Drive, Bella Vista, Australia).

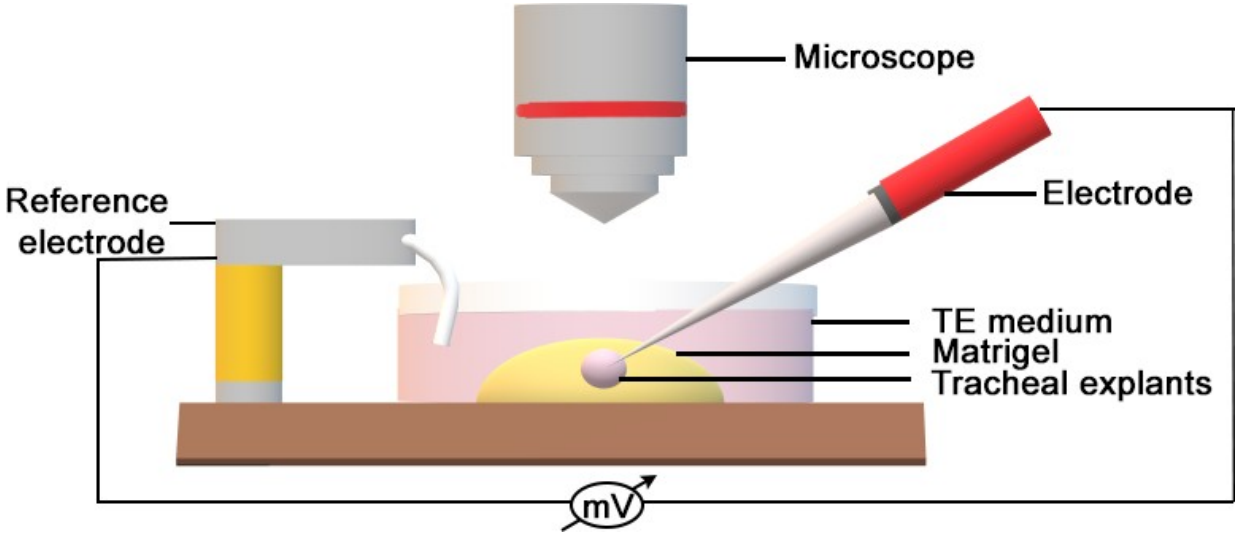

Figure 2. Experimental set up of tracheal explant experiments. Reference electrode was placed in the Ringer solution and the tracheal explant was positioned under the microscope. The recording electrode was controlled by a digital micromanipulator and observed through the microscope as approached the explant wall. Negative change in V_{te} indicated penetration of the explant wall and it was continuously recorded with a standardized voltmeter set-up during the experiment.

2.8.2 Ussing chamber

Ion transport measurements across freshly excised tracheal tissues were performed in a continuously perfused micro-Ussing chamber (57). Tracheas from 5-day-old WT and surviving *Slc26a9*$^{-/-}$ mice were removed, mounted on an insert with a circular open area of 0.01 mm^2 and placed between the two half cells of the Ussing chamber (Figure 3). V_{te} values were referenced to the basolateral side. The stabilization of the V_{te} and resistance (R_{te}) was performed under constant perfusion with Ringer solution at 37 °C. R_{te} was determined by applying short intermittent current pulses (ΔI = 0.5 µA) and the corresponding changes in V_{te} (ΔV_{te}) and basal

V_{te} were recorded continuously during the course of the experiment. R_{te} and the equivalent short circuit current (I_{sc}') were calculated according to Ohm's law ($R_{te} = \Delta V_{te}/\Delta I$).

To further assess transepithelial ion transport several activators and inhibitors compounds were used (Table 1).

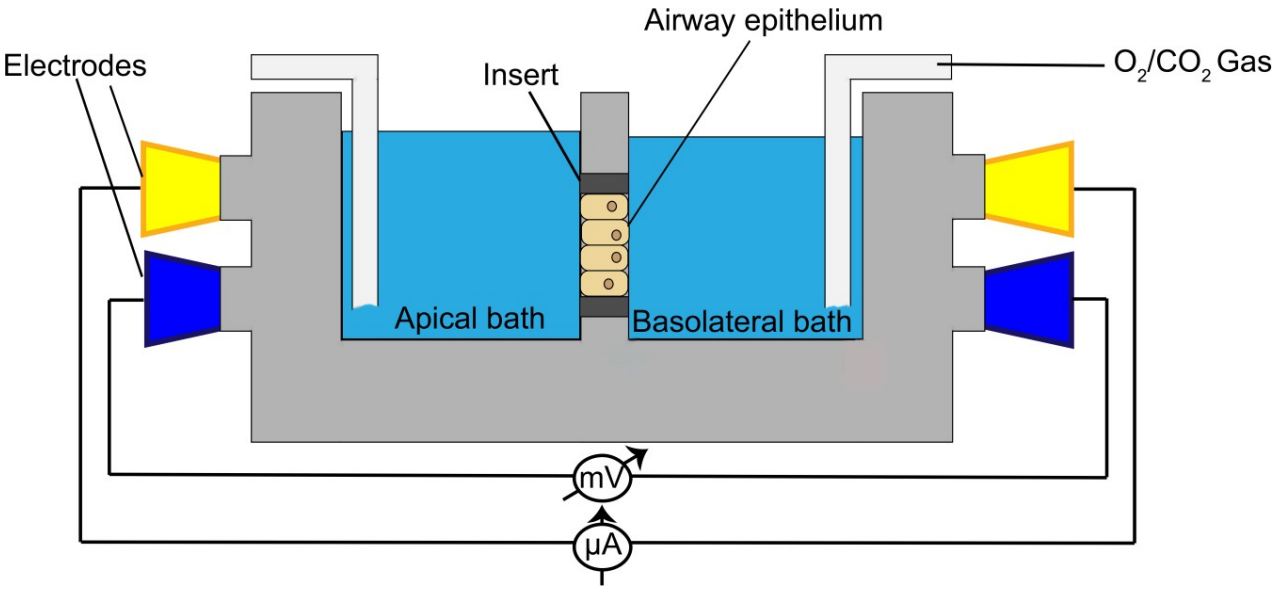

Figure 3. Experimental set up of Ussing chamber experiments. The airway epithelium was placed between the two half cells at the Ussing chamber and each side was filled with Ringer solution. Activators and inhibitors of ion channels or transporters were added either to the apical or basolateral side. Changes in V_{te} (mV) were continuously recorded. Intermittent current pulses were applied (ΔI = 0.5 µA) and I_{sc} was calculated according to the Ohm´s law ($R_{te} = \Delta V_{te}/\Delta I$).

Table 1. Summary of activators and inhibitors used to perform Ussing chamber experiments.

Substance	Effect	Final concentration	Side of application	Supplier
Amiloride	Blocker of the epithelial Na^+ channel, ENaC (77)	100 µM	Apical	Sigma-Aldrich, Steinheim, Germany
Forskolin	Activator of adenylyl cyclase resulting in an increase of intracellular cAMP concentration (83)	1 µM	Apical	Sigma-Aldrich, Steinheim, Germany
3-Isobutyl-1-methylxanthin (IBMX)	Inhibitor of cAMP and cyclic guanosine monophosphate phosphodiesterases. Consequently, protein kinase A is activated (83)	100 µM	Apical	Sigma-Aldrich, Steinheim, Germany
Uridine-5'-triphosphate (UTP)	Activator of P2Y2 receptor causing an elevation in intracellular Ca^{2+} (83)	100 µM	Apical	GE Healthcare Life Science, Freiburg, Germany
CFTR inhibitor 172*	Inhibitor of the epithelial Cl^- channel CFTR (55)	20 µM	Apical	Merck Millipore, Darmstadt, Germany
GlyH101*	Inhibitor of the epithelial Cl^- channels, CFTR and SLC26A9 (55, 63)	100 µM	Apical	Merck Millipore, Darmstadt, Germany
Bumetanide	Inhibitor of NKCC1 cotransporter (83)	100 µM	Basolateral	Sigma-Aldrich, Steinheim, Germany

*Both inhibitors were used in an attempt to differentiate CFTR- and SLC26A9-mediated Cl^- secretion. CFTR specific inhibitor, CFTRinh172, was added first and then GlyH101 was applied, assuming that the remaining inhibited current correspond to SLC26A9-mediated Cl^- secretion.

2.9 Flow cytometry

2.9.1 Isolation of single cells from lung homogenates for flow cytometry

For isolation of leukocytes, lungs from newborn mice were perfused through the right ventricle of the heart with 2.5 ml PBS, removed, transferred to RPMI-1640 (GE Healthcare Life Science, Freiburg, Germany), placed in a petri dish and minced with scissors in pieces no larger than 1 or 2 mm. Subsequently, each lung was transferred into 10 ml of PBS containing 300 U/mL collagenase type II (Worthington Biochemical, Lakewood, New Jersey, USA) and 0.15 mg/ml DNase I (Sigma-Aldrich, Steinheim, Germany), and incubated on a shaker with an orbital speed of 125 rpm for 30 minutes at 37°C. To obtain single cells suspension, the digested lungs were passed through a 100 µm filter (Sigma-Aldrich, Steinheim, Germany). The 100 µm filter was rinsed with 10 ml cold PBS to stop DNase reaction. Lung suspensions were centrifuged at 300 x *g* for 5 minutes at 4°C, supernatant was discarded and cells were incubated in 5 ml of red blood cell lysis buffer (BD Biosciences, Heidelberg, Germany) for 5 minutes at RT and sieved through a 40 µm filter (Sigma-Aldrich, Steinheim, Germany). Cells were resuspended in cRPMI medium containing RPMI-1640, 10% FBS (Thermo Fisher Scientific, Darmstadt, Germany), 0.1% 2-Mercaptoethanol (Thermo Fisher Scientific, Darmstadt, Germany) and 1% L-Glutamin (Thermo Fisher Scientific, Darmstadt, Germany).

2.9.2 Flow cytometry measurements

The cells were incubated with Fc Block (BD bioscience, Heidelberg, Germany) on ice. For surface staining, a master mix of the antibodies listed in Table 2 was prepared and added to the cell suspension and incubated for 30 minutes at 4°C (light protected). Total cell numbers and viability were assessed by trypan blue exclusion test (Sigma-Aldrich, Taufkirchen, Germany). Cells were fixed with intracellular fixation buffer to allow short term storage. Flow cytometry was performed with exclusion of nonviable cells and doublets by using the Multiparameter flow cytometry with an LSRFortessa cell analyzer (BD Biosciences, Heidelberg, Germany). Data were analyzed with Flow Jo software (v10; TreeStar, Ashland, Oregon, USA).

Cells were stained for detection of neutrophils ($CD45^+Ly6G^+CD11b^+$), monocytes ($CD45^+CD11c^+MHCII^+$), eosinophils ($CD45^+SinglecF^+CD64^-$) and T-cells ($CD45^+CD3^-$FSC-A).

Table 2. Antibody master mix for the detection of leukocytes from lung homogenates

Antibody	Clone	Fluorophore	Supplier	Dilution
CD45	30-F11	Phycoerythrin (PE)-CF594	BD Bioscience, Heidelberg, Germany	1:100
Ly6G (Lymphocyte antigen 6 complex locus G6D)	1A-8	Peridinin- chlorophyll-protein complex (PerCP)-cyanine (Cy) 5.5	BD Bioscience, Heidelberg, Germany	1:50
CD11b	M1/70	Qd605	Biolegend, San Diego, California, USA	1:100
CD11c	HL-3	Allophycocyanin (APC)-cyanine (Cy) Cy7	BD Bioscience, Heidelberg, Germany	1:200
MHCII (Major histocompatibility complex)	M5/114.15-2	V450	Biolegend, San Diego, California, USA	1:400
Siglec-F (Sialic acid-binding immunoglobulin-like lectin)	E50-2440	PE	BD Bioscience, Heidelberg, Germany	1:50
CD64	X54-5/7.1	Brilliant violet (BV) 711	Biolegend, San Diego, California, USA	1:50
CD3	17A2	Alexa flour 700	BD Bioscience, Heidelberg, Germany	1:50

2.10 Bronchoalveolar lavage

The trachea of juvenile (2-week-old) and adult WT and *Slc26a9*$^{-/-}$ mice (6-week-old) was cannulated, the left main stem bronchus ligated and right lung lobes were lavaged twice with sterile PBS (Thermo Fisher Scientific, Darmstadt, Germany) containing cOmplete Protease

Inhibitor (Sigma-Aldrich, Steinheim, Germany) with a volume of 17.5 µl/g body weight. BAL fluid was centrifuged at 300 x *g* for 5 minutes at 4°C. The cell pellet was suspended in 50 µl PBS, stained with trypan blue (Sigma-Aldrich, Steinheim, Germany) and counted using a Neubauer chamber (Karl Hecht, Sondheim v.d. Rhön, Germany). Total cell counts per recovered BAL volume were calculated. Differential cell counts of BAL volume on cytospin slides were performed after May-Grünwald-Giemsa (Merck, Darmstadt, Germany) staining as previously described (25).

2.11 Cytokine quantification

Two different protein quantification methods were used depending on the sensitivity required to read the specific cytokines: KC, MIP-2, IL-1α, IL-1β, IL-13, IL-5 and tumor necrosis factor alpha (TNF-α).

2.11.1 Enzyme-linked immunosorbent assay (ELISA)

Concentrations of the neutrophils-chemoattractant KC and MIP-2 were measured in lung homogenates from newborn WT and *Slc26a9*$^{-/-}$ mice by ELISA test. Additionally, the concentrations of the pro-inflammatory cytokines IL-1α and IL-1β were also analyzed using ELISA test. All ELISA test were performed according to the manufacturer's instructions using Quantikine® (R&D systems, Minneapolis, Minnesota, USA). Briefly, lung homogenates were applied to reaction chambers pre-coated with antibodies specific to the cytokine of interest, thus specifically immobilizing the cytokine of interest, and incubated 2 hours at room temperature. Subsequently, the solution in the wells was washed thoroughly and the secondary antibody specific for each cytokines of interest was added and incubated again for 2 hours at room temperature. Excessive secondary antibody was removed by repeated rinsing of the microplate wells and substrate solution was added immediately after. The concentration of cytokine was determined by colorimetric reaction catalyzed by the antibody linked enzyme. To measure the change in absorption, a micro plate reader (Mithras LB 940, Berthold Technologies GmbH & Co. KG, Bad Wildbad, Germany) set to 450 nm with wavelength correction at 540 nm was used. The final cytokine concentrations were derived from the standard curve determined for each assay. In accordance with the manufacturer's instructions the minimal detectable limit for each of the cytokines analyzed was: KC (2.0 pg/ml), MIP-2 (1.5 pg/ml), IL-1α (2.5 pg/ml) and IL-1β (2.31 pg/ml).

2.11.2 Cytometric bead assay (CBA)

Concentrations of TNF-α, IL-13 and IL-5 were measured in lung homogenates from newborn mice by using a CBA enhanced sensitivity flex sets (minimal detectable limit: 0.2 pg/ml; BD bioscience, Heidelberg, Germany). CBA was performed according to the manufacturer´s instructions. Briefly, the samples were centrifuged at 12000 x g for 2 minutes at 4°C and the supernatant transferred to a new autoclaved tube. Subsequently, 50 µl of the Mouse Flex Set Standard dilution or the samples were added to the appropriate tubes. Following, 20 µl of the mixed of Capture beads (previously vortexed) was added to each tube, mixed gently and then, incubated for 2 hours at room temperature. 20 µl of mixed Mouse Detection Reagent was added to each tube, mixed gently and incubated again for 2 hours at room temperature. After incubation, 1 ml of Wash buffer was added and centrifuged at 200 x g for 5 minutes, the supernatant was aspirated from each tube and 100 µl of the Enhanced Sensitivity Detection Reagent was added to each tube and incubated for 1 hour at room temperature. Then, tubes were washed as previously described and the excess of volume was aspirated and finally, 300 µl of Wash buffer was added to each tube and the samples were acquired on LSRFortessa flow cytometry (BD bioscience, Heidelberg, Germany).

2.12 Microbiology experiments

Lungs from newborn mice were homogenized under sterile conditions. Samples from each mouse were seeded on Columbia blood agar (Becton Dickinson, Heidelberg, Germany) and pre-reduced Schaedler agar (BioMérieux, Nürtingen, Germany) plates, incubated at 37°C, read after 48 hours. CFU per lung were counted.

2.13 RNA extraction and reverse transcription (RT) qPCR

2.13.1 RNA extraction

Lungs from newborn WT and *Slc26a9*$^{-/-}$ mice were transferred to 500 µl Trizol reagent (Thermo Fisher Scientific, Darmstadt, Germany) and tissue was homogenized using a tissue homogenizer (IKA, Staufen, Germany). Samples were left at room temperature for 20 minutes to disrupt cell nucleus and subsequently, 100 µl of chloroform (Sigma-Aldrich, Steinheim, Germany) was added. Samples were vortexed for 15 seconds, left at room temperature for 3 minutes and immediately after centrifuged at 12.000 x *g* for 10 minutes at 4°C. The upper aqueous phase was transferred to a fresh autoclaved 2 ml tubes. Each sample was placed on ice and 250 µl isopropanol (Carl Roth, Karlsruhe, Germany) was added, vortexed thoroughly for 10 seconds and incubated 10 minutes at room temperature. Incubation was followed by

centrifugation at 16.000 x *g* for 10 minutes at 4°C and supernatant was discarded. Pellet was washed with 1 ml of ice-cold 75% ethanol (Carl Roth, Karlsruhe, Germany) and centrifuged 16.000 x *g* for 5 minutes at 4°C. Supernatant was discarded and pellets were air-dried for 30 to 60 minutes and finally, re-suspended in nuclease-free H_2O (Thermo Fisher Scientific, Darmstadt, Germany). RNA concentration and purity were measured by a spectrophotometer (DeNovix, Wilmington, Delaware, USA).

2.13.2 RT-qPCR

cDNA was obtained by performing RT of 2 µg of total RNA with Superscript III reverse transcriptase (Thermo Fisher Scientific, Darmstadt, Germany) according to manufacturer's instructions. Real-time quantitative PCR was performed on an Applied Biosystems 7500 Real Time PCR system with TaqMan Universal PCR master mix and inventoried TaqMan gene expression assays (Applied Biosystems, Darmstadt, Germany) for *Tmem16A (*Mm00724407_m1), *Cftr* (Mm00445197_m1), sodium channel, nonvoltage-gated 1 alpha *(Scnn1a)* (Mm00803386_m1), sodium channel, nonvoltage-gated 1 beta *(Scnn1b)* (Mm00441215_m1), sodium channel, nonvoltage-gated 1 gamma *(Scnn1g)* (Mm00441228_m1), *Muc5b* (Mm00466391_m1) and beta actin (*Actb*) (Mm00607939_s1) according to manufacturer's instructions (purchased all from Thermo Fisher Scientific, Darmstadt, Germany). Relative fold changes of target gene expression were calculated from the efficiency of the PCR reaction and the crossing point deviation between samples from the different genotypes in relation to WT controls and normalization to the expression of the housekeeping gene, *Actb* (25, 91).

2.14 Statistics

Data were derived from at least 3 independent experiments. The results were analyzed with SigmaPlot version 12.5 software (Systat Software, Erkrath, Germany) and reported it as mean ± standard error of the mean (SEM). Survival curve was analyzed using the Kaplan Meier Log-rank test. Chi-square test was used for distribution analysis. Two groups comparison was performed with Mann-Whitney Rank Sum and for multiple group analysis two-way ANOVA was applied. $P < 0.05$ was accepted to indicate statistical significance.

3 Results

3.1 Genetic deletion of *Slc26a9* causes high mortality rate in newborn mice

To elucidate the *in vivo* role of SLC26A9 Cl^- channel, the *Slc26a9*$^{-/-}$ mice and WT littermate controls were characterized. First, the effect of the genetic deletion of *Slc26a9* on survival was evaluated by monitoring the pups from birth up to the age of 6 weeks. All WT mice survived throughout the duration of this survival study (Figure 4). However, within the first hours of life 48% mortality was observed in *Slc26a9*$^{-/-}$ mice compared to WT mice (Figure 4). After surviving the early neonatal period, no further survival disadvantages were detected up to the age of 6 weeks in *Slc26a9*$^{-/-}$ mice (Figure 4).

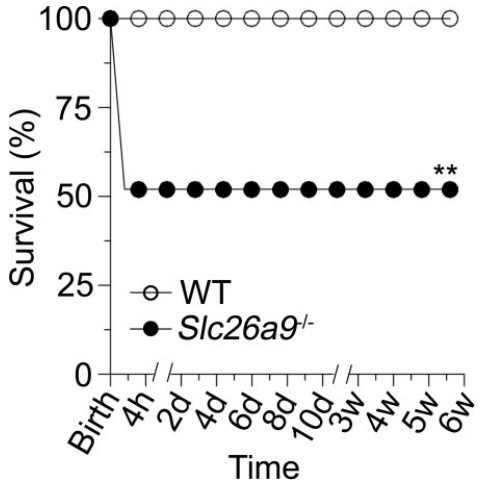

Figure 4. High and early mortality of newborn *Slc26a9*$^{-/-}$ mice. Survival curve of WT and *Slc26a9*$^{-/-}$ mice was performed by closely monitoring pups from birth up to week 6 of life. n = 107 - 244 mice per group. **P< 0.01 compared to WT mice.

3.2 Genetic deletion of *Slc26a9* causes spontaneous lung disease in newborn mice

In order to determine the cause of death of the newborn *Slc26a9*$^{-/-}$ mice, the phenotype of WT and *Slc26a9*$^{-/-}$ mice was investigated. If and how the genetic deletion of *Slc26a9* alters airway mucus content and morphology in newborn mice was evaluated by µCT and histology. To determine the impact of the genetic deletion of *Slc26a9* on fluid transport, lung liquid content as determine by wet/dry measurements was evaluated in newborn WT and *Slc26a9*$^{-/-}$ mice. Transepithelial ion transport and transcript levels of important ion channels were also

investigated. Furthermore, inflammatory cells and cytokines were evaluated in newborn WT and *Slc26a9*$^{-/-}$ mice.

3.2.1 Genetic deletion of *Slc26a9* produces early neonatal mortality due to deficient ventilation

The weight of newborn WT and *Slc26a9*$^{-/-}$ mice was evaluated as an indicator of their physical condition. Both, newborn WT and *Slc26a9*$^{-/-}$ mice showed similar body weight (Figure 5A). To determine if the newborn *Slc26a9*$^{-/-}$ mice showed external signs of disease, an observational study of their phenotype was conducted. The macroscopic inspection of pups shortly after birth revealed that newborn WT presented regular breathing and pink skin colour (Figure 5B and 5C). In contrast, newborn *Slc26a9*$^{-/-}$ displayed respiratory distress as evident from chest wall retraction and cyanotic appearance (Figure 5B and 5C). To further characterize the phenotype of newborn *Slc26a9*$^{-/-}$ mice, O_2 saturation levels were monitored. In comparison to newborn WT mice, newborn *Slc26a9*$^{-/-}$ mice exhibited significantly decreased O_2 saturation levels (Figure 5D).

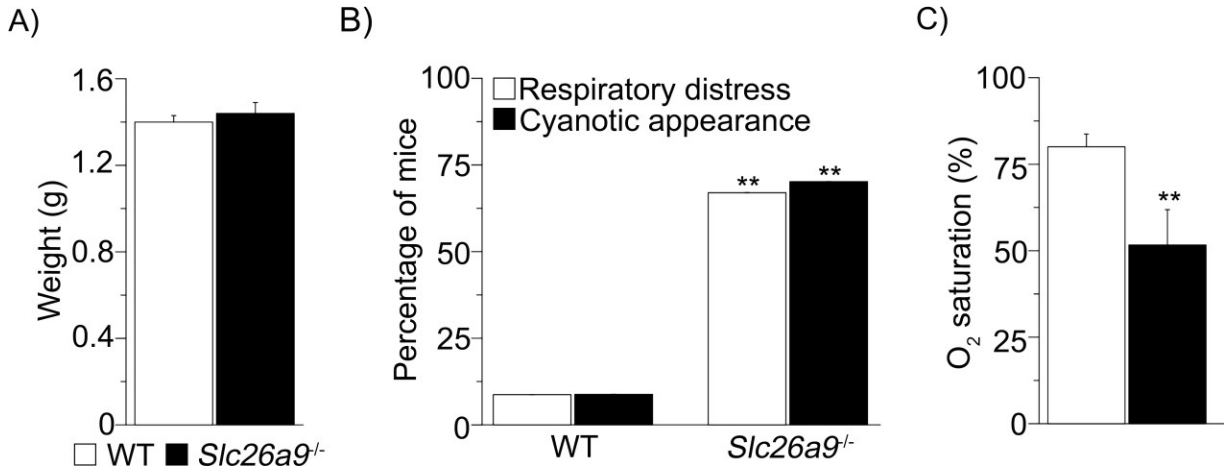

Figure 5. Respiratory distress and hypoxia in newborn *Slc26a9*$^{-/-}$ mice. All measurements were performed within the first hours of life. **(A)** Summary of body weights from WT and *Slc26a9*$^{-/-}$ mice. n= 14 – 24 mice per group. **(B)** Percentage of pups developing respiratory distress and/or cyanotic appearance. n= 136 – 244 mice per group. **(C)** Arterial oxygen saturation measurements of WT and *Slc26a9*$^{-/-}$ mice. n= 19 – 61 mice per group. ** $P < 0.01$ compared to WT.

Our breeding strategy also generated *Slc26a9*$^{+/-}$ mice, but none of the previously described observations were noted. Therefore, only WT and *Slc26a9*$^{-/-}$ mice were further investigated. Altogether, the data indicate that newborn *Slc26a9*$^{-/-}$ mice presented poor lung ventilation, which suggests that SLC26A9 is essential for normal air-breathing.

3.2.2 Genetic deletion of *Slc26a9* is associated with airway mucus obstruction in newborn mice

To investigate the cause of death of newborn *Slc26a9*$^{-/-}$ mice, we first studied airway and lung morphology by µCT. The experiments detected significantly elevated airway occlusion as determined by partial or complete opacification of the trachea and bronchi of the newborn *Slc26a9*$^{-/-}$ mice compared to WT mice (Figure 6A and 6B). Furthermore, the lung parenchyma of newborn WT mice displayed a homogenous lung texture and full aeration of the lung, while the newborn *Slc26a9*$^{-/-}$ lungs showed opacities in all lung lobules reflecting unventilated lung parenchyma i.e. atelectasis (Figure 6A).

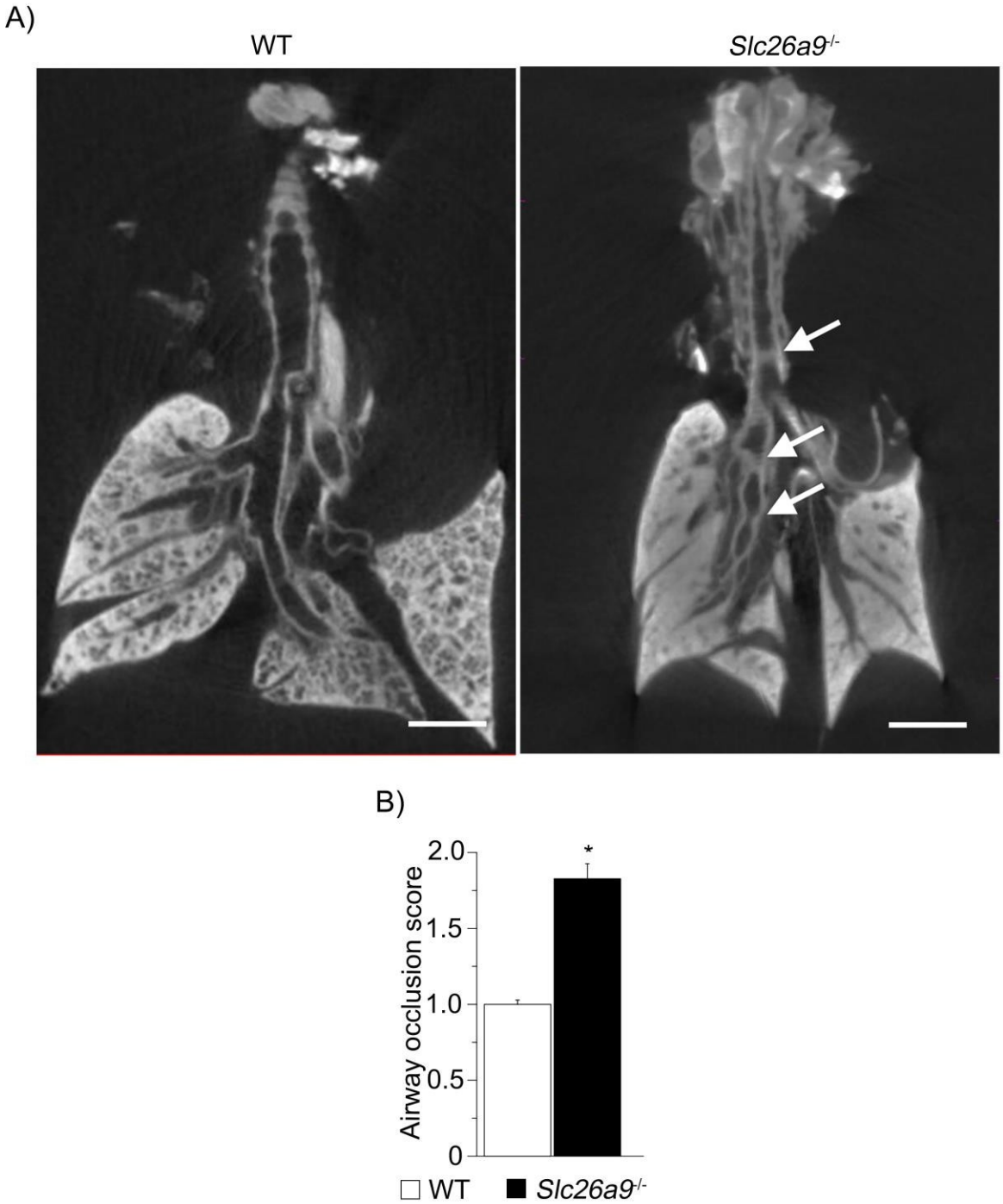

Figure 6. Airway occlusion in the tracheobronchial tree of newborn *Slc26a9*$^{-/-}$ mice. (A) Representative lung scans from newborn WT and *Slc26a9*$^{-/-}$ mice. Lung were perfused and fixed *in situ* to preserve luminal mucus. White arrows indicate airway occlusion. Scale: 1 mm. **(B)** Summary of airway occlusion score (0= none, 1= mild, and 2= severe airway occlusion). n= 5 – 7 mice per group. * P< 0.05 versus WT mice.

The obstruction of the tracheobronchial tree of the newborn *Slc26a9*$^{-/-}$ mice may indicate the presence of airway mucus plugging as has been shown in previous reports of βENaC-Tg mice

(92). Evaluation of AB-PAS stained-lung sections of newborn *Slc26a9*$^{-/-}$ mice confirmed severe airway mucus plugging in the lumen of the trachea, main axial airways and terminal bronchioles (Figure 7, 8 and 9) compared to newborn WT mice.

Whereas the trachea of WT mice showed low levels of AB-PAS positive signal (Figure 7A and 7B), the AB-PAS positive signal of newborn *Slc26a9*$^{-/-}$ mice is strongly located in the lumen, although some of the mucus seems to be still attached to the airway epithelium (Figure 7A and 7B). The number of goblet cells accounting for mucus producing cells did not differ in the epithelium of the newborn *Slc26a9*$^{-/-}$ mice versus newborn WT (Figure 7C).

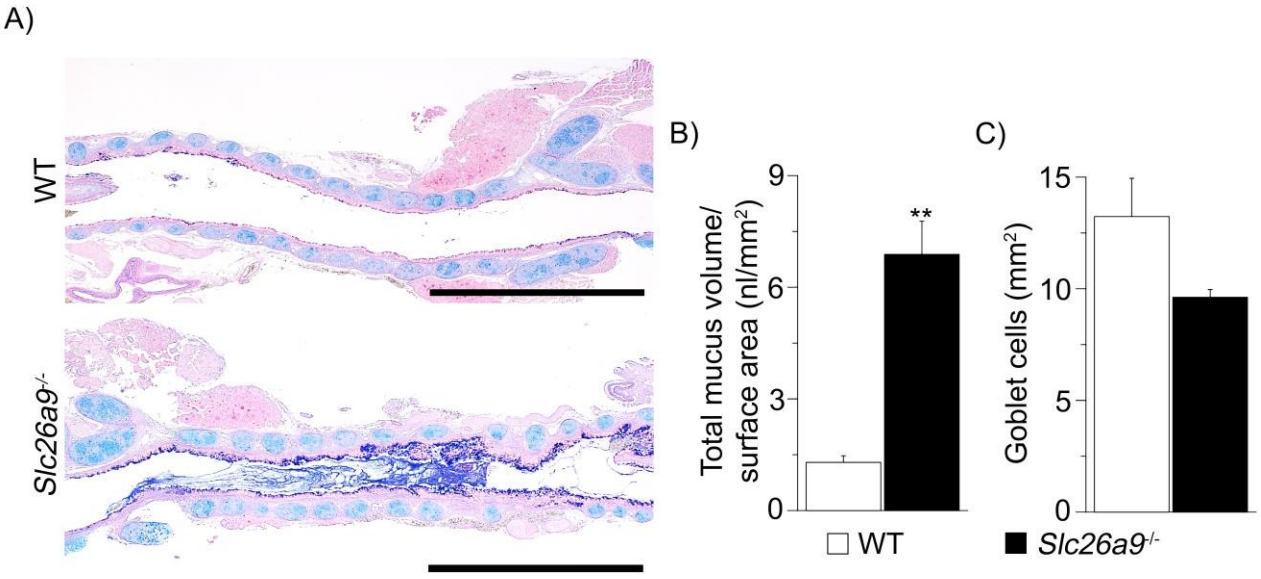

Figure 7. Severe mucus obstruction in the trachea of newborn *Slc26a9*$^{-/-}$ mice. (A) Representative images of AB-PAS stained-tracheas from newborn WT and *Slc26a9*$^{-/-}$ mice. Scale: 0.5 mm. **(B)** Quantification of total mucus content and **(C)** goblet cell counts in the trachea of newborn WT and *Slc26a9*$^{-/-}$ mice. n= 12 – 15 mice per group. ** P< 0.01 compared to WT mice.

Similarly to the observations in the trachea, main axial airways and terminal bronchioles of WT mice did not displayed detectable airway mucus obstruction by AB-PAS positive staining. Main axial airways (Figure 8A and 8B) and terminal bronchioles (Figure 9) of newborn *Slc26a9*$^{-/-}$ mice showed increased AB-PAS stained-material in the airway lumen compared to newborn WT mice. Further, the number of goblet cells did not change in the main axial airways of newborn *Slc26a9*$^{-/-}$ mice versus newborn WT mice (Figure 8C). Altogether, these results illustrate severe airway mucus obstruction in the newborn *Slc26a9*$^{-/-}$ mice.

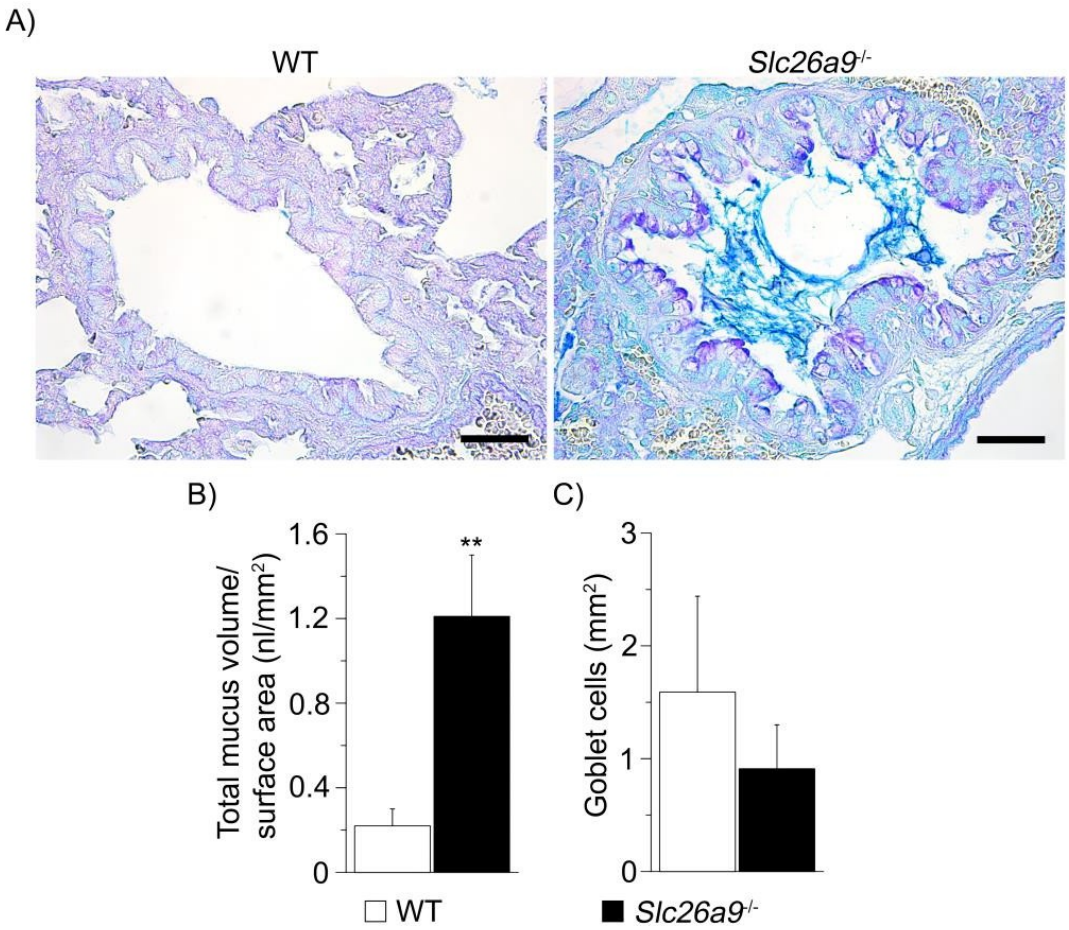

Figure 8. Severe mucus obstruction in the main axial airways of newborn *Slc26a9*$^{-/-}$ mice. **(A)** Representative images of AB-PAS stained-lungs from newborn WT and *Slc26a9*$^{-/-}$ mice. Scale: 20 µm. **(B)** Quantification of total mucus content and **(C)** goblet cell counts of newborn WT and *Slc26a9*$^{-/-}$ mice. n= 32 – 37 mice per group. ** P< 0.01 versus WT mice**.**

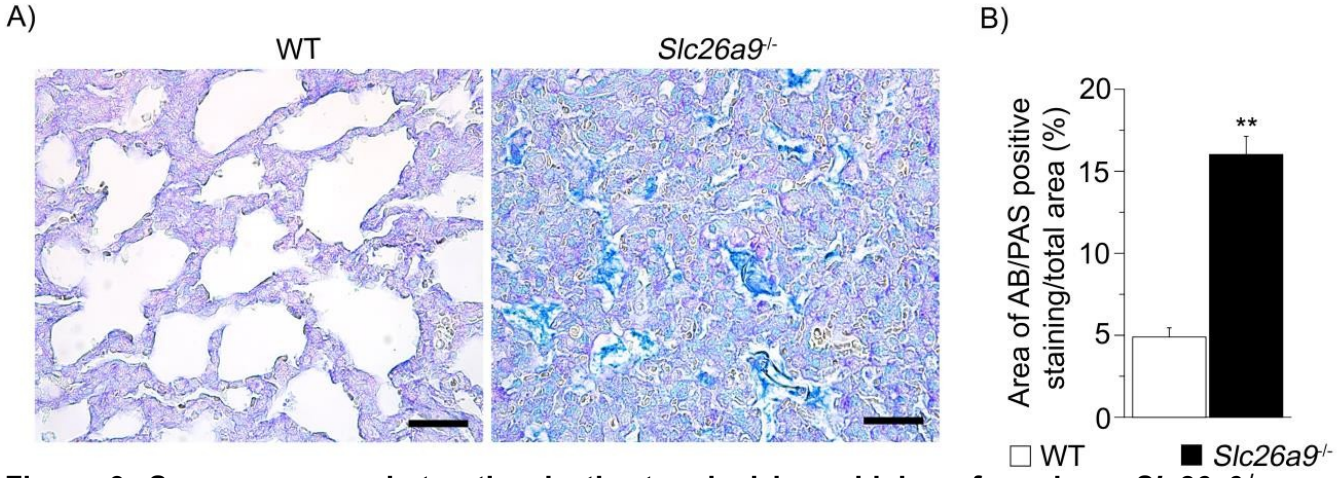

Figure 9. Severe mucus obstruction in the terminal bronchioles of newborn *Slc26a9*$^{-/-}$ mice. (A) Representative images of AB-PAS stained-lungs from newborn WT and *Slc26a9*$^{-/-}$ mice. Scale: 20 µm. **(B)** Quantification of total mucus content in the terminal bronchioles of newborn WT and *Slc26a9*$^{-/-}$ mice. n= 7 – 11 mice per group. ** P< 0.01 versus WT mice.

To test whether the airway mucus obstruction observed in the newborn *Slc26a9*$^{-/-}$ mice is accompanied by increased levels of mucin expression, real time RT-PCR and immunohistochemistry experiments were performed to determine *Muc5b*/MUC5B, one of the major macromolecular components of airway mucus. *Muc5b* mRNA expression was significantly elevated in lung homogenates from newborn *Slc26a9*$^{-/-}$ mice compared to WT mice (Figure 10A).

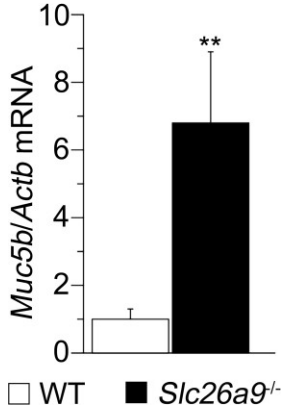

Figure 10. Elevated *Muc5b* transcript levels in newborn *Slc26a9*$^{-/-}$ mice compared to WT mice. Transcript levels of *Muc5b* whole lung homogenates of newborn WT and *Slc26a9*$^{-/-}$ mice. n=15 – 17 mice per group. *P< 0.05 and **P< 0.01 compared to WT mice.

Immunohistochemical experiments showed very low levels of MUC5B protein signal in the lung of newborn WT mice (Figures 11 and 12). In newborn *Slc26a9*$^{-/-}$ mice, MUC5B protein signal was strongly detected in the lumen of main axial airways and terminal bronchioles compared to WT mice (Figure 11). Furthermore, MUC5B signal correlates with AB-PAS positive staining in newborn *Slc26a9*$^{-/-}$ mice (Figure 8, 9 and 11). Negative controls of MUC5B did not exhibit any positive signal, confirming specific detection of MUC5B protein. Overall, the data demonstrate that lack of *Slc26a9* generates airway mucus obstruction throughout the whole respiratory tract and that MUC5B contributes to the early mucus plugging of the newborn *Slc26a9*$^{-/-}$ mice.

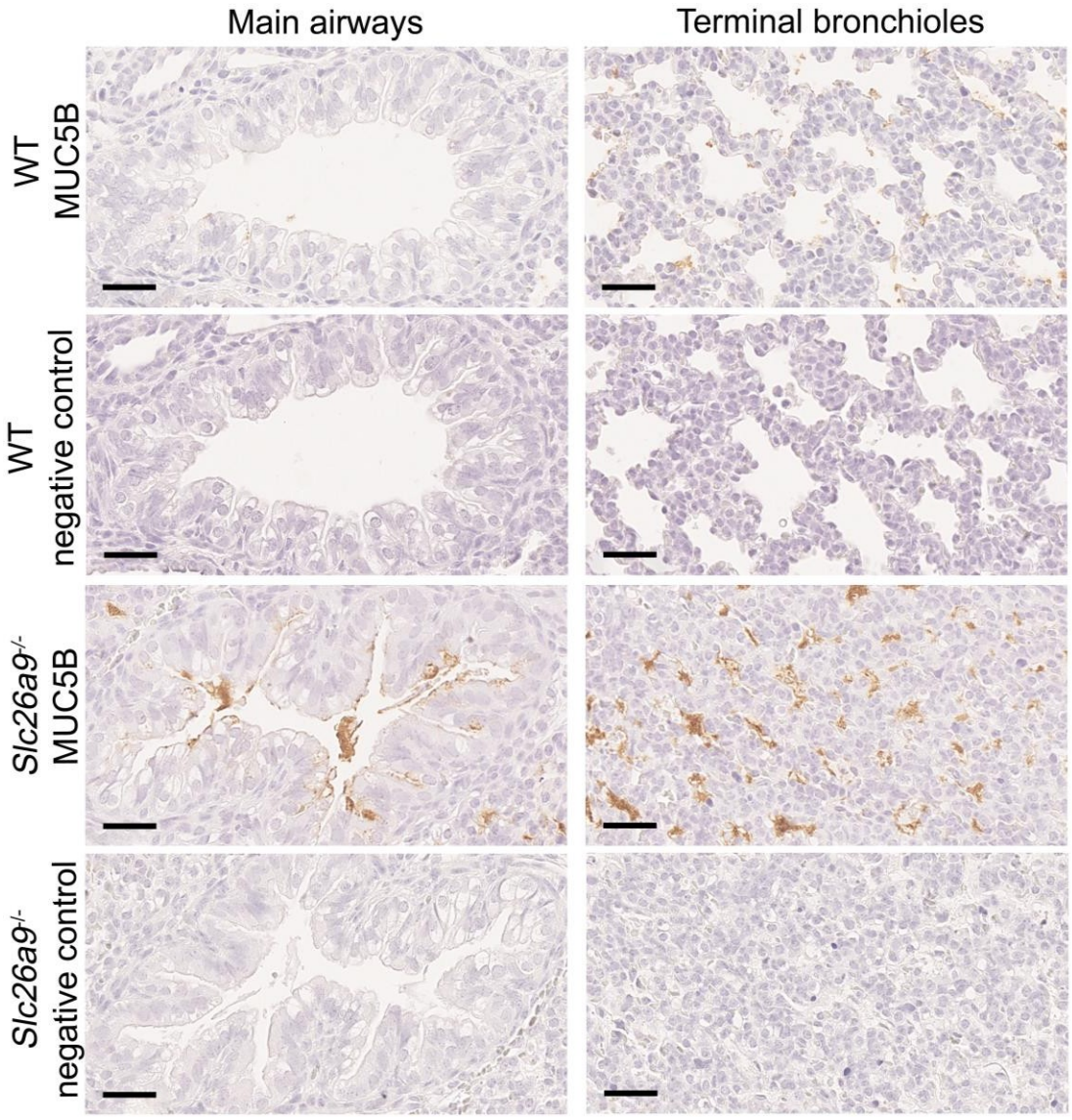

Figure 11. MUC5B protein expression is increased in mucus-obstructed airways of newborn *Slc26a9*$^{-/-}$ mice compared to WT mice. Representative images of MUC5B immunohistochemistry of main axial airways and terminal bronchioles from newborn WT and *Slc26a9*$^{-/-}$ mice. Negative controls that lack the primary antibody were included (second and fourth row). Scale: 20 µm. n= 3 – 5 mice per group.

3.2.3 Lack of *Slc26a9* changes ion transport in the airway epithelium of newborn mice

The dynamics of the airway ion transport change depending on the functional requirements of each developmental stage of the lung (93). In the newborn mice, the absorption of fetal lung liquid is particularly relevant to stablish efficient air-breathing adaptation (89, 93). To test if and how the absence of *Slc26a9* modifies fetal lung liquid content, wet/dry weight lung measurements were performed in newborn WT and *Slc26a9*$^{-/-}$ mice. No differences were detected when both genotypes were compared (Figure 12).

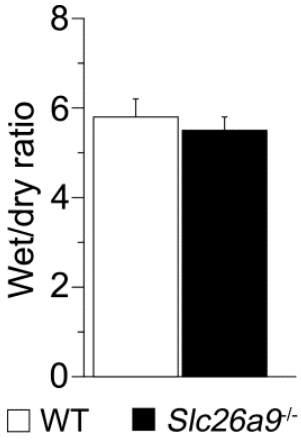

Figure 12. Genetic deletion of *Slc26a9* has no effect on lung liquid clearance in newborn mice. Wet to dry weight lung measurements of newborn WT and *Slc26a9*$^{-/-}$ mice. n= 7 – 22 mice per group.

The V_{te} was compared between WT and *Slc26a9*$^{-/-}$ cultured-tracheal explants from newborn mice. After the stabilization period with the recording electrode in Ringer solution, tracheal cysts were impaled. A successful impalement was determined as a strong and stable negative V_{te} as observed in Figure 13A. The results displayed significantly lower V_{te} in *Slc26a9*$^{-/-}$ versus WT cultured-tracheal explants under baseline conditions (Figure 13).

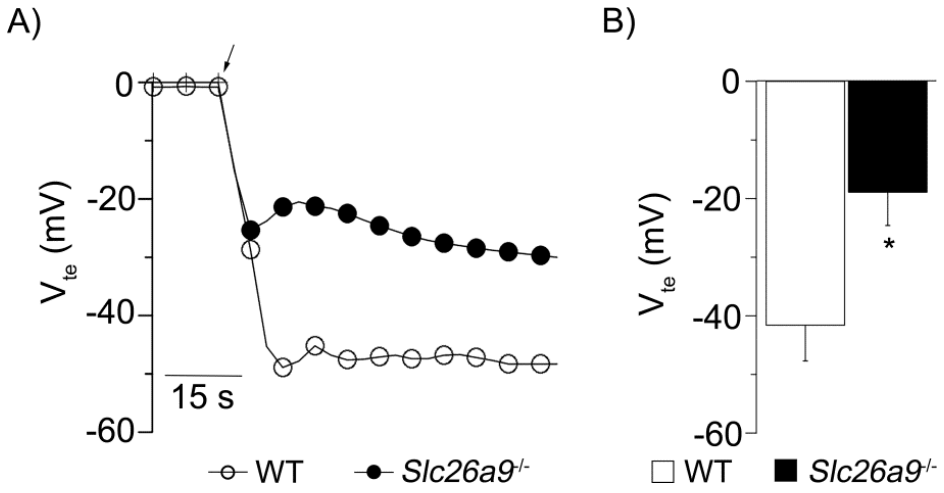

Figure 13. Changes in transepithelial ion transport in cultured-tracheal explants of newborn *Slc26a9*$^{-/-}$ mice compared to WT cultured-tracheal explants. (A) Representative recordings of V_{te} in cultured-tracheal explants from newborn WT and *Slc26a9*$^{-/-}$ mice. Arrow indicates the impalement of the explant. **(B)** Quantification of V_{te} for both genotypes. n= 5 – 8 mice per group. * P< 0.05 versus WT mice.

To investigate the mRNA levels of important players of the transepithelial ion transport such as the cAMP-activated Cl^- channel *Cftr*, Ca^{2+}-activated Cl^- channel *Tmem16a* and the subunits of the epithelial Na^+ channel ENaC (*Scnn1a*, *Scnn1b* and *Scnn1g*) in the airways, real time RT-PCR was performed in lung homogenates of newborn WT and *Slc26a9*$^{-/-}$ mice. Transcript levels of *Cftr* and *Tmem16a* did not differ between newborn WT and *Slc26a9*$^{-/-}$ mice (Figure 14A and 14B). mRNA levels of *Scnn1a* and *Scnn1g* subunits of ENaC were also unchanged when newborn WT and *Slc26a9*$^{-/-}$ mice were compared, whereas transcript levels of the *Scnn1b* subunit were 1.6-fold decreased in newborn *Slc26a9*$^{-/-}$ mice versus WT mice (Figure 14C-14E).

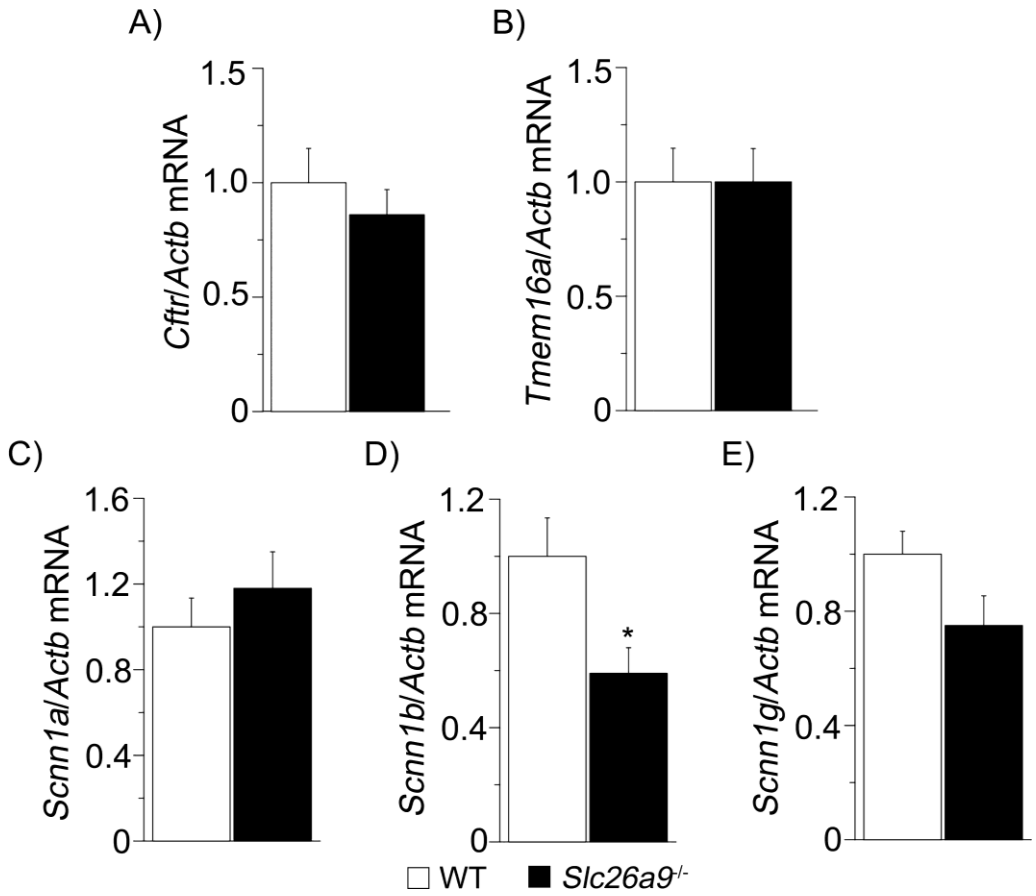

Figure 14. Transcript levels of *Cftr*, *Tmem16a* and subunits of *Scnn1* in lung homogenates of newborn WT and *Slc26a9*$^{-/-}$ mice. (A) Transcript levels of *Cftr*, **(B)** *Tmem16a*, **(C)** *Scnn1a*, **(D)** *Scnn1b* and **(E)** *Scnn1g* in lung homogenates of newborn WT and *Slc26a9*$^{-/-}$ mice. n= 16 – 19 mice per group. *P< 0.05 compared to WT mice.

Collectively, the data demonstrate that SLC26A9 is constitutively active under baseline conditions in the early neonatal airway epithelium and suggest that SLC26A9-mediated Cl^- secretion is pivotal for airway mucus clearance at birth.

3.2.4 Airway mucus obstruction of the newborn *Slc26a9*$^{-/-}$ mice is associated with hypoxic epithelial cell degeneration and inflammation in absence of detectable lung infection

To investigate if the muco-obstructive phenotype of newborn *Slc26a9*$^{-/-}$ mice leads to epithelial cell degeneration, resembling patients with CF and βENaC-Tg mice, the epithelial morphology of newborn WT and *Slc26a9*$^{-/-}$ mice was evaluated. An elevated number of degenerative epithelial cells were detected in the airway epithelium of newborn *Slc26a9*$^{-/-}$ mice compared to WT mice (Figure 15).

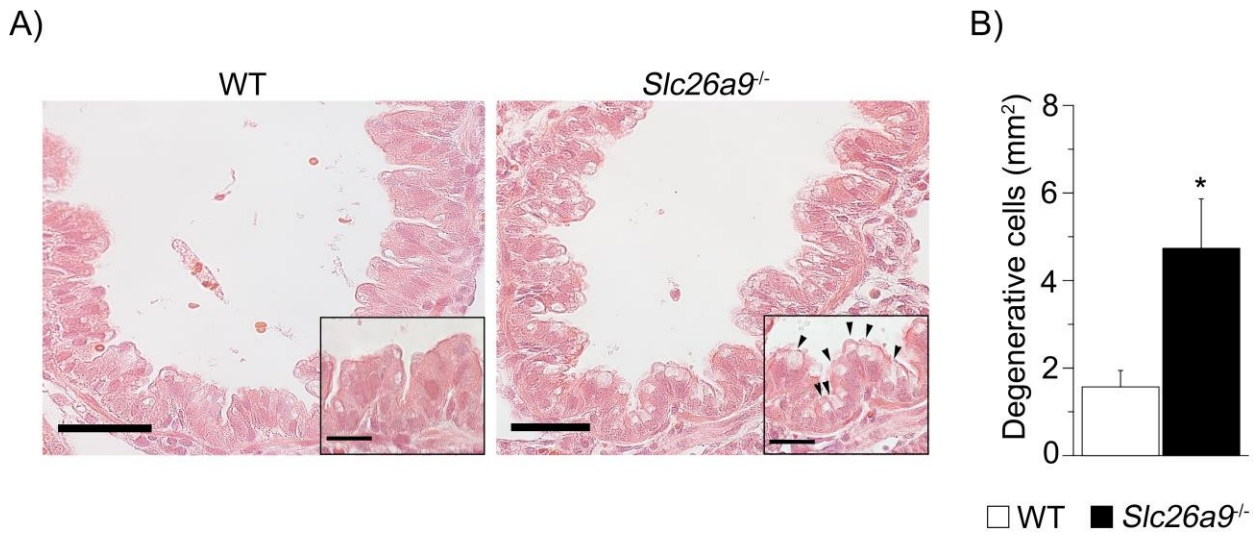

Figure 135. Increased epithelial cell degeneration in newborn *Slc26a9*$^{-/-}$ mice compared to WT mice. (A) Representative images of airway epithelium of newborn WT and *Slc26a9*$^{-/-}$ mice. The inserts represent a higher magnification of the same pictures. The black arrows depict degenerative epithelial cells. Scale: 20 µm and 10 µm. **(B)** Quantification of degenerative cells as determined from the number of degenerative epithelial cells per mm^2 of the basement membrane in newborn WT and *Slc26a9*$^{-/-}$ mice. 6 – 8 mice per group. *P<0.05 versus WT mice.

Hypoxic cells undergoing necrosis release inflammatory cytokines such as IL-1α, which triggers a transcriptional cascade that includes mucus hypersecretion and enhanced neutrophilic inflammation (22, 24). In order to compare the inflammatory phenotype between newborn WT and *Slc26a9*$^{-/-}$ mice, pro- and anti- inflammatory cytokines were studied in lung homogenates. Consistent with previous findings, the pro-inflammatory cytokine IL1α was elevated by 11-fold in lung homogenates of newborn *Slc26a9*$^{-/-}$ mice compared to newborn WT mice (Figure 16A). In addition, IL-1β and TNF-α were significantly increased in newborn *Slc26a9*$^{-/-}$ mice versus WT mice (Figure 16B and 16E). Furthermore, the levels of the neutrophil chemo-attractants, MIP-2 and KC were also augmented in newborn *Slc26a9*$^{-/-}$ mice compared to WT mice (Figure 16C and 16D). Conversely, levels of Th-2 cytokines IL-13 and IL-5 showed no differences when both genotypes were compared (Figure 16F and 16G).

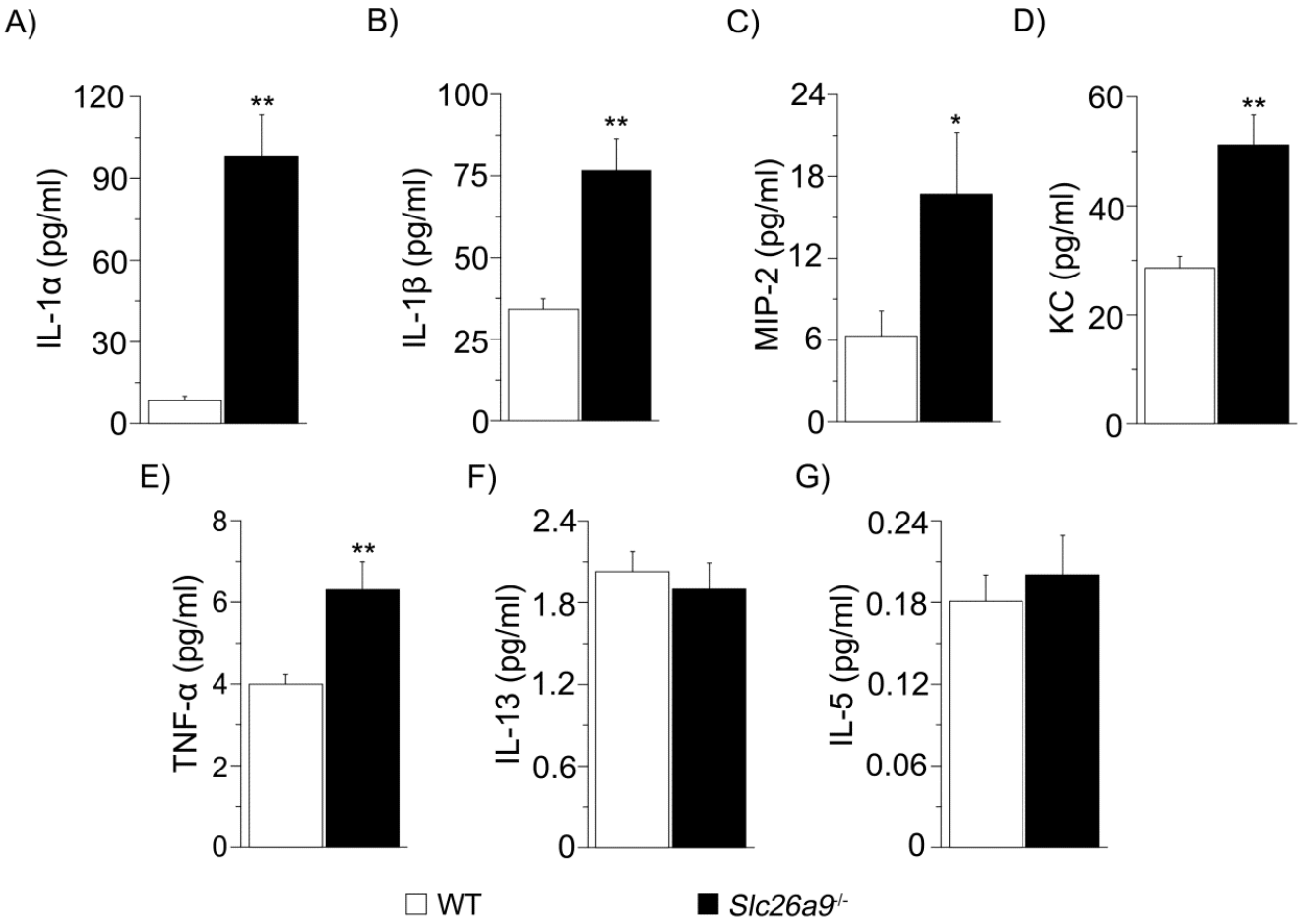

Figure 16. Increased levels of pro-inflammatory cytokines in newborn *Slc26a9*$^{-/-}$ mice compared to WT mice. Expression of **(A)** IL1-α, **(B)** IL-1β, neutrophil chemoattractants **(C)** MIP-2 and **(D)** KC, Th-1 cytokines **(E)** TNF-α, Th-2 cytokines **(F)** IL-13 and **(G)** IL-5 in lung homogenates of newborn WT and *Slc26a9*$^{-/-}$ mice. 5 – 8 mice per group. *P< 0.05 and **P< 0.01 compared to WT mice.

To further analyze the inflammatory phenotype of the newborn *Slc26a9*$^{-/-}$ mice, the contribution of inflammatory cells was investigated. In agreement with previous publications (22) and with the chemokines results (Figure 17), a higher percentage of neutrophils were displayed in newborn *Slc26a9*$^{-/-}$ mice compared to WT mice (Figure 17A). The percentage of monocytes, eosinophils and T cells remained unchanged when both genotypes were compared in newborn mice (Figure 17B-17D).

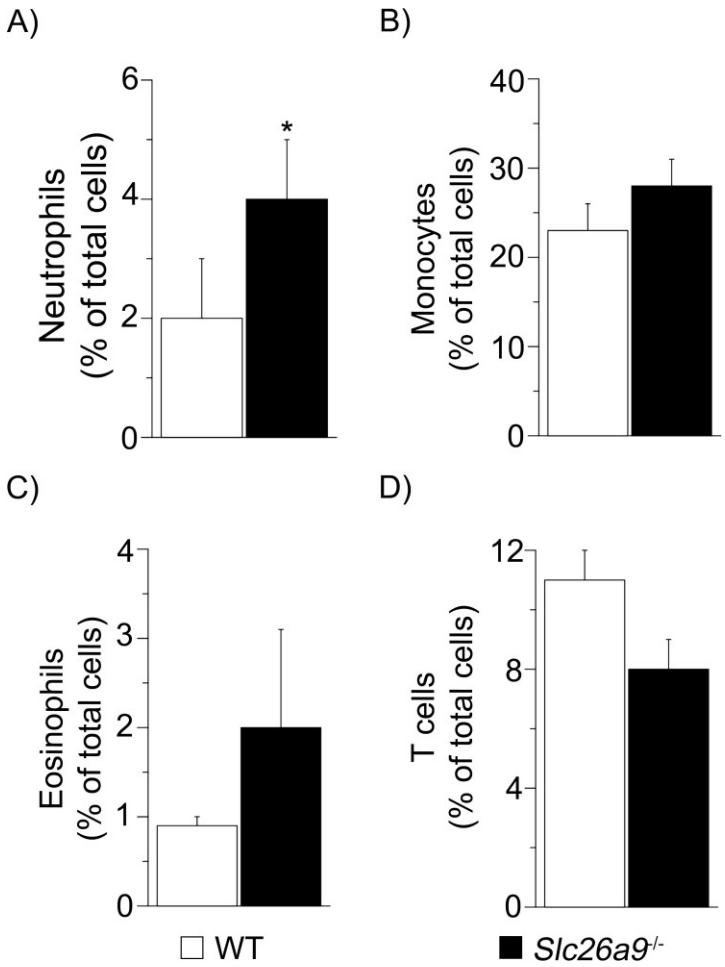

Figure 17. Neutrophilic airway inflammation in newborn *Slc26a9*$^{-/-}$ mice. Percentages of **(A)** neutrophils (CD45^{+}, Ly6G^{+} and CD11b^{+}), **(B)** monocytes (CD45^{+}, CD11c^{-}, MHCII^{+}), **(C)** eosinophils (CD45^{+}, SiglecF^{+}, CD64^{-}) and **(D)** T cells (CD45^{+}, CD3^{+}, FSC-A) were determined in lung homogenates of newborn WT and *Slc26a9*$^{-/-}$ mice. 6 – 11 mice per group. *P< 0.01 compared to WT mice.

Finally, to test whether the inflammatory phenotype observed in newborn *Slc26a9*$^{-/-}$ mice is associated with airway infection, lung homogenates were cultured on agar plates to assess for the growth of bacteria. No bacterial infection was detected by counting CFU in newborn WT or *Slc26a9*$^{-/-}$ mice (Figure 18).

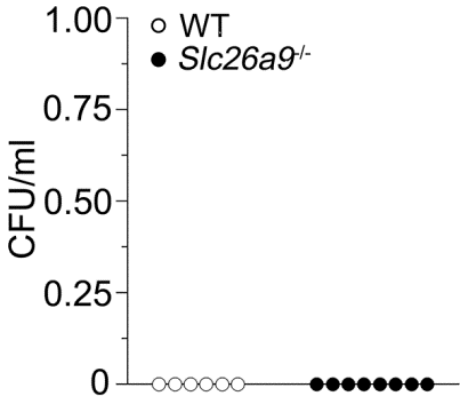

Figure18. Cultures of lung homogenates for detection of bacterial infection in newborn WT and *Slc26a9*$^{-/-}$ mice. CFU counts of lung homogenates after 48 hours of culture in newborn WT and *Slc26a9*$^{-/-}$ mice. 5 – 8 mice per group.

3.3 Developmental role of the SLC26A9 Cl^- channel in the lung

In the previous section a pivotal role of SLC26A9-mediated Cl^- secretion in newborn mice was demonstrated (See section 3.2.1), but if and how the absence of SLC26A9 affects the lung phenotype during postnatal development is not known. To investigate the postnatal development of the muco-obstructive and inflammatory phenotype observed at birth, longitudinal studies of WT and surviving *Slc26a9*$^{-/-}$ mice were performed. Experiments were performed at the juvenile stage, when postnatal alveologenesis (the final step of lung maturation) is taking place and in adult mice, when lung maturity has been reached (94-96). The bioelectrical properties of WT and surviving *Slc26a9*$^{-/-}$ tracheas were evaluated by performing Ussing chamber experiments in 5-day-old mice. Furthermore, juvenile and adult mice (2- and 6-week-old) were analyzed for mucus obstruction and structural lung damage by histology and the relative distribution of inflammatory cell was determined from BAL samples.

3.3.1 SLC26A9-mediated Cl^- secretion is not essential for transepithelial ion transport at postnatal day 5

Functional studies were performed in native tracheal tissue to evaluate the bioelectrical properties of 5 day-old WT and surviving *Slc26a9*$^{-/-}$ mice. Basal bioelectrical properties (V_{te} and R_{te}), amiloride-sensitive I_{sc}, cAMP-induced I_{sc}, UTP-induced I_{sc}, CFTRinh172-sensitive I_{sc}, GlyH101-sensitive I_{sc} and bumetanide-sensitive I_{sc} were compared between WT and surviving *Slc26a9*$^{-/-}$ mice in freshly excised tracheal tissue. These experiments demonstrated that basal V_{te} and R_{te} were no different in WT versus surviving *Slc26a9*$^{-/-}$ mice (Figure 19A, 19B and 19C). The amiloride-sensitive I_{sc} was normal when WT and surviving *Slc26a9*$^{-/-}$ mice were compared (Figure 19A and 19D). Elevation of intracellular cAMP and Ca^{2+} levels by addition of IBMX/forskolin and UTP, respectively, did not alter cAMP-induced I_{sc} and UTP-induced I_{sc} in the trachea of WT and surviving *Slc26a9*$^{-/-}$ mice (Figure 19A, 19E and 19F). WT and surviving *Slc26a9*$^{-/-}$ mice did not differ on CFTRinh172-sensitive I_{sc} and GlyH101-sensitive I_{sc} accounting for CFTR and SLC26A9-mediated Cl^- secretion, respectively (Figure 19A, 19G and 19H). Finally, bumetanide-sensitive I_{sc}, which reflects the inhibition of the basolateral NKCC1 co-transporter and thus, blocking the favorable driving force for the movement of Cl^- towards the apical surface, remain unchanged in surviving *Slc26a9*$^{-/-}$ versus WT mice (Figure 19A and 19I). Taking together, SLC26A9-mediated Cl^- secretion is not essential for lung health at the postnatal day 5.

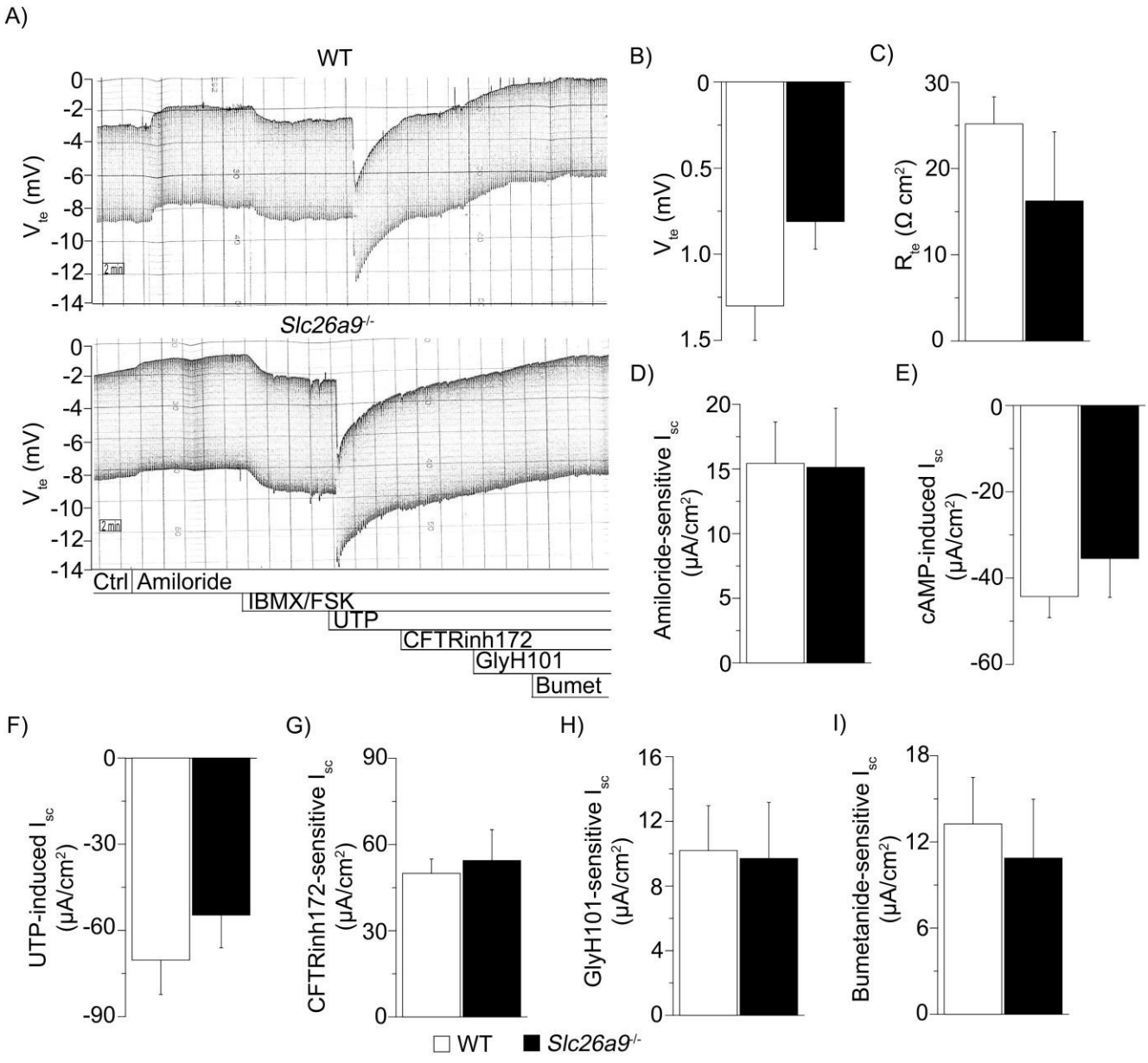

Figure 19. Unchanged epithelial ion transport in the trachea of 5-day-old surviving *Slc26a9*$^{-/-}$ mice compared to WT mice. (A) Representative Ussing chamber recordings of freshly excised tracheal tissue at postnatal day 5 of WT and surviving *Slc26a9*$^{-/-}$. Crtl: control or equilibration period, Fsk: forskoline and Bumet: bumetanide. Quantification of **(B)** basal V_{te}, **(C)** basal R_{te}, **(D)** amiloride-sensitive I_{sc}, **(E)** cAMP-induced I_{sc}, **(F)** UTP-induced I_{sc}, **(G)** CFTRinh172-sensitive I_{sc}, **(H)** GlyH101-sensitive I_{sc} and **(I)** bumetanide-sensitive I_{sc} in freshly excised trachea from WT and surviving *Slc26a9*$^{-/-}$ mice. n= 8 – 17 mice per group.

3.3.2 Effects of genetic deletion of *Slc26a9* on mucus airway obstruction in juvenile and adult mice

In order to determine how the absence of *Slc26a9* affects lung development over the time and whether the surviving *Slc26a9*$^{-/-}$ mice exhibit a muco-obstructive phenotype similar to newborn mice (See section 3.2), longitudinal morphometric studies were performed at the juvenile and adult ages (2 and 6 weeks of age). Juvenile WT mice did not display detectable AB-PAS positive signal (Figure 20A, first column). However, AB-PAS lung stained-sections of surviving *Slc26a9*$^{-/-}$ mice showed high levels of variation within the group at the juvenile and adult stage: ~30% of surviving *Slc26a9*$^{-/-}$ mice displayed slight airway mucus obstruction and goblet cells (Figure 20A, second column), while the remaining 70% did not exhibit detectable AB-PAS positive material or goblet cells (Figure 20A, third column). Consistently, the quantification of AB-PAS lung stained-sections showed a trend towards increase in surviving juvenile and adult *Slc26a9*$^{-/-}$ mice compared to WT mice (Figure 20B). The number of goblet cells did not differ between genotypes within the same age group, but at the juvenile stage an upward tendency is observed (Figure 20C). Interestingly, goblet cell counts of surviving adult *Slc26a9*$^{-/-}$ mice are diminished compared to the same genotype at the juvenile stage (Figure 20C).

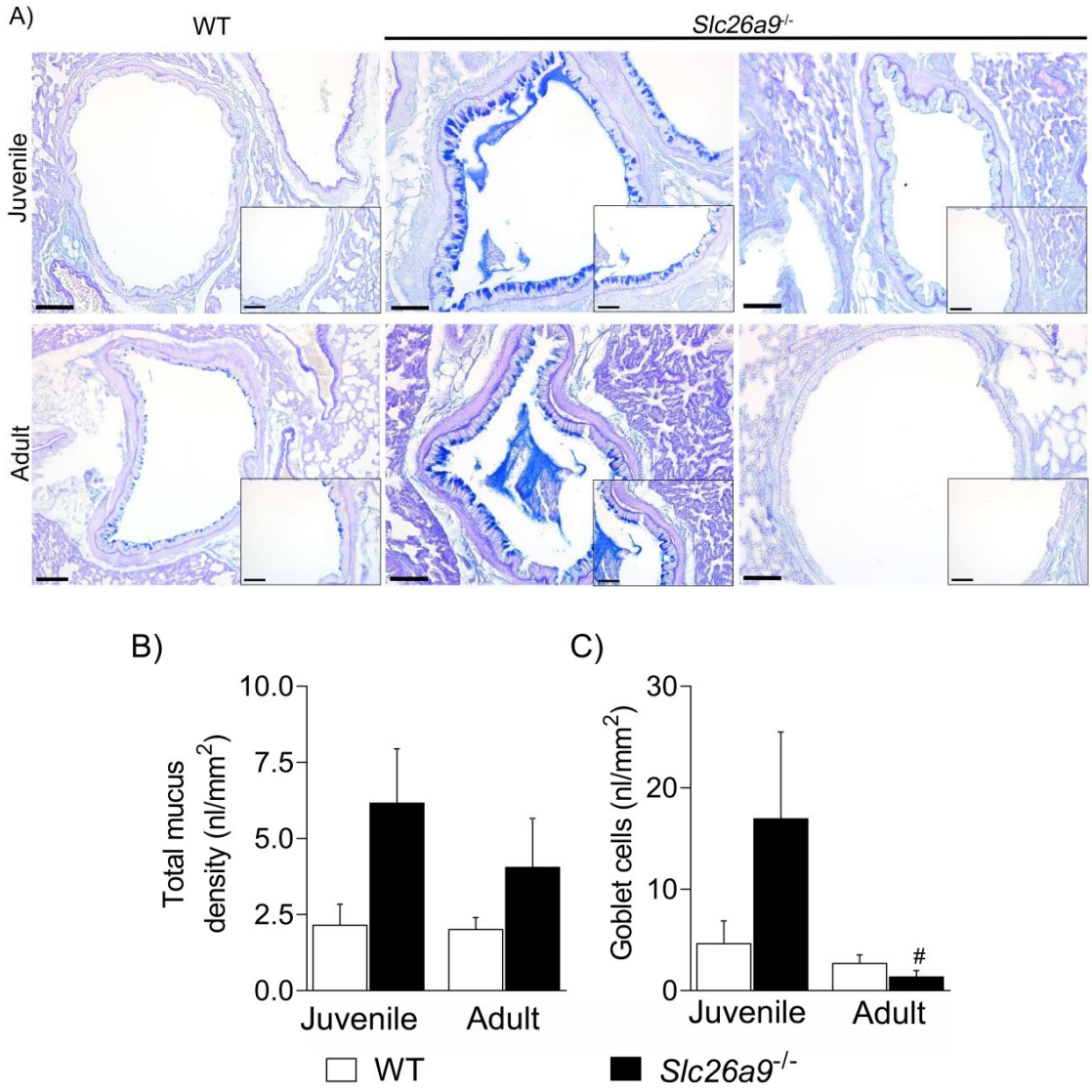

Figure 20. Airway mucus content in surviving juvenile and adult *Slc26a9*$^{-/-}$ mice. (A) Representative AB-PAS images of juvenile (2-week-old) and adult (6-week-old) WT and *Slc26a9*$^{-/-}$ mice. Inserts depict a higher magnification of the airway epithelium. Scale: 60 µm and 20 µm. n= 5 – 10 mice per group. **(B)** Quantification of total mucus content and **(C)** goblet cell counts of juvenile (2-week-old) and adult (6-week-old) WT and *Slc26a9*$^{-/-}$ mice. n= 5 – 10 mice per group. # P< 0.01 compared to the same genotype at the juvenile stage.

3.3.3 Effects of genetic deletion of *Slc26a9* on airway morphology and lung structure in juvenile and adult mice

Because severe lung damage occurs early and persist throughout life of patients with CF and in the mouse model of CF-like lung disease, βENaC-Tg mice (86, 102), quantitative longitudinal studies of structural lung damage were performed as parameters of alveolar diameter in the lung of juvenile and adult WT and surviving *Slc26a9*$^{-/-}$ mice. Histological sections showed that alveolar size and architecture were unchanged in surviving *Slc26a9*$^{-/-}$ mice versus WT mice at both time points analyzed (Figure 21A and 21B). Morphometric quantification of distal airspace enlargement by measuring the MLI indicated similar distances of alveolar walls in juvenile and adult WT and surviving *Slc26a9*$^{-/-}$ mice (Figure 21A and 21B). Similarly, lung volumes did not differ between WT and surviving *Slc26a9*$^{-/-}$ at any of the time points analyzed (Figure 21C). Altogether, the data demonstrate that lack of *Slc26a9* does not cause spontaneous structural lung damage under physiological conditions at the juvenile and adult stage of life.

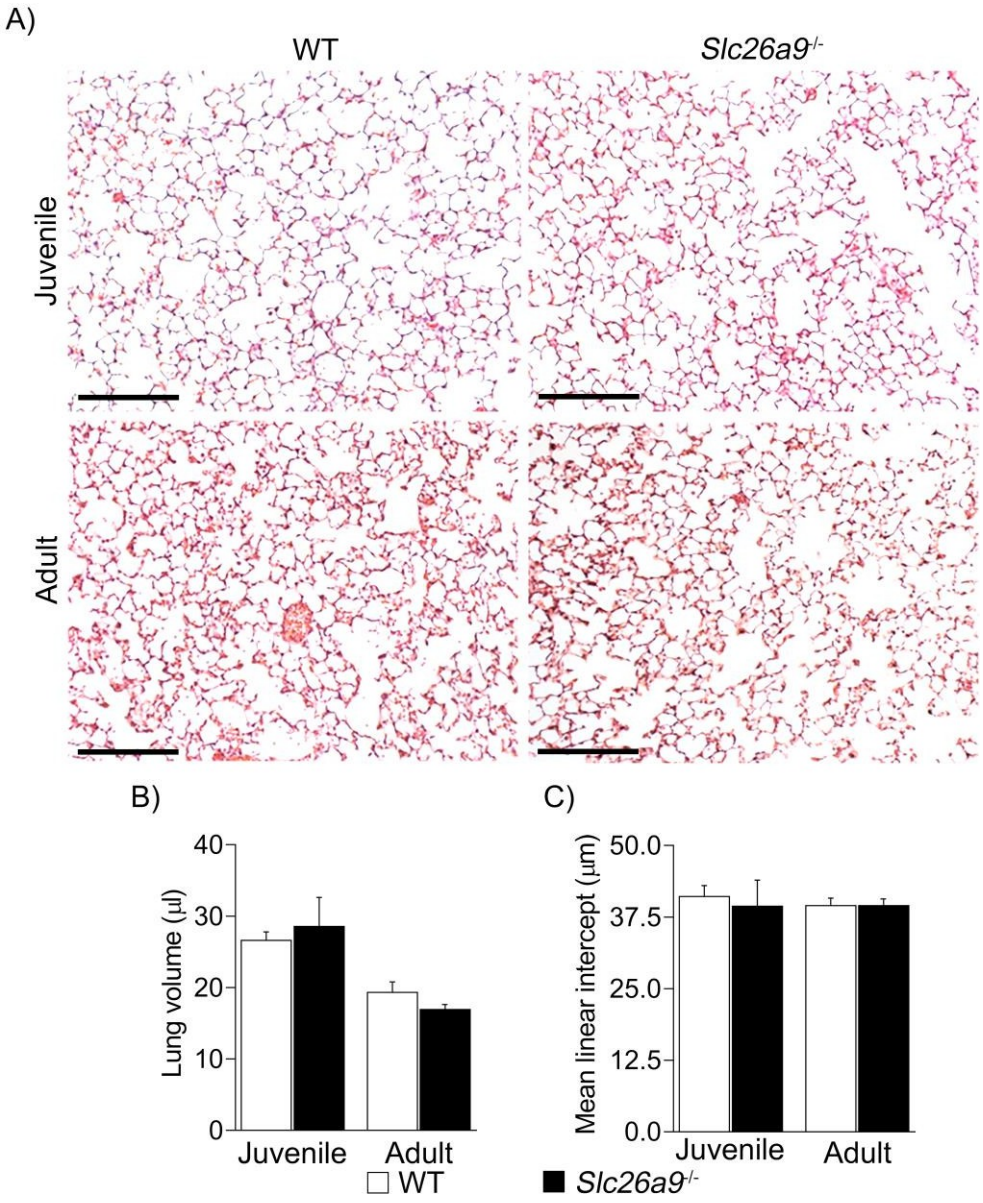

Figure 21. Absence of structural lung damage in surviving juvenile and adult *Slc26a9*$^{-/-}$ mice. (A) Representative lung morphology pictures of juvenile (2-week-old) and adult (6-week-old) WT and surviving *Slc26a9*$^{-/-}$ mice. Scale: 100 µm. **(B)** MLI and **(C)** lung volume in juvenile (2-week-old) and adult (6-week-old) WT and surviving *Slc26a9*$^{-/-}$ mice. n= 3 – 24 mice per group.

3.3.4 Resolution of inflammation in surviving juvenile and adult *Slc26a9*$^{-/-}$ mice

To assess whether the surviving *Slc26a9*$^{-/-}$ mice exhibit an inflammatory phenotype (as observed in the newborn mice; see section 3.1.4), the number of degenerative cells in the airway epithelium and differential counts of inflammatory cells were analyzed in juvenile and adult WT and surviving *Slc26a9*$^{-/-}$ mice. The quantification of airway epithelial cell degeneration showed

similar abundance between juvenile and adult WT and surviving *Slc26a9*$^{-/-}$ mice at both time points analyzed (Figure 22).

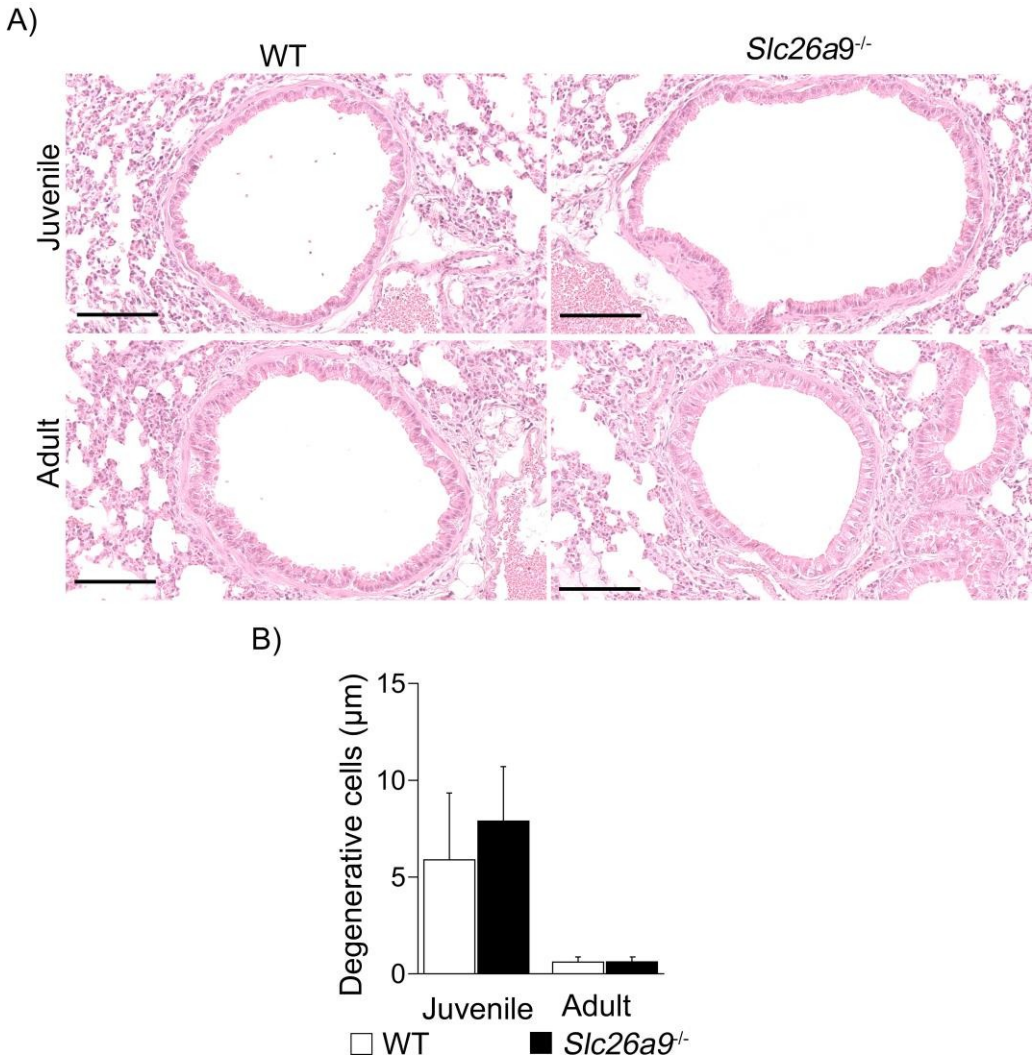

Figure 22. Unchanged number of degenerative cells in surviving juvenile and adult *Slc26a9*$^{-/-}$ mice compared to WT mice. (A) Representative airway morphology pictures of juvenile (2-week-old) and adult (6-week-old) WT and surviving *Slc26a9*$^{-/-}$ mice. Scale: 100 µm. (B) Quantification of necrotic cells count of juvenile (2-week-old) and adult (6-week-old) WT and surviving *Slc26a9*$^{-/-}$ mice. n= 5 – 10 mice per group.

To evaluate the role of *Slc26a9* on airway inflammation in a longitudinal manner, BAL from WT and surviving *Slc26a9*$^{-/-}$ mice were analyzed and the absolute and relative counts of inflammatory cell types were determined. Total cells, macrophages and neutrophils were significantly increased at the juvenile and adult stage in the lungs of surviving *Slc26a9*$^{-/-}$ mice compared to WT mice (Figure 23A, 23B and 23C). Interestingly, the number of neutrophils of

surviving adult *Slc26a9*$^{-/-}$ mice was significantly reduced compared to the same genotype at the juvenile stage (Figure 23C). Lymphocytes and eosinophils did not differ at the tested time points between WT and surviving *Slc26a9*$^{-/-}$ mice (Figure 23D and 23E).

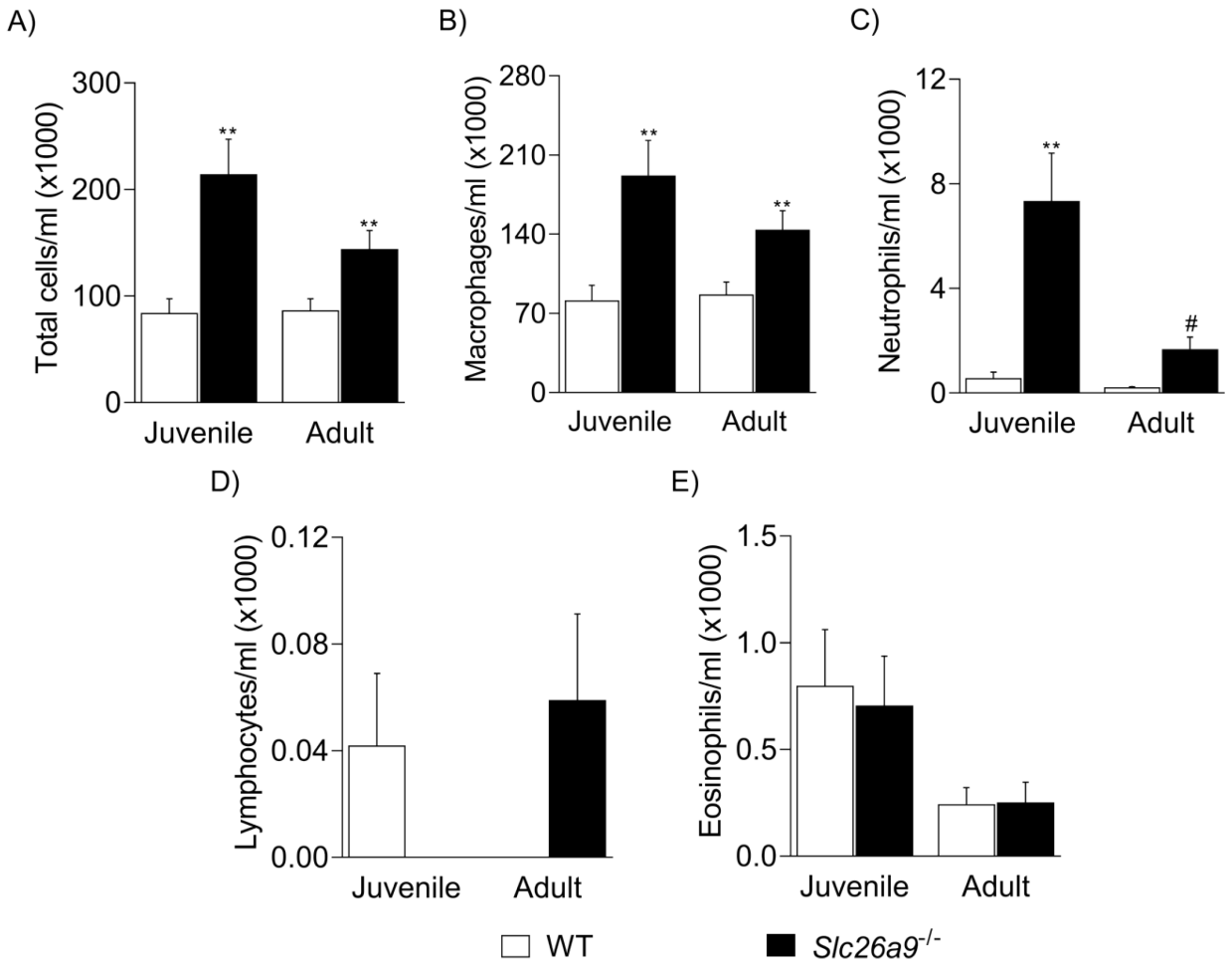

Figure 23. Airway inflammation detected in BAL of surviving juvenile and adult *Slc26a9*$^{-/-}$ mice. BAL cell counts from juvenile (2-week-old) and adult (6-week-old) WT and surviving *Slc26a9*$^{-/-}$ mice: **(A)** total cells, **(B)** macrophages, **(C)** neutrophils, **(D)** lymphocytes and **(E)** eosinophils. n= 8 – 22 mice per group. **P<0.01 compared to WT mice at the same age and # P< 0.01 compared to the same genotype at juvenile stage.

3.4 Genetic deletion of *Slc26a9* decreases survival of βENaC-Tg mice with CF-like lung disease

To assess the role of SLC26A9 as a modifier of mortality in the context of muco-obstructive lung disease *in vivo*, *Slc26a9*$^{+/-}$ mice were intercrossed with βENaC-Tg mice. The survival of WT, *Slc26a9*$^{+/-}$, *Slc26a9*$^{-/-}$, βENaC-Tg, βENaC-Tg/*Slc26a9*$^{+/-}$ and βENaC-Tg/*Slc26a9*$^{-/-}$ mice were

monitored from birth up to the age of 6 weeks. At birth, all genotypes were represented according to the Mendelian ratios (Figure 24A), suggesting that all mice survive the intrauterine period. All WT animals survive from birth up to the age of 6 week-old (Figure 24B). Consistently with previous findings (see section 3.1) newborn *Slc26a9*$^{-/-}$ presented an increased mortality ~ 50% soon after birth compared to WT mice (Figure 24B). *Slc26a9*$^{+/-}$ mice did not differ from WT mice (Figure 24B). ~25% of βENaC-Tg mice die in the first two weeks of life (Figure 24B), which is known from previous publications (25, 77) and a similar trend is observed for the βENaC-Tg/*Slc26a9*$^{+/-}$ (Figure 24B). The overall mortality observed in the βENaC-Tg/*Slc26a9*$^{-/-}$ mice group was of ~80% and significantly lower compared to all other genotypes (Figure 24B). In the βENaC-Tg/*Slc26a9*$^{-/-}$ mice, mortality began in the early neonatal period and persist until the second week of life (Figure 24B).

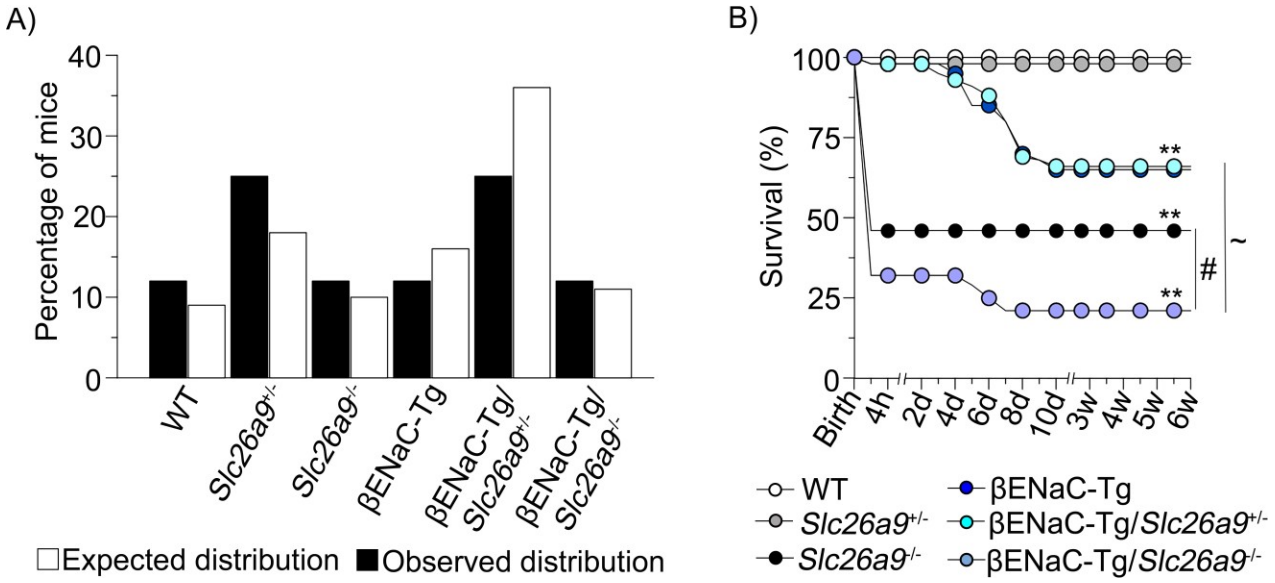

Figure 24. Increased neonatal mortality was detected in βENaC-Tg/*Slc26a9*$^{-/-}$ mice. (A) Mendelian distribution after birth and **(B)** survival curve of WT, *Slc26a9*$^{+/-}$, *Slc26a9*$^{-/-}$, βENaC-Tg, βENaC-Tg/*Slc26a9*$^{+/-}$ and βENaC-Tg/*Slc26a9*$^{-/-}$ mice. The survival curve was performed by following newborn mice from birth up to the age of 6 weeks. n = 21 – 88 mice per group. ** P< 0.01 compared to WT mice, ~ P< 0.01 compared to βENaC-Tg and βENaC-Tg/*Slc26a9*$^{+/-}$ mice and # P< 0.05 compared to *Slc26a9*$^{-/-}$ mice.

4 Discussion

The epithelial Cl^- channel SLC26A9 is one of the most promising modifiers and therapeutic candidates to compensate the impaired CFTR-mediated Cl^- secretion in patients with CF (34, 46, 48, 58, 59, 63). However, the relevance of the epithelial Cl^- channel SLC26A9 under physiological conditions is not fully understood. Here, the *Slc26a9*$^{-/-}$ mouse was characterized at different developmental stages (newborn, juvenile and adult) to investigate how SLC26A9 contributes to lung health. Moreover, it was determined how the genetic deletion of *Slc26a9* modifies mortality in the context of CF-like lung disease by evaluating survival of the βENaC-Tg/*Slc26a9*$^{-/-}$ mice.

4.1 Role of the epithelial Cl^- channel SLC26A9 in the early neonatal lung

4.1.1 SLC26A9-mediated Cl^- secretion is constitutively active in the airways after birth

In order to ensure an efficient transition from the uterine life to the air-breathing environment, the lung epithelium of the neonatal lung undergoes critical changes of the fluid transport phenotype from a secretory to an absorptive epithelium, which reflect the functional requirements at different developmental stages (93, 97). It is well known that reabsorption of fetal lung liquid is driven by ENaC, being the α subunit a critical component (89), but the complex regulation of the ion transport at birth is not fully understood. Hence, the role of SLC26A9 Cl^- channel during early neonatal adaptation was assessed. The impact of the genetic deletion of *Slc26a9* on vital functions of the newborn lung such as lung liquid content (wet/dry measurements) was evaluated. Cultured-tracheal explants from newborn mice and freshly excised tracheas from 5-day-old mice were studied to determine the contribution of SLC26A9 Cl^- channel to the transepithelial ion transport. The expression of other important ion channels (*Cftr*, *Tmem16a*, *Scnn1a, Scnn1b* and *Scnn1g*) was also investigated.

Defective fetal lung liquid absorption results in respiratory distress and early death in the alpha-ENaC-deficient (*αENaC*$^{-/-}$) mice soon after birth. Furthermore, a characteristic waterlogged appearance of the lung has been observed when fetal lung liquid absorption fails (89). The absence of the distinctive waterlogged appearance and changes in fetal lung fluid content in newborn *Slc26a9*$^{-/-}$ lungs as determined by wet/dry measurements (Figure 12), suggests that the genetic deletion of *Slc26a9* does not alter the re-absorption of fetal lung liquid.

Previous studies in heterologous systems have shown that SLC26A9 is constitutively active when inserted in the plasma membrane (46, 48, 63). In this line, the lower transepithelial

potential difference detected in cultured-tracheal explants from newborn *Slc26a9*$^{-/-}$ mice compared to cultured-tracheal explants from WT mice (Figure 13) suggests that SLC26A9 is constitutively active in the airway epithelium under physiological conditions during the early neonatal period. This study shows, for the first time, the *in vivo* contribution of SLC26A9 Cl^- channel to the transepithelial ion transport of the airway epithelium under baseline conditions (Figure 13) and suggest that SLC26A9-mediated Cl^- secretion is essential to adapt to postnatal air-breathing conditions.

In the airway epithelium, fluid secretion and absorption is tightly regulated by coordinate movement of ions to maintain ASL height and consequently, proper MCC (98). The complex interplay of epithelial ion channels may include mutual influence on plasma membrane trafficking (47) or transcription. Here, the transcript levels of the main contributors to fluid homeostasis (*Cftr*, *Tmem16a*, *Scnn1a, Scnn1b* and *Scnn1g*) in the airway epithelium of newborn mice were studied (99) to determine if the genetic deletion of *Slc26a9* modifies their expression. The results revealed normal levels of *Cftr* and *Tmem16a* in the lung of newborn *Slc26a9*$^{-/-}$ mice compared to newborn WT mice (Figure 14), suggesting that neither of them is up-regulated to compensate the absence of *Slc26a9*, even under conditions of a pro-inflammatory phenotype (100). Further, the lack of mutual compensation of TMEM16A and CFTR has been observed in βENaC-Tg mice (45). The mRNA levels of the βENaC subunit in the lung of *Slc26a9*$^{-/-}$ mice (Figure 14) were significantly lower compared to WT mice. Decreased expression of ENaC subunits have been associated with a switch to a pro-secretory mechanism in presence of inflammatory cytokines such as TNF-α and IL-1β (Figure 16B and 16E) (100, 102–104). This may suggest that reduced levels of the β subunit act as a compensatory mechanism in the lungs of newborn *Slc26a9*$^{-/-}$ mice in order to counterbalance the airway surface dehydration due to the absence of the SLC26A9- mediated Cl^- secretion.

Interestingly, Ussing chamber experiments of the trachea at postnatal day 5 did not detect differences between WT and surviving *Slc26a9*$^{-/-}$ mice either in transepithelial potential difference or short-circuit current (Figure 19). This last observation is supported by bioelectrical experiments performed in native tracheal and bronchial tissue from adult *Slc26a9*$^{-/-}$ mice (8 – 20 weeks of life), where no contribution of SLC26A9 to airway Cl^- secretion was reported in the airway epithelium under physiological conditions (57). Altogether, the electrophysiological studies (Figure 13 and 19) presented here, in combination with previous bioelectrical experiments on murine tissue suggest an age-dependent regulation of SLC26A9 activity with a crucial role at the early postnatal adaptation of pulmonary tissue.

4.1.2 Lack of SLC26A9-mediated Cl^- secretion is associated with airway mucus obstruction and inflammation in newborn mice

In the healthy lung, the airway mucus layer lining the epithelium acts as a protective barrier against irritants, allergens and pathogens (105). Ion channels contribute to airway mucus homeostasis by maintaining a balance between fluid secretion and absorption. However, excessive mucin secretion and/or accumulation due to defective transepithelial ion transport leads to airway mucus plugging and consequently, to limited airflow (20, 77, 105–109). To investigate the consequences of the lack of SLC26A9-mediated Cl^- secretion, survival, airway mucus content, lung morphology and inflammatory phenotype were analyzed in newborn WT and *Slc26a9*$^{-/-}$ mice.

In the newborn *Slc26a9*$^{-/-}$ mice, the absence of SLC26A9-mediated Cl^- secretion caused severe airway mucus plugging throughout the respiratory tract (Figures 7, 8, 9 and 10). Airway mucus plugging in newborn *Slc26a9*$^{-/-}$ mice was associated with distinctive signs of respiratory distress such as irregular breathing, gasping, cyanosis and wall chest retraction (Figure 5). All these symptoms that have been previously described in mouse models of early neonatal lung disease (89, 110, 111). Impaired ventilation in newborn *Slc26a9*$^{-/-}$ mice was confirmed by decreased O_2 levels (Figure 5) and observations of atelectasis in the lung (Figure 6). Similar observations have been documented in patients with CF and chronic obstructive pulmonary disease (COPD), where mucus plugging and loss of gas exchange can restricts normal ventilation (112). This muco-obstructive lung phenotype of *Slc26a9*$^{-/-}$ mice resulted in significantly increased mortality within 30 minutes of life (Figure 4). This result might be explained by the absence of efficient MCC as a consequence of defective SLC26A9-mediated Cl^- secretion at birth and thus, in absence of SLC26A9 the lung fails to efficiently adapt to the new air-breathing conditions.

In the developing lung, mucins are expressed from an early embryonic stage in the forming bronchioles and alveolar saccules (113). At the time of birth and continuously through life in non-disease conditions, MUC5B is abundantly expressed in the lung of mice and humans (113, 114). It has been suggested that MUC5B is essential to maintain MCC (113, 115). However, the up-regulation of MUC5B is associated with the pathogenesis of muco-obstructive lung diseases, such as CF, chronic bronchitis and COPD (25, 116–118). In agreement with these publications, increased mRNA and protein levels of *Muc5b*/MUC5B were highly detected in newborn *Slc26a9*$^{-/-}$ mice (Figures 10 and 11). Overall, the data demonstrate that MUC5B contributes to mucus plugging in the lung of newborn *Slc26a9*$^{-/-}$ mice. These data is in line with previous publications

showing that MUC5B strongly contributes to airway mucus plugging in a model of muco-obstructive lung disease, the βENaC-Tg mice (119, 120).

The data in this work demonstrates that *Slc26a9*$^{-/-}$ mice develop spontaneous muco-obstructive lung disease at the early neonatal stage associated with up-regulation of MUC5B expression. However, how SLC26A9 contributes to the regulation of mucins in the airway epithelium of neonatal mice remains unknown. Previous studies have determined that severe hypoxic environment generated by airway mucus obstruction leads to airway epithelial necrosis and an inflammatory phenotype, activating a transcriptional cascade that induces mucin biosynthesis (15, 22–24). This muco-inflammatory phenotype has been documented in patients with CF (79, 92, 121, 122), and in the βENaC-Tg mice (22). The bioelectric studies, histological analysis, O_2 measurements and evidence of atelectasis in the lung of newborn *Slc26a9*$^{-/-}$ mice (Figure 5 – 9 and Figure 13), suggests that a similar mechanism may be taking place in the lung of newborn *Slc26a9*$^{-/-}$ mice. Similarly to observations in βENaC-Tg mice (22, 25, 77, 83), the results presented here showed that the hypoxic environment generated by mucus plugging in newborn *Slc26a9*$^{-/-}$ mice triggers epithelial cell degeneration (Figure 15), release of pro-inflammatory cytokines (Figure 16A-16D) and mild neutrophilic inflammation in the lung (Figure 17A). It was previously reported that the pro-inflammatory cytokine, IL-1α triggers hypoxia-driven inflammation leading to neutrophilic inflammation and mucin hypersecretion (22, 23). IL-1α acts as a danger-associated molecular pattern molecule and in the context of cellular hypoxia can be released through two mechanisms: passively from degenerative cells (Figure 15) and actively through the activation of the inflammasome, Nod-like receptor protein 3 (NLRP3) via reactive oxygen species (ROS) (22, 23, 123). The inflammasome NLRP3 is also responsible for IL-1β secretion, which in turn further increase the secretion of IL-1α (124, 125). In this study, the production of ROS and expression of NLRP3 were not measured. However, since the lack of SLC26A9-mediated Cl^- secretion generates airway mucus obstruction (Figures 7, 8 and 9), a state of oxygen-deprivation (Figures 5 and 6) and elevated levels of IL-1α and IL-1β (Figure 16A and 16B) in the lung of *Slc26a9*$^{-/-}$ mice shortly before death, it may be that this pathway is activated. Moreover, a hypoxic environment activates macrophages that further induce IL-1β and TNF-α (Figure 16E and Figure 25) (126, 127). IL-1α and IL-1β are known to activate IL1-R under hypoxic conditions to induce mucin biosynthesis via SAM pointed domain-containing Ets (SPDEF) transcription factor and the endoplasmic reticulum to nucleus signaling 2 (ERN2) (15, 128, 129) (Figure 25). In this line, a previous report has shown that SPDEF regulates baseline MUC5B expression in the respiratory epithelium. Therefore, it might be interesting to study the

expression of SPDEF in the context of muco-obstructive lung disease in newborn *Slc26a9*$^{-/-}$ mice (130). Furthermore, the defective mucus hydration due to the absence of SLC26A9-mediated Cl^- secretion (Figure 13) further aggravates the muco-obstructive phenotype observed in newborn *Slc26a9*$^{-/-}$ mice (Figure 25), in agreement with observations in other muco-obstructive lung diseases (15).

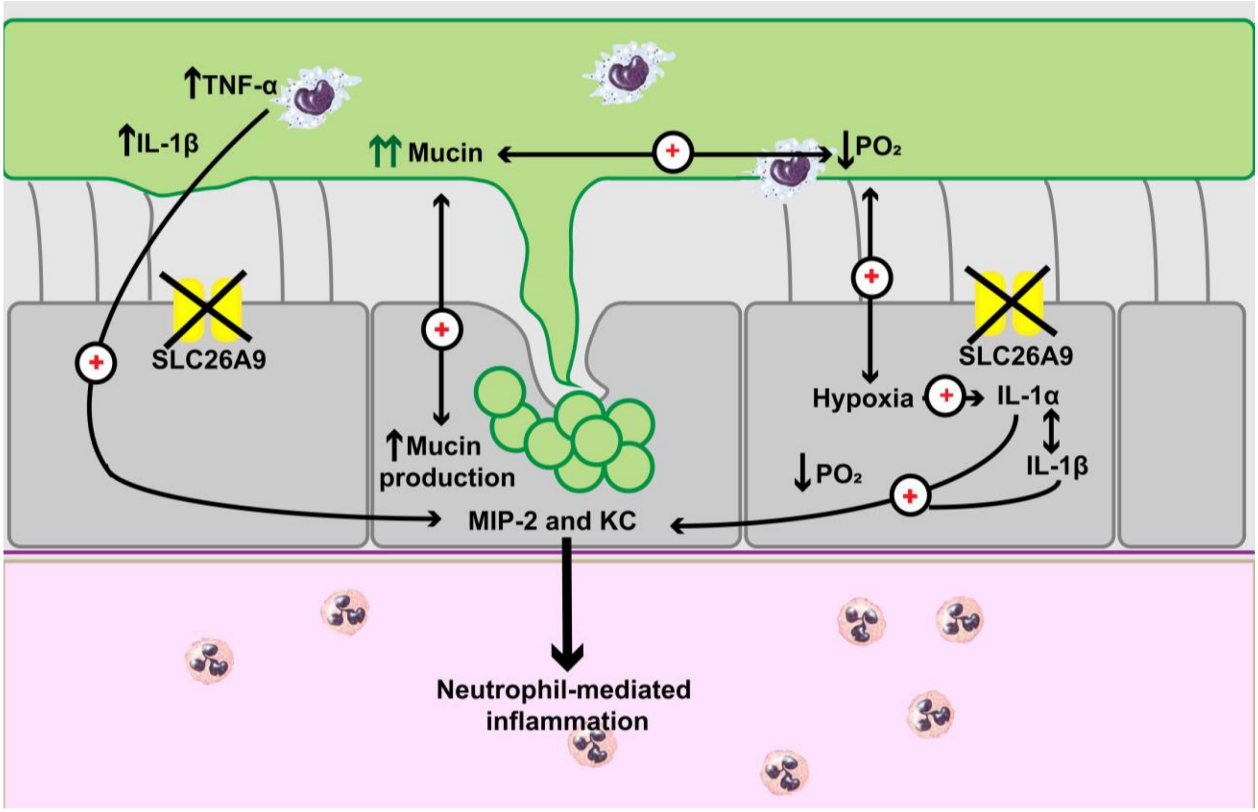

Figure 25. Schematic overview of how the absence of SLC26A9-mediated Cl^- secretion impacts the airway epithelium in newborn mice. Poor airway surface hydration due to the absence of SLC26A9-mediated Cl^- secretion causes airway mucus plugging in the lung of newborn *Slc26a9*$^{-/-}$ mice. Hypoxia-driven inflammation via IL-1α is generated and IL-1β further increase levels of IL-1α. Activated macrophages undergoing hypoxia also induce IL-1β and TNF-α secretion. IL-1α and IL-1β activate IL-1R generating a transcriptional cascade that induces airway mucin biosynthesis. IL-1α is responsible for neutrophilic inflammation and the release of neutrophil chemoattractant, MIP-2 and KC.

Airway infection is the main cause of airway inflammation in patients with CF (131). However, early signs of inflammation are observed in asymptomatic infants with CF without airway bacterial colonization (79) and in βENaC-Tg mice housed in a pathogen-free environment (132). Secretion of IL-1α activates a transcriptional cascade that results in neutrophil-mediated inflammation (Figure 17D, 17E) in a sterile environment (Figure 18) (22). The absence of lung

infection in newborn *Slc26a9*$^{-/-}$ mice (Figure 19) supports the notion that mucus plugging can trigger airway inflammation in the absence of bacteria (22).

4.2 Resolution of airway mucus obstruction and inflammation in surviving *Slc26a9*$^{-/-}$ mice

Once the *Slc26a9*$^{-/-}$ mice survive the neonatal stage, no further mortality is observed up to the age of 6 weeks (Figure 4). Therefore, surviving *Slc26a9*$^{-/-}$ mice were studied to determine if and how the early muco-inflammatory phenotype changes over time. The pulmonary phenotype of WT and *Slc26a9*$^{-/-}$ mice was examined at the juvenile and adult stage of life (2- and 6-week-old, respectively). Similarly, to the analysis of newborn mice, airway mucus content, lung morphology and inflammatory phenotype were evaluated in juvenile and adult mice.

Neutrophilic inflammation persists in surviving *Slc26a9*$^{-/-}$ mice at the juvenile stage (Figure 23). Interestingly, when the inflammatory cells of surviving *Slc26a9*$^{-/-}$ mice at juvenile and adult stage were compared, neutrophils were reduced by 80% in the adult stage compared to the juvenile phase (Figure 23). This result together with the observation that only 30% of the surviving *Slc26a9*$^{-/-}$ mice presented moderate levels of airway mucus obstruction (Figure 20) might suggest that surviving *Slc26a9*$^{-/-}$ mice slowly resolve the initial muco-inflammatory phenotype observed in newborn mice. These findings are supported by a previous study showing that the absence of SLC26A9-mediated Cl^- secretion has not impact on airway mucus content in adult mice (57). This question could be further addressed by measuring the inflammation levels in mice of more advanced ages to determine if there is an improvement compared to earlier endpoints.

The resolution of the inflammatory phenotype in surviving *Slc26a9*$^{-/-}$ mice might be related to the amiloration of airway mucus obstruction. As discussed above (see section 4.1.2) airway mucus obstruction has been associated with high levels of inflammation. In this line, at week 6 of age when the airway mucus plugging is resolved in *Slc26a9*$^{-/-}$ mice, neutrophilic inflammation is 30-fold lower compared to βENaC-Tg mice at the same age, which displayed a chronic airway mucus obstruction (25). These reduce levels of inflammation compared to other models of muco-obstructive lung disease such as βENaC-Tg mice might helped to explained the absence of structural lung damage in surviving *Slc26a9*$^{-/-}$ mice (Figure 21), suggesting that low levels of inflammation are insufficient to cause alveolar damage.

Based on the histological, immunological and bioelectrical findings, it was hypothesized that under physiological conditions SLC26A9-mediated Cl^- secretion is essential for airway mucus hydration in newborn mice, but dispensable at later stages. This is supported by the increased mortality restricted to newborn *Slc26a9*$^{-/-}$ mice (Figure 4) and lack of muco-obstructive phenotype in surviving juvenile and adult *Slc26a9*$^{-/-}$ mice (Figures 20) (57). Whether this age-dependent pulmonary phenotype of the *Slc26a9*$^{-/-}$ mice reflect changes on the ion transport pathways through different stages of lung development (from the perinatal lung to adulthood) remains unknown and further research is necessary. This question might be addressed by studying the transcripts and protein levels of *Slc26a9*/SLC26A9 in a longitudinal manner. However, the identification of the specific mechanism regulating SLC26A9 and its signaling pathways might be more difficult to prove. Previous reports have suggested a regulation via WNK kinases (54, 55). Our data indicates that SLC26A9 function is vital to maintain airway mucus hydration at the critical period of air-breathing adaptation, therefore oxygen sensing regulation might also be possible. Unraveling the molecular mechanisms associated to SLC26A9 regulation under physiological and pathophysiological conditions may lead to a better understanding of SLC26A9 function and its potential therapeutic applications in the context of CF and other muco-obstructive lung diseases.

4.3 Role of the epithelial Cl^- channel SLC26A9 as a modifier of muco-obstructive lung diseases

Lung disease severity in patients with CF has hereditability of 0.54 to 0.8 due to non-CF genetic modifiers (133, 134). *SLC26A9* has been discussed as one of the genetic modifiers that contribute to phenotype variation in CF (135). In previous publications, different genetic variants of *SLC26A9* gene have been associated with higher risk of developing CF-related diabetes, prenatal exocrine pancreatic damage, meconium ileus and muco-obstructive lung diseases such as asthma, diffuse bronchiectasis and CF (50, 56–61, 136). Therefore, it was investigated if the genetic deletion of *Slc26a9* modifies the severity of mortality of CF-like lung disease *in vivo* to test its role as a genetic modifier in CF.

The experiments revealed that genetic deletion of *Slc26a9* increases the mortality rate of βENaC-Tg mice by ~40% (Figure 24). Such a strong impact of a Cl^- channel on the pathogenesis of CF-like lung disease has been previously demonstrated by the absence of CFTR function in the βENaC-Tg mice (83). The βENaC-Tg/*Cftr*$^{-/-}$ mice revealed elevated neonatal airway mucus obstruction, epithelial cell degeneration and increase mortality compared to single-transgenic βENaC-Tg mice (83). It might be speculated that the absence of *Slc26a9*$^{-/-}$

also aggravates the severity of early mucus obstruction in βENaC-Tg mice, thus explaining the elevated mortality of the βENaC-Tg/*Slc26a9*$^{-/-}$ mice. It would be interesting to study the pulmonary phenotype in newborn mice to determine if the augmented mortality of βENaC-Tg/*Slc26a9*$^{-/-}$ is due to an exacerbated airway mucus plugging. Furthermore, investigating the time course of the pulmonary phenotype of βENaC-Tg/*Slc26a9*$^{-/-}$ mice (e.g. mucus content, inflammation and structural lung damage) in a developmental manner may help to elucidate the role of *Slc26a9* in a chronic muco-inflammatory environment that resembles CF lung disease.

The genetic deletion of *Slc26a9* also modifies survival of *Cftr*$^{-/-}$ mice by increasing mortality in newborn mice (49). Interestingly, most of the double mutants (*Slc26a9*$^{-/-}$/*Cftr*$^{-/-}$ mice), disappeared before the weaning period, when the litter was still with their mothers and therefore, it was not possible to determine their cause of death. However, it was suggested that intestinal obstruction or a combination of both, airway and intestinal obstruction was responsible of the early death of *Slc26a9*$^{-/-}$/*Cftr*$^{-/-}$ mice (49). It would be interesting to investigate whether the additional loss of *Slc26a9* in *Cftr*$^{-/-}$ mice worsens lung disease compared to defects observed in the models alone and therefore, helps to explain the high levels of mortality of *Slc26a9*$^{-/-}$/*Cftr*$^{-/-}$ mice.

4.4 Genetic deletion of *Slc26a9* does not generate a model of CF-like lung disease

A comparison of findings in the *Slc26a9* and the above mentioned model of CF-like lung disease, βENaC-Tg mouse are displayed in table 3. Both mouse models, the *Slc26a9*$^{-/-}$ and the βENaC-Tg mice, displayed spontaneous muco-obstructive lung disease with a similar mortality rate (Table 3). However, important and distinctive differences can be noted: (i) *Slc26a9*$^{-/-}$ mice presented an acute muco-obstructive phenotype shortly after birth, while βENaC-Tg mice showed a chronic airway mucus plugging that evolves over the first days of life and does not resolve by itself, (ii) the mucus in *Slc26a9*$^{-/-}$ mice was observed throughout the whole respiratory tree (trachea, main axial airways and terminal bronchioles), whereas mucus plugging in βENaC-Tg mice slowly progress from the trachea to the main axial proximal and distal airways and (iii) neutrophilic inflammation strongly decreased over time in *Slc26a9*$^{-/-}$ mice, while is chronic in βENaC-Tg mice. The pulmonary phenotype of patients with CF is also presented for comparison with CF lung disease. Altogether, this table shows that *Slc26a9*$^{-/-}$ mice does not represent a mouse model of CF lung disease, because they lack the chronicity and slow progression that characterize CF lung disease.

Table 3. Pulmonary phenotypes of *Slc26a9*$^{-/-}$ mice, βENaC-Tg mice and patients with CF

	***Slc26a9*$^{-/-}$ mice**	**βENaC-Tg mice**	**Patients with CF**
Genetic defect	Deletion of exons 2 – 5 of *Slc26a9* gene (66)	βENaC overexpression (77)	CFTR mutations (28)
Disease mortality	48% of pulmonary mortality within 30 minutes of life	50% of pulmonary mortality within the first 2 weeks of life (25, 77)	90% of pulmonary mortality in early adulthood (80)
Ion transport defect	Reduced basal transepithelial potential difference Reduced upregulation of Cl^- secretion in type 2 inflammation (57)	Increased ENaC-mediated Na^+ absorption (77, 83) Normal cAMP-dependent Cl^- secretion (77, 83)	Increased ENaC-mediated Na^+ absorption (13, 137) Deficient cAMP-dependent Cl^- secretion (13, 138)
Onset of pulmonary disease	Acute phenotype. Restrictive to the neonatal stage	Chronic phenotype. Starts at day 3 of life and persist up to adulthood (25)	Chronic phenotype. Starts at early childhood and persist over time (79, 139, 140)
Airway mucus obstruction	Mucus plugging No goblet metaplasia	Mucus plugging Goblet cell metaplasia (25)	Mucus plugging Goblet cell metaplasia (79, 139)
Localization of airway mucus plugging	Whole respiratory tree, including trachea, main axial airways and terminal bronchioles	Starts in the trachea and extends to the main axial proximal and distal airways over time (25)	Whole respiratory tree (79, 139)
Airway inflammation	Neutrophilic inflammation, but decrease over time	Chronic neutrophilic inflammation Transient eosinophilia (25)	Chronic neutrophilic inflammation (141)
Airway infection	No spontaneous infection	Low level of spontaneous infection with environmental and oropharyngeal species (81)	Chronic bacterial infection (*Pseudomonas aeruginosa* and other pathogens) (141, 142)

The distinctive features displayed by newborn *Slc26a9*$^{-/-}$ mice: acute onset of the disease, respiratory distress, cyanotic appearance, reduced O_2 saturation and atelectasis of the lung (Figures 4 and 5) seem to resemble the pathophysiological symptoms of respiratory distress syndrome (RSD) in full-term babies (143–145). The first manifestations of RSD in full-term babies occur between 10 minutes to 12 hours after birth (146), while the first symptoms of diseases in the *Slc26a9*$^{-/-}$ mice appeared within 30 minutes of life (Figure 4). Multiple factors contribute to the development of RSD in full-term babies (severe birth asphyxia, meconium aspiration, cesarean section, among others) (147, 148). However, if and how the SLC26A9 Cl^- channel contributes or act as a modifier of RSD it is completely unknown and beyond the scope of this project.

4.5 Conclusions

Taken together, the results presented here indicate that the epithelial Cl^- channel SLC26A9 contributes to lung health in newborn mice, but is not essential at the juvenile and adult stages of life. Newborn *Slc26a9*$^{-/-}$ mice revealed acute respiratory distress, which is characterized by severe airway mucus obstruction, hypoxia and neonatal death. Furthermore, the pulmonary phenotype of newborn *Slc26a9*$^{-/-}$ mice is fostered by reduced transepithelial ion transport and sterile inflammation. The data demonstrate that SLC26A9-mediated Cl^- secretion is critical to maintain mucus homeostasis in newborn mice, suggesting a critical role in the period of air-breathing adaptation. At the juvenile and adult stages, surviving *Slc26a9*$^{-/-}$ mice showed clear signs of resolution of the muco-inflammatory phenotype as demonstrated by reduced airway mucus content and inflammatory cells over time. Additionally, the observation that *Slc26a9* acts as a modifier of CF-like lung disease in βENaC-Tg mice, suggests that ASL dehydration and consequently, airway mucus dehydration is aggravated in the βENaC-Tg/*Slc26a9*$^{-/-}$ mice in the context of CF-like lung disease.

In summary, our findings shed light on how SLC26A9 impacts the airway epithelial function in a developmental manner and offers first insights of its role in the context of CF-like lung disease, supporting a crucial role of SLC26A9 in muco-obstructive lung diseases such as CF and its potential benefit as therapeutic target in patients with CF.

5 Summary

5.1 Summary

The alternative chloride channel SLC26A9, member of the SoLute Carrier 26 family, has been genetically involved in the pathogenesis of airway mucus obstruction in CF, allergic disease and diffuse non-CF bronchiectasis, supporting a potential role of SLC26A9 as a modifier in muco-obstructive lung diseases. Furthermore, *in vivo* experiments in a mouse model of Th2-driven airway disease revealed that SLC26A9-mediated chloride secretion is critical to prevent airway mucus obstruction, supporting the potential contribution of SLC26A9 to airway surface hydration in the airway epithelium. These findings support SLC26A9 as a promising therapeutic target in CF to potentially bypass the impaired CFTR-mediated chloride secretion. Nevertheless, the *in vivo* role of SLC26A9 under physiological conditions remains unclear. Hence, in this work, the function of SLC26A9 was investigated in a developmental manner (newborn, juvenile and adult stage) by characterizing the pulmonary phenotype of *Slc26a9*$^{-/-}$ mice. Furthermore, we evaluated how the genetic deletion of *Slc26a9* changes the mortality rate of βENaC-Tg mice, which is a mouse model of CF-like lung disease.

Newborn *Slc26a9*$^{-/-}$ mice displayed severe acute respiratory distress due to muco-inflammatory phenotype leading to significant mortality. The mucus plugging of the newborn *Slc26a9*$^{-/-}$ mice was extended throughout the whole respiratory tree. The experiments also demonstrated that airway mucus plugging limits ventilation in newborn *Slc26a9*$^{-/-}$ mice and trigger neutrophil-mediated inflammation probably via epithelial hypoxic necrosis releasing IL-1α. Interestingly, this muco-obstructive phenotype was not observed at the juvenile and adult stage. However, neutrophilic inflammation persists up to adulthood in the lungs of surviving *Slc26a9*$^{-/-}$ mice, but trends to decrease over time, suggesting that surviving *Slc26a9*$^{-/-}$ mice resolve the initial muco-inflammatory phenotype. By monitoring the double mutant βENaC-Tg/*Slc26a9*$^{-/-}$ mice and littermate controls, it was determined that the deletion of *Slc26a9* increases the mortality of βENaC-Tg mice.

In summary, the data demonstrate for the first time that SLC26A9-mediated Cl^-/fluid secretion is particularly relevant for lung health at birth. These findings suggest a critical role of SLC26A9 to maintain airway surface hydration and mucus clearance at the air-breathing adaptation period. The longitudinal characterization of the *Slc26a9*$^{-/-}$ mice revealed an age-dependent resolution of the initial muco-inflammatory phenotype. However, the implications of this airway disease

resolution process on the pathogenesis of muco-obstructive lung diseases, including CF is not yet clear. Furthermore, the modification of survival in βENaC-Tg/*Slc26a9*$^{-/-}$ mice, implicates that *Slc26a9* might impact the lung phenotype in a pathophysiological context. Finally, unravelling the understanding of SLC26A9 function in the pathogenesis of muco-obstructive lung diseases may lead to improve non-CFTR directed therapies for patients with CF.

5.2 Zusammenfassung

Der alternative Cl^- Kanal SLC26A9, Mitglied der SoLute Carrier 26 Proteinfamilie, wird als wichtiger genetischer Modulator in der Pathogenese der muko-obstruktiven Lungenerkrankung wie Mukoviszidose (CF), allergischen Erkrankungen und diffusen Non-CF-Bronchiektasien diskutiert. *In-vivo*-Experimente an einem Mausmodell mit induzierter Th2-Inflammationbelegen, dass SLC26A9 die SLC26A9-vermittelte Chloridsekretion entscheidend ist, um eine Obstruktion des Atemwegsschleims zu verhindern, was den möglichen Beitrag von SLC26A9 zur Oberflächenhydratation der Atemwege im Atemwegsepithel unterstützt. Diese Ergebnisse unterstreichen das Potenzial von SLC26A9 als vielversprechende therapeutische Zielstruktur und Krankheits"modifikator", um die durch eine Mutation von CFTR verringerte Cl^- Leitfähigkeit auszugleichen und den Mukustransport in Patienten mit CF und auch möglicherweise anderen muko-obstruktiven Lungenerkrankungen zu verbessern. Dennoch ist die Rolle von SLC26A9 unter physiologischen Bedingungen *in vivo* wenig verstanden. Deshalb wurde in dieser Arbeit die Funktion von SLC26A9 longitudinal untersucht, indem der pulmonale Phänotyp von *Slc26a9*$^{-/-}$ Mäusen charakterisiert wurde. Darüber hinaus wurde evaluiert, inwiefern die genetische Deletion von *Slc26a9* die Mortalität vom βENaC-Tg Mäusen, die eine CF- ähnliche Lungenerkrankung aufweisen, beeinflusst.

Neugeborene *Slc26a9*$^{-/-}$ Mäuse wiesen aufgrund des muko-entzündlichen Phänotyps eine schwere akute Atemnot auf, die zu einer signifikanten Mortalität führte. Das Muko-obstruktion in den neugeborenen *Slc26a9*$^{-/-}$ Mäusen war in der gesamten Lunge. Die Experimente zeigten auch, dass die Muko-obstruktion die Ventilation bei neugeborenen *Slc26a9*$^{-/-}$ Mäusen einschränkt und eine durch Neutrophile-vermittelte Entzündung auslöst, etwa über eine epitheliale hypoxische Nekrose, die IL-1α freisetzt. Interessanterweise wurde dieser muko-obstruktive Phänotyp im Jugend- und Erwachsenenstadium nicht beobachtet. Die neutrophile Entzündung bleibt jedoch in der Lunge überlebender *Slc26a9*$^{-/-}$ Mäuse bis zum Erwachsenenalter bestehen. Die Entzündungsparameter nehmen jedoch im Laufe der Entwicklung ab, was darauf hindeutet, dass überlebende *Slc26a9*$^{-/-}$ Mäuse den anfänglichen

muko-entzündlichen Phänotyp überwinden. Das Monitoring der doppelmutanten βENaC-Tg/*Slc26a9*$^{-/-}$ Mäuse- ergab, dass die Deletion von Slc26a9 die Mortalität von βENaC-Tg-Mäusen signifikant erhöht.

Zusammenfassend zeigen die Daten erstmals, dass die SLC26A9-vermittelte Cl^-/sekretion für die Lungengesundheit bei der Geburt besonders relevant ist. Diese Ergebnisse legen nahe, dass SLC26A9 eine entscheidende Rolle bei der Aufrechterhaltung der Flüssigkeitszufuhr auf der Atemwegsoberfläche und der mukoziliäre Clearance bei der Anpassung an die Atmung spielt. Die longitudinale Charakterisierung der *Slc26a9*$^{-/-}$ Mäuse ergab eine altersabhängige Auflösung des initialen muko-inflammatorischen Phänotyps. Die Auswirkungen dieses Auflösungsprozesses für Atemwegserkrankungen auf die Pathogenese von mukoobstruktiven Lungenerkrankungen, einschließlich CF, sind jedoch noch nicht klar. Weiterhin deuten die Ergebnisse daraufhin, dass die Deletion von SLC26A9 im CF-Mausmodell die Mortalität weiter erhöht und SLC26A9 damit im pathogenetischen Kontext von mukoobstruktiven Lungenerkrankungen relevant ist. Schließlich könnte die Aufklärung der Funktion von SLC26A9 bei der Pathogenese von mukoobstruktiven Lungenerkrankungen zu einer Verbesserung der nicht-CFTR-gerichteten Therapien für Patienten mit CF führen.

6 References

1. Riordan JR, Rommens JM, Kerem BS, Alon NOA, Rozmahel R, Grzelczak Z, Zielenski J, Lok SI, Plavsic N, Chou JL, Drumm ML, Iannuzzi MC, Collins FS, Tsui LC. Identification of the cystic fibrosis gene: Cloning and characterization of complementary DNA. *Science (80-)* 1989;doi:10.1126/science.2475911.

2. Riordan JR. CFTR function and prospects for therapy. *Annu Rev Biochem* 2008;77:701-726.

3. Rommens J, Kerem B, Alon N, Rozmahel R, Grzelczak Z, Zielenski J, Lok S, Plavsic N, Chou J, Et A. Identification of the cystic fibrosis gene: cloning and characterization of complementary DNA. *Science (80-)* 1989;245:1066–1073.

4. Kerem BS, Rommens JM, Buchanan JA, Markiewicz D, Cox TK, Chakravarti A, Buchwald M, Tsui LC. Identification of the cystic fibrosis gene: Genetic analysis. *Science (80-)* 1989;doi:10.1126/science.2570460.

5. Csanády L, Vergani P, Gadsby DC. Structure, Gating, and Regulation of the CFTR Anion Channel. *Physiol Rev* 2019;doi:10.1152/physrev.00007.2018.

6. Linsdell P, Tabcharani JA, Rommens JM, Hou Y-X, Chang X-B, Tsui L-C, Riordan JR, Hanrahan JW. Permeability of Wild-Type and Mutant Cystic Fibrosis Transmembrane Conductance Regulator Chloride Channels to Polyatomic Anions. *J Gen Physiol* 2002;doi:10.1085/jgp.110.4.355.

7. Poulsen JH, Fischer H, Illek B, Machen TE. Bicarbonate conductance and pH regulatory capability of cystic fibrosis transmembrane conductance regulator. *Proc Natl Acad Sci* 2006;doi:10.1073/pnas.91.12.5340.

8. Berger HA, Anderson MP, Gregory RJ, Thompson S, Howard PW, Maurer RA, Mulligan R, Smith AE, Welsh MJ. Identification and regulation of the cystic fibrosis transmembrane conductance regulator-generated chloride channel. *J Clin Invest* 1991;doi:10.1172/JCI115450.

9. Picciotto MR, Cohn JA, Bertuzzi G, Greengard P, Nairn AC. Phosphorylation of the cystic fibrosis transmembrane conductance regulator. *J Biol Chem* 1992;

10. Engelhardt JF, Zepeda M, Cohn JA, Yankaskas JR, Wilson JM. Expression of the cystic fibrosis gene in adult human lung. *J Clin Invest* 1994;doi:10.1172/JCI117028.

11. Jiang Q, Engelhardt JF. Cellular heterogeneity of CFTR expression and function in the lung: Implications for gene therapy of cystic fibrosis. *Eur J Hum Genet* 1998;doi:10.1038/sj.ejhg.5200158.

12. Saint-Criq V, Gray MA. Role of CFTR in epithelial physiology. *Cell Mol Life Sci* 2017;doi:10.1007/s00018-016-2391-y.

13. Boucher RC. Airway Surface Dehydration in Cystic Fibrosis: Pathogenesis and Therapy. *Annu Rev Med* 2007;doi:10.1146/annurev.med.58.071905.105316.

14. Fahy J V., Dickey BF. Airway Mucus Function and Dysfunction. *N Engl J Med* 2010;363:2233–2247.

15. Boucher RC. Muco-Obstructive Lung Diseases. *N Engl J Med* 2019;doi:10.1056/NEJMra1813799.

16. Knowles MR, Boucher RC. Mucus clearance as a primary innate defense mechanism for mammalian airways. *J Clin Invest* 2002;doi:10.1172/JCI0215217.

17. Button B, Cai LH, Ehre C, Kesimer M, Hill DB, Sheehan JK, Boucher RC, Rubinstein M. A periciliary brush promotes the lung health by separating the mucus layer from airway epithelia. *Science (80-)* 2012;doi:10.1126/science.1223012.

18. Mall MA, Galietta LJV. Targeting ion channels in cystic fibrosis. *J Cyst Fibros* 2015;14:561–570.

19. Stutts MJ, Canessa CM, Olsen JC, Hamrick M, Cohn JA, Rossier BC, Boucher RC. CFTR as a cAMP-dependent regulator of sodium channels. *Science (80-)* 1995;doi:10.1126/science.7543698.

20. Mall M, Bleich M, Greger R, Schreiber R, Kunzelmann K. The amiloride-inhibitable Na+ conductance is reduced by the cystic fibrosis transmembrane conductance regulator in normal but not in cystic fibrosis airways. *J Clin Invest* 1998;doi:10.1172/JCI2729.

21. Knowles MR, Boucher RC. Mucus clearance as a primary innate defense mechanism for mammalian airways. *J Clin Invest* 2008;doi:10.1172/jci15217.

22. Fritzsching B, Zhou-Suckow Z, Trojanek JB, Schubert SC, Schatterny J, Hirtz S, Agrawal R, Muley T, Kahn N, Sticht C, Gunkel N, Welte T, Randell SH, Länger F, Schnabel P, Herth FJF, Mall MA. Hypoxic epithelial necrosis triggers neutrophilic inflammation via IL-1 receptor signaling in cystic fibrosis lung disease. *Am J Respir Crit Care Med* 2015;191:902–913.

23. Chen CJ, Kono H, Golenbock D, Reed G, Akira S, Rock KL. Identification of a key pathway required for the sterile inflammatory response triggered by dying cells. *Nat Med* 2007;13:851–856.

24. Montgomery ST, Mall MA, Kicic A, Stick SM. Hypoxia and sterile inflammation in cystic fibrosis airways: Mechanisms and potential therapies. *Eur Respir J* 2017;49:1–13.

25. Mall MA, Harkema JR, Trojanek JB, Treis D, Livraghi A, Schubert S, Zhou Z, Kreda SM, Tilley SL, Hudson EJ, O'Neal WK, Boucher RC. Development of chronic bronchitis and emphysema in β-epithelial Na+ channel-overexpressing mice. *Am J Respir Crit Care Med* 2008;177:730–742.

26. Peroni DG, Boner AL. Atelectasis: Mechanisms, diagnosis and management. *Paediatr Respir Rev* 2000;doi:10.1054/prrv.2000.0059.

27. Duo-Neng L, Zhong-Xi H, Zheng G, Xi-Xiang Y, Xian-Zhong G. Cystic Fibrosis Nature Review . *C - Comput Model Eng Sci* 2016;1–19.doi:10.1038/nrdp.2015.10.

28. Virant-Young D, Thomas J, Woiderski S, Powers M, Carlier J, McCarty J, Kupchick T, Larder A. Cystic Fibrosis: A Novel Pharmacologic Approach to Cystic Fibrosis Transmembrane Regulator Modulation Therapy. *J Am Osteopath Assoc* 2015;doi:10.7556/jaoa.2015.112.

29. Balázs A, Mall MA. Role of the SLC26A9 Chloride Channel as Disease Modifier and Potential Therapeutic Target in Cystic Fibrosis. *Front Pharmacol* 2018;9:1–9.

30. Gentzsch M, Mall MA. Ion Channel Modulators in Cystic Fibrosis. *Chest* 2018;doi:10.1016/j.chest.2018.04.036.

31. Davies JC, Moskowitz SM, Brown C, Horsley A, Mall MA, McKone EF, Plant BJ, Prais D, Ramsey BW, Taylor-Cousar JL, Tullis E, Uluer A, McKee CM, Robertson S, Shilling RA, Simard C, Van Goor F, Waltz D, Xuan F, Young T, Rowe SM. VX-659–Tezacaftor–

Ivacaftor in patients with cystic fibrosis and one or two Phe508del alleles. *N Engl J Med* 2018;

32. Keating D, Marigowda G, Burr L, Daines C, Mall MA, McKone EF, Ramsey BW, Rowe SM, Sass LA, Tullis E, McKee CM, Moskowitz SM, Robertson S, Savage J, Simard C, Van Goor F, Waltz D, Xuan F, Young T, Taylor-Cousar JL. VX-445-tezacaftor-ivacaftor in patients with cystic fibrosis and one or two Phe508del alleles. *N Engl J Med* 2018;doi:10.1056/NEJMoa1807120.

33. Kerem E, Kerem B. The relationship between genotype and phenotype in cystic fibrosis. *Curr Opin Pulm Med* 1995;doi:10.1097/00063198-199511000-00004.

34. Blackman SM, Commander CW, Watson C, Arcara KM, Strug LJ, Stonebraker JR, Wright FA, Rommens JM, Sun L, Pace RG, Norris SA, Durie PR, Drumm ML, Knowles MR, Cutting GR. Genetic modifiers of cystic fibrosis-related diabetes. *Diabetes* 2013;62:3627-3635.

35. Waller MD, Simmonds NJ. Phenotypic variability of R117H-CFTR expression within monozygotic twins. *Paediatr Respir Rev* 2016;doi:10.1016/j.prrv.2016.06.009.

36. Picci L, Cameran M, Scarpa M, Pradal U, Melotti P, Assael BM, Castellani C. TG15 T5 allele in clinically discordant monozygotic twins with cystic fibrosis [5]. *Am J Med Genet Part A* 2007;doi:10.1002/ajmg.a.31849.

37. Matthias Welsner Svenja Straßburg CT and SS. Use of ivacaftor in late diagnosed cystic fibrosis monozygotic twins heterozygous for F508del and R117H-7T – a case report. *BMC Pulm Med* 2019;19:6.

38. Drumm ML, Ziady AG, Davis PB. Genetic Variation and Clinical Heterogeneity in Cystic Fibrosis. *Annu Rev Pathol Mech Dis* 2011;doi:10.1146/annurev-pathol-011811-120900.

39. Schechter MS. Non-Genetic Influences on Cystic Fibrosis Lung Disease: The Role of Sociodemographic Characteristics, Environmental Exposures, and Healthcare Interventions. *Semin Respir Crit Care Med* 2003;doi:10.1055/s-2004-815660.

40. Salvatore F, Scudiero O, Castaldo G. Genotype-phenotype correlation in cystic fibrosis: The role of modifier genes. *Am J Med Genet* 2002;doi:10.1002/ajmg.10461.

41. Li H, Salomon JJ, Sheppard DN, Mall MA, Galietta LJ. Bypassing CFTR dysfunction in cystic fibrosis with alternative pathways for anion transport. *Curr Opin Pharmacol* 2017;34:91–97.

42. Justin D Walter, Marta Sawicka and RD. Cryo-EM structures and functional characterization of murine Slc26a9 reveal mechanism of uncoupled chloride transport. *Elife* 2019;8:.

43. Geertsma ER, Chang YN, Shaik FR, Neldner Y, Pardon E, Steyaert J, Dutzler R. Structure of a prokaryotic fumarate transporter reveals the architecture of the SLC26 family. *Nat Struct Mol Biol* 2015;doi:10.1038/nsmb.3091.

44. Sharma AK, Rigby AC, Alper SL. STAS domain structure and function. *Cell Physiol Biochem* 2011;doi:10.1159/000335104.

45. Fanning AS, Anderson JM. PDZ domains: Fundamental building blocks in the organization of protein complexes at the plasma membrane. *J Clin Invest* 1999;doi:10.1172/JCI6509.

46. Lohi H, Kujala M, Mäkelä S, Lehtonen E, Kestilä M, Saarialho-Kere U, Markovichand D, Kere J. Functional characterization of three novel tissue-specific anion exchangers SLC26A7, -A8, and -A9. *J Biol Chem* 2002;277:14246–14254.

47. Bertrand CA, Mitra S, Mishra SK, Wang X, Zhao Y, Pilewski JM, Madden DR, Frizzell RA. The CFTR trafficking mutation F508del inhibits the constitutive activity of SLC26A9. *Am J Physiol - Lung Cell Mol Physiol* 2017;312:L912–L925.

48. Chang MH, Plata C, Sindic A, Ranatunga WK, Chen AP, Zandi-Nejad K, Chan KW, Thompson J, Mount DB, Romero MF. Slc26a9 is inhibited by the R-region of the cystic fibrosis transmembrane conductance regulator via the STAS domain. *J Biol Chem* 2009;284:28306–28318.

49. Liu X, Li T, Riederer B, Lenzen H, Ludolph L, Yeruva S, Tuo B, Soleimani M, Seidler U. Loss of Slc26a9 anion transporter alters intestinal electrolyte and HCO3- transport and reduces survival in CFTR-deficient mice. *Pflugers Arch Eur J Physiol* 2015;doi:10.1007/s00424-014-1543-x.

50. Miller MR, Soave D, Li W, Gong J, Pace RG, Boëlle PY, Cutting GR, Drumm ML,

Knowles MR, Sun L, Rommens JM, Accurso F, Durie PR, Corvol H, Levy H, Sontag MK, Strug LJ. Variants in solute carrier SLC26A9 modify prenatal exocrine pancreatic damage in cystic fibrosis. *J Pediatr* 2015;166:1152-1157.e6.

51. Chang MH, Plata C, Zandi-Nejad K, Sincrossed D Signić A, Sussman CR, Mercado A, Broumand V, Raghuram V, Mount DB, Romero MF. Slc26a9-Anion exchanger, channel and Na+ transporter. *J Membr Biol* 2009;228:125–140.

52. Guo M, Du Y, Gokey JJ, Ray S, Bell SM, Adam M, Sudha P, Perl AK, Deshmukh H, Potter SS, Whitsett JA, Xu Y. Single cell RNA analysis identifies cellular heterogeneity and adaptive responses of the lung at birth. *Nat Commun* 2019;doi:10.1038/s41467-018-07770-1.

53. Plasschaert LW, Žilionis R, Choo-Wing R, Savova V, Knehr J, Roma G, Klein AM, Jaffe AB. A single-cell atlas of the airway epithelium reveals the CFTR-rich pulmonary ionocyte. *Nature* 2018;560:377–381.

54. Dorwart MR, Shcheynikov N, Wang Y, Stippec S, Muallem S. SLC26A9 is a Cl- channel regulated by the WNK kinases. *J Physiol* 2007;584:333–345.

55. Salomon JJ, Spahn S, Wang X, Füllekrug J, Bertrand CA, Mall MA. Generation and functional characterization of epithelial cells with stable expression of SLC26A9 Cl^- channels. *Am J Physiol - Lung Cell Mol Physiol* 2016;310:L593–L602.

56. Bakouh N, Bienvenu T, Thomas A, Ehrenfeld J, Liote H, Roussel D, Duquesnoy P, Farman N, Viel M, Cherif-Zahar B, Amselem S, Taam RA, Edelman A, Planelles G, Sermet-Gaudelus I. Characterization of SLC26A9 in patients with CF-like lung disease. *Hum Mutat* 2013;34:1404–1414.

57. Anagnostopoulou P, Riederer B, Duerr J, Michel S, Binia A, Agrawal R, Liu X, Kalitzki K, Xiao F, Chen M, Schatterny J, Hartmann D, Thum T, Kabesch M, Soleimani M, Seidler U, Mall MA. SLC26A9-mediated chloride secretion prevents mucus obstruction in airway inflammation. *J Clin Invest* 2012;122:3629–3634.

58. Strug LJ, Gonska T, He G, Keenan K, Ip W, Boëlle P-Y, Lin F, Panjwani N, Gong J, Li W, Soave D, Xiao B, Tullis E, Rabin H, Parkins MD, Price A, Zuberbuhler PC, Corvol H, Ratjen F, Sun L, Bear CE, Rommens JM. Cystic fibrosis gene modifier *SLC26A9*

modulates airway response to CFTR-directed therapeutics. *Hum Mol Genet* 2016;25:ddw290.

59. Soave D, Miller MR, Keenan K, Li W, Gong J, Ip W, Accurso F, Sun L, Rommens JM, Sontag M, Durie PR, Strug LJ. Evidence for a causal relationship between early exocrine pancreatic disease and cystic fibrosis-related diabetes: A mendelian randomization study. *Diabetes* 2014;doi:10.2337/db13-1464.

60. Blackman SM, Hsu S, Vanscoy LL, Collaco JM, Ritter SE, Naughton K, Cutting GR. Genetic modifiers play a substantial role in diabetes complicating cystic fibrosis. *J Clin Endocrinol Metab* 2009;doi:10.1210/jc.2008-2186.

61. Anh-Thu N. Lam, Melis A. Aksit, Briana Vecchio-Pagan, Celeste A. Shelton, Derek L. Osorio, Arianna F. Anzmann, Loyal A. Goff, David C. Whitcomb, Scott M. Blackman GRC. Increased expression of anion transporter SLC26A9 delays diabetes onset in cystic fibrosis. *J Clin Invest* 2019;Volume 1:

62. Sun L, Rommens JM, Corvol H, Li W, Li X, Chiang TA, Lin F, Dorfman R, Busson PF, Parekh R V., Zelenika D, Blackman SM, Corey M, Doshi VK, Henderson L, Naughton KM, O'neal WK, Pace RG, Stonebraker JR, Wood SD, Wright FA, Zielenski J, Clement A, Drumm ML, Boëlle PY, Cutting GR, Knowles MR, Durie PR, Strug LJ. Multiple apical plasma membrane constituents are associated with susceptibility to meconium ileus in individuals with cystic fibrosis. *Nat Genet* 2012;44:562–569.

63. Bertrand CA, Zhang R, Pilewski JM, Frizzell RA. SLC26A9 is a constitutively active, CFTR-regulated anion conductance in human bronchial epithelia. *J Gen Physiol* 2009;133:421–438.

64. Loriol C, Dulong S, Avella M, Gabillat N, Borgese F, Ehrenfeld J. Cellular Physiology and Biochemistr y Biochemistry Characterization of SLC26A9 , Facilitation of Cl- Transport by Bicarbonate. 2008;2:.

65. Avella M, Loriol C, Boulukos K, Borgese F, Ehrenfeld J. SLC26A9 stimulates CFTR expression and function in human bronchial cell lines. *J Cell Physiol* 2011;doi:10.1002/jcp.22328.

66. Xu J, Song P, Miller ML, Borgese F, Barone S, Riederer B, Wang Z, Alper SL, Forte JG, Shull GE, Ehrenfeld J, Seidler U, Soleimani M. Deletion of the chloride transporter

Slc26a9 causes loss of tubulovesicles in parietal cells and impairs acid secretion in the stomach. *Proc Natl Acad Sci* 2008;105:17955–17960.

67. Henriksnäs J, Phillipson M, Storm M, Engstrand L, Soleimani M, Holm L. Impaired mucus-bicarbonate barrier in Helicobacter pylori- infected mice . *Am J Physiol Liver Physiol* 2006;doi:10.1152/ajpgi.00017.2006.

68. Singh AK, Liu Y, Riederer B, Engelhardt R, Thakur BK, Soleimani M, Seidler U. Molecular transport machinery involved in orchestrating luminal acid-induced duodenal bicarbonate secretion in vivo. *J Physiol* 2013;doi:10.1113/jphysiol.2013.254854.

69. Demitrack ES, Soleimani M, Montrose MH. Damage to the gastric epithelium activates cellular bicarbonate secretion via SLC26A9 Cl − /HCO 3 − exchange . *Am J Physiol Liver Physiol* 2010;doi:10.1152/ajpgi.00037.2010.

70. Howlett M, Chalinor H V., Buzzelli JN, Nguyen N, Van Driel IR, Bell KM, Fox JG, Dimitriadis E, Menheniott TR, Giraud AS, Judd LM. IL-11 is a parietal cell cytokine that induces atrophic gastritis. *Gut* 2012;doi:10.1136/gutjnl-2011-300539.

71. Xu J, Henriksnas J, Barone S, Witte D, Shull GE, Forte JG, Holm L, Soleimani M. SLC26A9 is expressed in gastric surface epithelial cells, mediates Cl-/HCO3- exchange, and is inhibited by NH4+. *Am J Physiol Cell Physiol* 2005;289:C493-505.

72. Snouwaert JN, Brigman KK, Latour AM, Malouf NN, Boucher RC, Smithies O, Koller BH. An animal model for cystic fibrosis made by gene targeting. *Science (80-)* 1992;257:1083–1088.

73. Ratcliff R, Evans MJ, Cuthbert AW, MacVinish LJ, Foster D, Anderson JR, Colledge WH. Production of a severe cystic fibrosis mutation in mice by gene targeting. *Nat Genet* 1993;doi:10.1038/ng0593-35.

74. Colledge WH, Abella BS, Southern KW, Ratcliff R, Jiang C, Cheng SH, MacVinish LJ, Anderson JR, Cuthbert AW, Evans MJ. Generation and characterization of a ΔF508 cystic fibrosis mouse model. *Nat Genet* 1995;doi:10.1038/ng0895-445.

75. Zeiher BG, Eichwald E, Zabner J, Smith JJ, Puga AP, McCray PB, Capecchi MR, Welsh MJ, Thomas KR. A mouse model for the ΔF508 allele of cystic fibrosis. *J Clin Invest* 1995;doi:10.1172/JCI118253.

76. Guilbault C, Saeed Z, Downey GP, Radzioch D. Cystic fibrosis mouse models. *Am J Respir Cell Mol Biol* 2007;36:1–7.

77. Mall M, Grubb BR, Harkema JR, O'Neal WK, Boucher RC. Increased airway epithelial Na+ absorption produces cystic fibrosis-like lung disease in mice. *Nat Med* 2004;doi:10.1038/nm1028.

78. Boucher RC. An overview of the pathogenesis of cystic fibrosis lung disease. *Adv Drug Deliv Rev* 2002;doi:10.1016/S0169-409X(02)00144-8.

79. Sly PD, Brennan S, Gangell C, De Klerk N, Murray C, Mott L, Stick SM, Robinson PJ, Robertson CF, Ranganathan SC. Lung disease at diagnosis in infants with cystic fibrosis detected by newborn screening. *Am J Respir Crit Care Med* 2009;180:146–152.

80. Zhou Z, Duerr J, Johannesson B, Schubert SC, Treis D, Harm M, Graeber SY, Dalpke A, Schultz C, Mall MA. The ENaC-overexpressing mouse as a model of cystic fibrosis lung disease. *J Cyst Fibros* 2011;doi:10.1016/S1569-1993(11)60021-0.

81. Gehrig S, Duerr J, Weitnauer M, Wagner CJ, Graeber SY, Schatterny J, Hirtz S, Belaaouaj A, Dalpke AH, Schultz C, Mall MA. Lack of neutrophil elastase reduces inflammation, mucus hypersecretion, and emphysema, but not mucus obstruction, in mice with cystic fibrosislike lung disease. *Am J Respir Crit Care Med* 2014;189:1082–1092.

82. Wagner CJ, Schultz C, Mall MA. Neutrophil elastase and matrix metalloproteinase 12 in cystic fibrosis lung disease. *Mol Cell Pediatr* 2016;doi:10.1186/s40348-016-0053-7.

83. Johannesson B, Hirtz S, Schatterny J, Schultz C, Mall MA. CFTR regulates early pathogenesis of chronic obstructive lung disease in βenac-overexpressing mice. *PLoS One* 2012;doi:10.1371/journal.pone.0044059.

84. Weibel ER. Stereological methods (Vol.1). Practical Methods for Biological Morphometry. *Stereol methods (Vol1)*, Third. London: Academic Press Limited; 1979. p. 415.

85. Scherle W. A simple method for volumetry of organs in quantitative stereology. *Mikroskopie* 1970;

86. Vasilescu DM, Knudsen L, Ochs M, Weibel ER, Hoffman EA. Optimized murine lung preparation for detailed structural evaluation via micro-computed tomography. *J Appl Physiol* 2012;doi:10.1152/japplphysiol.00550.2011.

87. Juan C. Tapia, Narayanan Kasthuri, Kenneth Hayworth, Richard Schalek, Jeff W. Lichtman, Stephen J Smith and JB. High contrast en bloc staining of neuronal tissue for field emission scanning electron microscopy. *Nat Protoc* 2012;7:193–206.

88. Thiesse J, Namati E, Sieren JC, Smith AR, Reinhardt JM, Hoffman EA, McLennan G. Lung structure phenotype variation in inbred mouse strains revealed through in vivo micro-CT imaging. *J Appl Physiol* 2010;109:1960–1968.

89. Hummler, Edith; Pierre barker; John Gatzy, Friederich Beermann, Chantal Verdumo, Andrea Schmidt RB& BCR. Early death due to defective neonatal lung liquid clearance in alphaENaC deficient mice. *Nat Genet* 1996;12:325–8.

90. Krochmal EM, Ballard ST, Yankaskas JR, Boucher RC, Gatzy JT. Volume and ion transport by fetal rat alveolar and tracheal epithelia in submersion culture. *Am J Physiol* 1989;256:F397-407.

91. Pfaffl MW. A new mathematical model for relative quantification in real-time RT-PCR. *Nucleic Acids Res* 2001;

92. Wielpütz MO, Eichinger M, Zhou Z, Leotta K, Hirtz S, Bartling SH, Semmler W, Kauczor HU, Puderbach M, Mall MA. In vivo monitoring of cystic fibrosis-like lung disease in mice by volumetric computed tomography. *Eur Respir J* 2011;doi:10.1183/09031936.00149810.

93. Olver RE, Walters D V., M. Wilson S. Developmental Regulation of Lung Liquid Transport. *Annu Rev Physiol* 2004;66:77–101.

94. Mund SI, Stampanoni M, Schittny JC. Developmental alveolarization of the mouse lung. *Dev Dyn* 2008;doi:10.1002/dvdy.21633.

95. Schittny JC, Mund SI, Stampanoni M. Evidence and structural mechanism for late lung alveolarization. *Am J Physiol Cell Mol Physiol* 2008;doi:10.1152/ajplung.00296.2007.

96. Branchfield K, Li R, Lungova V, Verheyden JM, McCulley D, Sun X. A three-dimensional study of alveologenesis in mouse lung. *Dev Biol* 2016;doi:10.1016/j.ydbio.2015.11.017.

97. Barker PM, Olver RE. Invited Review: Clearance of lung liquid during the perinatal period. *J Appl Physiol* 2015;doi:10.1152/japplphysiol.00092.2002.

98. Hollenhorst MI, Richter K, Fronius M. Ion Transport by Pulmonary Epithelia. *J Biomed Biotechnol* 2011;doi:10.1155/2011/174306.

99. Frizzell RA, Hanrahan JW. Physiology of epithelial chloride and fluid secretion. *Cold Spring Harb Perspect Med* 2012;doi:10.1101/cshperspect.a009563.

100. Anagnostopoulou P, Dai L, Schatterny J, Hirtz S, Duerr J, Mall MA. Allergic airway inflammation induces a pro-secretory epithelial ion transport phenotype in mice. *Eur Respir J* 2010;36:1436–1447.

101. Hahn A, Salomon JJ, Leitz D, Feigenbutz D, Korsch L, Lisewski I, Schrimpf K, Millar-Büchner P, Mall MA, Frings S, Möhrlen F. Expression and function of Anoctamin 1/TMEM16A calcium-activated chloride channels in airways of in vivo mouse models for cystic fibrosis research. *Pflugers Arch Eur J Physiol* 2018;470:1335–1348.

102. Dagenais A, Fréchette R, Yamagata Y, Yamagata T, Carmel JF, Clermont ME, Brochiero E, Massé C, Berthiaume Y. Downregulation of ENaC activity and expression by TNF-α in alveolar epithelial cells. *Am J Physiol - Lung Cell Mol Physiol* 2004;

103. Yamagata T, Yamagata Y, Nishimoto T, Hirano T, Nakanishi M, Minakata Y, Ichinose M, Dagenais A, Berthiaume Y. The regulation of amiloride-sensitive epithelial sodium channels by tumor necrosis factor-alpha in injured lungs and alveolar type II cells. *Respir Physiol Neurobiol* 2009;doi:10.1016/j.resp.2008.12.008.

104. Roux J, Kawakatsu H, Gartland B, Pespeni M, Sheppard D, Matthay MA, Canessa CM, Pittet JF. Interleukin-1β decreases expression of the epithelial sodium channel α-subunit in alveolar epithelial cells via a p38 MAPK-dependent signaling pathway. *J Biol Chem* 2005;doi:10.1074/jbc.M410561200.

105. Zhou-Suckow Z, Duerr J, Hagner M, Mall MA. Airway mucus, inflammation and remodeling: emerging links in the pathogenesis of chronic lung diseases. *Cell Tissue Res* 2017;doi:10.1007/s00441-016-2562-z.

106. Kreda SM, Davis CW, Rose MC. CFTR, mucins, and mucus obstruction in cystic fibrosis. *Cold Spring Harb Perspect Med* 2012;doi:10.1101/cshperspect.a009589.

107. Mall MA. Unplugging mucus in cystic fibrosis and chronic obstructive pulmonary disease. *Ann Am Thorac Soc* 2016. doi:10.1513/AnnalsATS.201509-641KV.

108. Matsui H, Grubb BR, Tarran R, Randell SH, Gatzy JT, Davis CW, Boucher RC. Evidence for periciliary liquid layer depletion, not abnormal ion composition, in the pathogenesis of cystic fibrosis airways disease. *Cell* 1998;doi:10.1016/S0092-8674(00)81724-9.

109. Regnis JA, Robinson M, Bailey DL, Cook P, Hooper P, Chan HK, Gonda I, Bautovich G, Bye PTP. Mucociliary clearance in patients with cystic fibrosis and in normal subjects. *Am J Respir Crit Care Med* 1994;doi:10.1164/ajrccm.150.1.8025774.

110. Wan H, Xu Y, Ikegami M, Stahlman MT, Kaestner KH, Ang S-L, Whitsett JA. Foxa2 is required for transition to air breathing at birth. *Proc Natl Acad Sci* 2004;doi:10.1073/pnas.0404424101.

111. Clark JC, Wert SE, Bachurski CJ, Stahlman MT, Stripp BR, Weaver TE, Whitsett JA. Targeted disruption of the surfactant protein B gene disrupts surfactant homeostasis, causing respiratory failure in newborn mice. *Proc Natl Acad Sci* 2006;doi:10.1073/pnas.92.17.7794.

112. Fraser KL, Elizabeth Tullis D, Sasson Z, Hyland RH, Thornley KS, Hanly PJ. Pulmonary hypertension and cardiac function in adult cystic fibrosis: Role of hypoxemia. *Chest* 1999;doi:10.1378/chest.115.5.1321.

113. Roy MG, Rahmani M, Hernandez JR, Alexander SN, Ehre C, Ho SB, Evans CM. Mucin production during prenatal and postnatal murine lung development. *Am J Respir Cell Mol Biol* 2011;doi:10.1165/rcmb.2010-0020RC.

114. Buisine MP, Devisme L, Copin MC, Durand-Réville M, Gosselin B, Aubert JP, Porchet N. Developmental mucin gene expression in the human respiratory tract. *Am J Respir Cell Mol Biol* 1999;20:209–218.

115. Roy MG, Livraghi-Butrico A, Fletcher AA, McElwee MM, Evans SE, Boerner RM, Alexander SN, Bellinghausen LK, Song AS, Petrova YM, Tuvim MJ, Adachi R, Romo I, Bordt AS, Bowden MG, Sisson JH, Woodruff PG, Thornton DJ, Rousseau K, De La Garza MM, Moghaddam SJ, Karmouty-Quintana H, Blackburn MR, Drouin SM, Davis CW, Terrell KA, Grubb BR, O'Neal WK, Flores SC, *et al.* Muc5b is required for airway defence. *Nature* 2014;doi:10.1038/nature12807.

116. Kirkham S, Kolsum U, Rousseau K, Singh D, Vestbo J, Thornton DJ. MUC5B is the major

mucin in the gel phase of sputum in chronic obstructive pulmonary disease. *Am J Respir Crit Care Med* 2008;doi:10.1164/rccm.200803-391OC.

117. Henderson AG, Ehre C, Button B, Abdullah LH, Cai LH, Leigh MW, DeMaria GC, Matsui H, Donaldson SH, Davis CW, Sheehan JK, Boucher RC, Kesimer M. Cystic fibrosis airway secretions exhibit mucin hyperconcentration and increased osmotic pressure. *J Clin Invest* 2014;doi:10.1172/JCI73469.

118. Anderson WH, Coakley RD, Button B, Henderson AG, Zeman KL, Alexis NE, Peden DB, Lazarowski ER, Davis CW, Bailey S, Fuller F, Almond M, Qaqish B, Bordonali E, Rubinstein M, Bennett WD, Kesimer M, Boucher RC. The relationship of mucus concentration (hydration) to mucus osmotic pressure and transport in chronic bronchitis. *Am J Respir Crit Care Med* 2015;doi:10.1164/rccm.201412-2230OC.

119. Roy MG, Livraghi-Butrico A, Fletcher AA, McElwee MM, Evans SE, Boerner RM, Alexander SN, Bellinghausen LK, Song AS, Petrova YM, Tuvim MJ, Adachi R, Romo I, Bordt AS, Bowden MG, Sisson JH, Woodruff PG, Thornton DJ, Rousseau K, De La Garza MM, Moghaddam SJ, Karmouty-Quintana H, Blackburn MR, Drouin SM, Davis CW, Terrell KA, Grubb BR, O'Neal WK, Flores SC, *et al.* Muc5b is required for airway defence. *Nature* 2014;505:412–416.

120. Livraghi-Butrico A, Grubb BR, Wilkinson KJ, Volmer AS, Burns KA, Evans CM, O'Neal WK, Boucher RC. Contribution of mucus concentration and secreted mucins Muc5ac and Muc5b to the pathogenesis of muco-obstructive lung disease. *Mucosal Immunol* 2017;10:395–407.

121. Stick SM, Brennan S, Murray C, Douglas T, von Ungern-Sternberg BS, Garratt LW, Gangell CL, De Klerk N, Linnane B, Ranganathan S, Robinson P, Robertson C, Sly PD. Bronchiectasis in Infants and Preschool Children Diagnosed with Cystic Fibrosis after Newborn Screening. *J Pediatr* 2009;doi:10.1016/j.jpeds.2009.05.005.

122. Sly PD, Gangell CL, Chen L, Ware RS, Ranganathan S, Mott LS, Murray CP, Stick SM. Risk Factors for Bronchiectasis in Children With Cystic Fibrosis. *Surv Anesthesiol* 2014;doi:10.1097/01.sa.0000443983.90197.36.

123. Groß O, Yazdi AS, Thomas CJ, Masin M, Heinz LX, Guarda G, Quadroni M, Drexler SK, Tschopp J. Inflammasome Activators Induce Interleukin-1α Secretion via Distinct

Pathways with Differential Requirement for the Protease Function of Caspase-1. *Immunity* 2012;doi:10.1016/j.immuni.2012.01.018.

124. Fettelschoss A, Kistowska M, LeibundGut-Landmann S, Beer H-D, Johansen P, Senti G, Contassot E, Bachmann MF, French LE, Oxenius A, Kundig TM. Inflammasome activation and IL-1 target IL-1 for secretion as opposed to surface expression. *Proc Natl Acad Sci* 2011;doi:10.1073/pnas.1109176108.

125. Cullen SP, Kearney CJ, Clancy DM, Martin SJ. Diverse Activators of the NLRP3 Inflammasome Promote IL-1β Secretion by Triggering Necrosis. *Cell Rep* 2015;doi:10.1016/j.celrep.2015.05.003.

126. Hempel SL, Monick MM, Hunninghake GW. Effect of Hypoxia on Release of IL-1 and TNF by Human Alveolar Macrophages. *Am J Respir Cell Mol Biol* 1996;doi:10.1165/ajrcmb.14.2.8630267.

127. Netea MG, Simon A, Van De Veerdonk F, Kullberg BJ, Van Der Meer JWM, Joosten LAB. IL-1β processing in host defense: Beyond the inflammasomes. *PLoS Pathog* 2010;doi:10.1371/journal.ppat.1000661.

128. Chen G, Ribeiro CMP, Sun L, Okuda K, Kato T, Gilmore RC, Martino MB, Dang H, Abzhanova A, Lin JM, Hull-Ryde EA, Volmer AS, Randell SH, Livraghi-Butrico A, Deng Y, Scherer PE, Stripp BR, O'Neal WK, Boucher RC. XBP1S Regulates MUC5B in a Promoter Variant-Dependent Pathway in IPF Airway Epithelia. *Am J Respir Crit Care Med* 2019;doi:10.1164/rccm.201810-1972oc.

129. Fujisawa T, Chang MMJ, Velichko S, Thai P, Hung LY, Huang F, Phuong N, Chen Y, Wu R. NF-κB mediates IL-1β- and IL-17A-induced MUC5B expression in airway epithelial cells. *Am J Respir Cell Mol Biol* 2011;doi:10.1165/rcmb.2009-0313OC.

130. Chen G, Volmer AS, Wilkinson KJ, Deng Y, Jones LC, Yu D, Bustamante-Marin XM, Burns KA, Grubb BR, O'Neal WK, Livraghi-Butrico A, Boucher RC. Role of spdef in the regulation of muc5b expression in the airways of naive and mucoobstructed mice. *Am J Respir Cell Mol Biol* 2018;doi:10.1165/rcmb.2017-0127OC.

131. Armstrong DS, Hook SM, Jamsen KM, Nixon GM, Carzino R, Carlin JB, Robertson CF, Grimwood K. Lower airway inflammation in infants with cystic fibrosis detected by

newborn screening. *Pediatr Pulmonol* 2005;40:500–510.

132. Livraghi-Butrico A, Kelly EJ, Klem ER, Dang H, Wolfgang MC, Boucher RC, Randell SH, O'Neal WK. Mucus clearance, MyD88-dependent and MyD88-independent immunity modulate lung susceptibility to spontaneous bacterial infection and inflammation. *Mucosal Immunol* 2012;5:397–408.

133. Vanscoy LL, Blackman SM, Collaco JM, Bowers A, Lai T, Naughton K, Algire M, McWilliams R, Beck S, Hoover-Fong J, Hamosh A, Cutler D, Cutting GR. Heritability of lung disease severity in cystic fibrosis. *Am J Respir Crit Care Med* 2007;doi:10.1164/rccm.200608-1164OC.

134. Mekus F, Ballmann M, Bronsveld I, Bijman J, Veeze H, Tümmler B. Categories of δF508 homozygous cystic fibrosis twin and sibling pairs with distinct phenotypic characteristics. *Twin Res* 2000;doi:10.1375/136905200320565256.

135. O'Neal WK, Knowles MR. Cystic Fibrosis Disease Modifiers: Complex Genetics Defines the Phenotypic Diversity in a Monogenic Disease. *Annu Rev Genomics Hum Genet* 2018;doi:10.1146/annurev-genom-083117-021329.

136. Sun L, Rommens JM, Corvol H, Li W, Li X, Chiang TA, Lin F, Dorfman R, Busson PF, Parekh R V., Zelenika D, Blackman SM, Corey M, Doshi VK, Henderson L, Naughton KM, O'neal WK, Pace RG, Stonebraker JR, Wood SD, Wright FA, Zielenski J, Clement A, Drumm ML, Boëlle PY, Cutting GR, Knowles MR, Durie PR, Strug LJ. Multiple apical plasma membrane constituents are associated with susceptibility to meconium ileus in individuals with cystic fibrosis. *Nat Genet* 2012;44:562–569.

137. Boucher RC, Stutts MJ, Knowles MR, Cantley L, Gatzy JT. Na+ transport in cystic fibrosis respiratory epithelia. Abnormal basal rate and response to adenylate cyclase activation. *J Clin Invest* 1986;doi:10.1172/JCI112708.

138. Sheppard DN, Ostedgaard LS. Understanding how cystic fibrosis mutations cause a loss of Cl- channel function. *Mol Med Today* 1996;doi:10.1016/1357-4310(96)10028-9.

139. Mall M, Boucher RC. Pathogenesis of Pulmonary Disease in Cystic Fibrosis. *Cyst Fibros 21st Century* 2005. doi:10.1159/000088489.

140. M.O. W, M. P, A. K-S, M. S, E. F, O. S, S. L, M. S, J. B, H.-U. K, M. E, M.A. M. Magnetic

resonance imaging detects changes in structure and perfusion, and response to therapy in early cystic fibrosis lung disease. *Am J Respir Crit Care Med* 2014;doi:10.1164/rccm.201309-1659OC.

141. Pereira LCR, Moreira EAMH, Bennemann GD, Moreno YMF, Buss ZDS, Barbosa E, Ludwig-Neto N, Wilhelm Filho D, Fröde TS. Influence of inflammatory response, infection, and pulmonary function in cystic fibrosis. *Life Sci* 2014;doi:10.1016/j.lfs.2014.06.002.

142. Sagel SD, Gibson RL, Emerson J, McNamara S, Burns JL, Wagener JS, Ramsey BW, Konstan M, Chatfield B, Retsch-Bogart G, Waltz DA, Acton J, Zeitlin P, Hiatt P, Moss R, Wagener J, Omlor G, Borowitz D, Rosenfeld M. Impact of Pseudomonas and Staphylococcus Infection on Inflammation and Clinical Status in Young Children with Cystic Fibrosis. *J Pediatr* 2009;doi:10.1016/j.jpeds.2008.08.001.

143. Liu J. Respiratory Distress Syndrome in Full-term Neonates. *J Neonatal Biol* 2012;S1:1-2.

144. Bouziri A, Slima S Ben, Hamdi A, Menif K, Belhadj S, Khaldi A, Kechaou W, Kazdaghli K, Jaballah N Ben. Acute respiratory distress syndrome in infants at term and near term about 23 cases. *Tunisie Medicale* 2007;

145. Faix RG, Viscardi RM, DiPietro MA, Nicks JJ. Adult respiratory distress syndrome in full-term newborns. *Pediatrics* 1989;

146. Liu J, Shi Y, Dong JY, Zheng T, Li JY, Lu LL, Liu JJ, Liang J, Zhang H, Feng ZC. Clinical characteristics, diagnosis and management of respiratory distress syndrome in full-term neonates. *Chin Med J (Engl)* 2010;doi:10.3760/cma.j.issn.0366-6999.2010.19.004.

147. Liu J, Yang N, Liu Y. High-risk factors of respiratory distress syndrome in term neonates: A retrospective case-control study. *Balkan Med J* 2014;doi:10.5152/balkanmedj.2014.8733.

148. Wang J, Liu X, Zhu T, Yan C. Analysis of neonatal respiratory distress syndrome among different gestational segments. *Int J Clin Exp Med* 2015;

Own publications

Original articles

Millar-Büchner P, Philp AR, Gutierrez N, Villanueva S, Kerr B, Flores CA. **(2016)** Severe changes in colon epithelium in the *Mecp2*-null mouse model of Rett syndrome". Mol Cell Pediatr. Dec;3 (1):37. Epub 2016 Nov 21. doi: 10.1186/s40348-016-0065-3

Philp AR, Riquelme TT, Millar-Büchner P, González R, Sepúlveda FV, Cid LP, Flores CA. **(2018)** Kcnn4 is a modifier gene of intestinal cystic fibrosis preventing lethality in the Cftr-F508del mouse. Sci Rep. 2018 Jun 18; 8(1):9320. doi: 10.1038/s41598-018-27465-3

Hahn A, Salomon JJ, Leitz D, Feigenbutz D, Korsch L, Lisewski I, Schrimpf K, Millar-Büchner P, Mall MA, Frings S, Möhrlen F. **(2018)** Expression and function of Anoctamin 1/TMEM16A calcium- activated chloride channels in airways of in vivo mouse models for cystic fibrosis research. Pflugers Arch. 2018 Sep; 470(9):1335-1348. doi: 10.1007/s00424-018-2160-x

Vega G., Güequén A., Johansson M., Arike L., Martínez-Abad B., Scudieri P., Pedemonte N., Millar-Büchner P., Philp A.R, Galietta L.J.V., Hansson G.C, and Flores C.A. **(2019)** Normal Calcium-Activated Anion Secretion in a Mouse Selectively Lacking TMEM16A in Intestinal Epithelium. Front. Physiol., 13 June 2019. doi: 10.3389/fphys.2019.00694

Published abstracts

Salomon J.J., Millar-Büchner P., Spahn S., Wagner W., Mall M.A. **(2019)**. Early death in *Slc26a9*-deficient mice is due to airway mucus obstruction associated with epithelial necrosis and neutrophilic inflammation. American Journal of Respiratory and Critical Care Medicine 2019;199: A2837

Poster presentations

Millar-Büchner P., Salomon J.J., Spahn S., Mall M. **(2015)** Role of SLC26A9 Cl^- channel in lung disease. 3rd Winter Training School: Evolutionary Medicine & Development of Respiratory Disease, Borstel, Germany

Millar-Büchner P., Salomon J.J., Mall M. **(2016)** Characterization of the pulmonary phenotype of adult *Slc26a9* knockout mice. Annual meeting of Deutsches Zentrum für Lungenforschung (DZL), Hannover, Germany

Millar-Büchner P., Salomon J.J., Mall M. **(2016)** Characterization of SLC26A9 in the lung of adult mice. Annual meeting of European Young Investigators Meeting (EYIM), Paris, France

Millar-Büchner P., Salomon J.J., Sphan S., Mall M. **(2017)** Lack of SLC26A9 Cl^- channel produced neonatal mortality due to airway mucus plugging. Annual meeting of Deutsches Zentrum für Lungenforschung (DZL), Munich, Germany

Millar-Büchner P., Salomon J.J., Spahn S., Wagner W., Löser T., Schatterny J., Butz S., Mall M.A. **(2018)** *Slc26a9* deficiency triggers early onset of airway mucus obstruction and neonatal mortality. Annual meeting of Deutsches Zentrum für Lungenforschung (DZL), Bad Nauheim, Germany

Millar-Büchner P., Salomon J.J., Sphan S., Mall M. **(2018)** Early onset airway mucus plugging and neonatal mortality in *Slc26a9*-deficient mice. Annual meeting of European Young Investigators Meeting (EYIM), Paris, France

Millar-Büchner P., Salomon J.J., Sphan S., Mall M. **(2018)** Early neonatal mortality of *Slc26a9*-deficient mice is triggered by airway mucus obstruction. Annual meeting of ECFS Basic science conference, Loutraki, Greece

Millar-Büchner P., Salomon J.J., Sphan S., Wagner W., Löser T., Schatterny J., Butz S., Mall M.A. **(2019)** Lack of SLC26A9 Cl^- channel produces early onset of airway mucus obstruction and neonatal mortality in mice. Annual meeting of Deutsches Zentrum für Lungenforschung (DZL), Mannheim, Germany

Millar-Büchner P., J.J. Salomon, S. Spahn, W. Wagner, T. Löse[3], J. Schatterny, S. Butz, M.A. Mall. **(2019)** Increased mortality and early onset of airway mucus obstruction of the *Slc26a9*-deficient mice. Annual meeting of ECFS Basic science conference, Dubrovnik, Croatia

Oral presentations

Characterization of SLC26A9 in the lung of adult mice. European Young Investigators Meeting (EYIM), **February 2016**, Paris, France

Early onset airway mucus plugging and neonatal mortality in *Slc26a9*-deficient mice. European Young Investigators Meeting (EYIM), **February 2018**, Paris, France

Early neonatal mortality of *Slc26a9*-deficient mice is triggered by airway mucus obstruction. ECFS Basic science conference, **March 2018**, Loutraki, Greece

Increased mortality and early onset of airway mucus obstruction of the *Slc26a9*-deficient mice. ECFS Basic science conference, **April 2019**, Dubrovnik, Croatia

Honors and awards

Young fellows travel award from the European cystic fibrosis society (ECFS), **March 2018**, Loutraki, Greece

Travel grant from Mukoviszidose e.V. to attend the European cystic fibrosis society (ECFS) basic science conference, **April 2019**, Dubrovnik, Croatia

Curriculum vitae

Personal information

Last name, first name:	Millar Büchner, Pamela
Date of birth:	05-09-1990
Place of birth:	Valdivia, XIV Región de los Ríos, Chile
Nationality:	Chilean
Marital status:	Married

School background

1997 – 2004	Primary education at Escuela Particular N°1 Nuestra Señora del Carmen, Valdivia, Chile
2005 – 2008	High school at Instituto Inmaculada Concepción, Valdivia, Chile

Academic background

2009 – 2012	Bachelor degree in Biology at Universidad Austral de Chile, Valdivia, Chile
2009 – 2013	Biologist degree at Universidad Austral de Chile, Valdivia, Chile
2015 – present	PhD student at the Translational Lung Research Center (TLRC), Medical faculty of University of Heidelberg, Heidelberg, Germany

Professional background

2013 – 2014	Research assistant at Molecular Biophysics and Physiology laboratory, Centro de Estudios Científicos (CECs), Valdivia, Chile

Acknowledgements

I would like to thank:

Prof. Dr. Marcus Mall for his excellent supervision and for giving me the opportunity to work in this very interesting project; for his critical thinking about the results, his valuable advice and unwavering support and encouragement throughout my PhD studies.

Dr. Johanna Salomon for her supervision and constructive criticism of my project. For the time invested in many meetings to discuss new results. For her patience and help with my countless questions! (Both science related and unrelated) and for proof-reading this thesis.

Dr. Carlos Flores for participating of my TAC meetings. For his input and helpful suggestions about the project. For his encouragement and friendly support.

Dr. Claudius Wagner for his always valuable advice and for proofreading this thesis.

Jolanthe Schatterny and Simone Butz for their valuable experimental support and for their willingness to arrive earlier in the morning and rescue me from night shifts! Willi Wagner, Timo Löser and Martin Finke for their technical advice and help to analyze the µCT data. Inge Frommer for performing the osmium-impregnation technique. Dr. Matthias Hagner and Dr. Michelle Paulsen for their technical advice with the flow cytometry experiments. Prof. Dr. Stephan Frings, Dr. Frank Möhrlen and Frederike Auer for their technical advice and for welcome me into their laboratory to perform my experiments.

Dr. Ayca Seyhan-Agircan, Dr. Claudius Wagner, Stella Jianghui Zhu, Stephanie Hirtz, Dr. Anita Balazs and Dr. Zhe Zhou-Suckow for their support and advice. For all the ideas, books and movies recommendations. I am grateful for all the great conversations and for lots of fun that we have together.

My husband, Fredy, for always being there for me, for believing in me and encourage me to achieve my goals. For putting a smile in my face every day.

My parents Erica and Jaime, and my brother Cristián, for their endless support. For bearing with me through the difficult times that living abroad sometimes means and the daily talks that make me feel closer to you. For teaching me to be persistent and pursue my dreams. Francisca Araneda for her friendship throughout all chapters of my life. ¡Muchísimas gracias a todos!

Eidesstattliche Versicherung

1. Bei der eingereichten Dissertation zu dem Thema: **“Role of the epithelial Cl^- channel SLC26A9 in the murine airway epithelium”** handelt es sich um meine eigenständig erbrachte Leistung.

2. Ich habe nur die angegebenen Quellen und Hilfsmittel benutzt und mich keiner unzulässigen Hilfe Dritter bedient. Insbesondere habe ich wörtlich oder sinngemäß aus anderen Werken übernommene Inhalte als solche kenntlich gemacht.

3. Die Arbeit oder Teile davon habe ich bislang nicht an einer Hochschule des In- oder Auslands als Bestandteil einer Prüfungs- oder Qualifikationsleistung vorgelegt.

4. Die Richtigkeit der vorstehenden Erklärungen bestätige ich.

5. Die Bedeutung der eidesstattlichen Versicherung und die strafrechtlichen Folgen einer unrichtigen oder unvollständigen eidesstattlichen Versicherung sind mir bekannt. Ich versichere an Eides statt, dass ich nach bestem Wissen die reine Wahrheit erklärt und nichts verschwiegen habe.

Heidelberg, den 21.Octoker 2019 P. Millar Büchner